EXPERIMENTAL STUDY OF SOLID PROPELLANT COMBUSTION INSTABILITY

A THESIS SUBMITTED TO
THE GRADUATE SCHOOL OF NATURAL AND APPLIED SCIENCES
OF
MIDDLE EAST TECHNICAL UNIVERSITY

BY

AYÇA ÇEKİÇ

IN PARTIAL FULFILLMENT OF THE REQUIREMENTS
FOR
THE DEGREE OF MASTER OF SCIENCE
IN
MECHANICAL ENGINEERING

DECEMBER 2005

Approval of the Graduate School of Natural and Applied Sciences

_____

Prof. Dr. Canan ÖZGEN

Director

I certify that this thesis satisfies all the requirements as a thesis for the degree of Master of Science.

_____

Prof. Dr. S. Kemal İDER

Head of Department

This is to certify that we have read this thesis and that in our opinion it is fully adequate, in scope and quality, as a thesis for the degree of Master of Science.

_____

Asst. Prof. Abdullah ULAŞ

Supervisor

Examining Committee Members

Prof. Dr. Demir BAYKA	(METU, ME)	_____
Asst. Prof. Dr. Abdullah ULAŞ	(METU, ME)	_____
Prof. Dr. Mehmet ÇALIŞKAN	(METU, ME)	_____
Prof. Dr. Sinan AKMANDOR	(METU, AEE)	_____
Dr. Mehmet Ali AK	(TÜBİTAK-SAGE)	_____

I hereby declare that all information in this document has been obtained and presented in accordance with academic rules and ethical conduct. I also declare that, as required by these rules and conduct, I have fully cited and referenced all material and results that are not original to this work.

Name, Last Name : Ayça ÇEKİÇ
Signature :

ABSTRACT

EXPERIMENTAL STUDY OF SOLID PROPELLANT COMBUSTION INSTABILITY

ÇEKİÇ, Ayça
M.S., Department of Mechanical Engineering
Supervisor: Asst. Prof. Dr. Abdullah ULAŞ

December 2005, 129 pages

In this study, experimental investigation of solid propellant combustion instability using an end burning T-Burner setup is performed. For this purpose, a T-Burner setup is designed, analyzed, constructed and tested with all its sub components. T-Burner setup constructed is mainly composed of a base part, a control panel and the T-Burner itself. Combustion chamber, pressure stabilization mechanism, pressurization system, measurement instruments and data acquisition systems form the T-Burner.

Pressure stabilization mechanism is utilized in two different alternatives, first of which is by the use of nitrogen gas and a small surge tank with a cavitating venturi. This is a brand new approach for this kind of system. The second alternative is the use of a choked nozzle for pressure stabilization.

Resonance frequencies of the system with the two different pressure stabilization mechanisms are experimentally evaluated. Helmholtz frequency of the

T-burner constructed is calculated and no Helmholtz instability is observed in the system.

Constructed T-Burner setup is operated for a specific solid propellant. System worked successfully and pressure data are obtained. Pressure data revealed oscillatory behaviour. Decay and growth rates of pressure oscillations are used for the calculation of pressure response of the propellant tested.

By the use of this T-Burner comparison of the behavior of different propellants can be performed. It can be used as a test device for measuring quantitatively the response of a burning propellant to unsteady motions.

Keywords: T-Burner, Combustion Instability, Experimental, Solid Propellant

ÖZ

KATI YAKITLARDAKİ YANMA KARARSIZLIKLARININ DENEYSEL İNCELENMESİ

ÇEKİÇ, Ayça
Yüksek Lisans, Makina Mühendisliği Bölümü
Tez Yöneticisi: Y. Doç. Dr. Abdullah ULAŞ

Aralık 2005, 129 sayfa

Bu çalışmada, katı yakıt yanma kararsızlığı uçtan yanmalı T-Yakıcı deney düzeneği kullanılarak deneysel olarak incelenmiştir. Bu amaçla, bir T-Yakıcı deney düzeneği bütün alt sistemleri ile birlikte tasarlanmış, analizleri yapılmış, üretilmiş ve test edilmiştir. Üretilen T-Yakıcı deney düzeneği temel olarak bir kaideden, bir kontrol panelinden ve T-Yakıcı'nın kendisinden oluşmaktadır. T-Yakıcı ise yanma odasından, basınç sabitleme düzeneğinden, basınçlandırma sisteminden, ölçüm cihazlarından ve veri toplama sisteminden oluşmaktadır.

Sistemin basınç sabitleme mekanizması için iki alternatif kullanılmıştır. İlk alternatif, nitrojen gazı, küçük bir tank ve ona bağlı kavitasyonlu ventüriden oluşmaktadır. Bu yaklaşım T-Yakıcı sistemlerinde ilk defa denenmektedir. İkinci alternatifte ise basınç sabitlemek için lüle kullanılmaktadır.

Sistemin rezonans frekansları her iki basınç sabitleme mekanizması için de deneysel olarak elde edilmiştir. T-Yakıcı sisteminin Helmholtz frekansı hesaplanmış ve sistemde herhangi bir Helmholtz kararsızlığı gözlenmemiştir.

Üretilen T-Yakıcı deney düzeneği tanımlı bir katı yakıt için denenmiştir. Sistem başarı ile çalışmış, basınç verisi elde edilmiştir. Alınan basınç verisi salınımlı karakter göstermiştir. Basınç salınımlarının azalma ve artma oranları, denenen yakıtın basınç tepkisini hesaplamakta kullanılmıştır.

Bu T-Yakıcı deney düzeneği kullanılarak değişik yakıtların davranışları niceliksel olarak karşılaştırılabilir. Ayrıca bu düzenek yanan bir yakıtın zamandan bağımsız hareketlere karşı niteliksel tepkisini ölçmekte de kullanılabilir.

Anahtar Kelimeler: T-Yakıcı, Yanma Kararsızlığı, Deneysel, Katı Yakıt

To My Family

ACKNOWLEDGMENTS

I would like to express my sincere gratitude to Asst. Prof. Dr. Abdullah ULAŞ and Dr. Mehmet Ali AK, for their endless support, guidance and for helpful discussions we have made throughout the study.

TÜBİTAK SAGE who supported this work is also greatly acknowledged.

I would like to send my thanks to the TÜBİTAK-SAGE Propulsion Division members for their help and understanding.

I am grateful to my colleagues at TÜBİTAK-SAGE, especially İlke AYDINCAK.

My special thanks go to Dr. L. Oktay GÖNÇ for his endless support and friendship.

I am indebted to Kürşat KARAİL, both for his forbearance and for his invaluable assistance in the preparation of this thesis.

Finally, the greatest thanks go to my family who supported and encouraged me throughout my whole life. It would be impossible without their patience and understanding.

TABLE OF CONTENTS

LIST OF TABLES

LIST OF FIGURES

LIST OF SYMBOLS

F_{thrust}	Thrust
$\dot{m}$	Mass flow rate
c	Equivalent velocity
A_{ex}	Nozzle exit area
P_{ex}	Nozzle exit pressure
P	Pressure
u	Velocity
ν	Velocity of gases leaving propellant combustion zone
a	Speed of sound
ρ	Density
A_b	Admittance function
r_b	Burning rate
C	Pre-exponential factor
R	Response function
γ	Specific Heat Ratio
T	Temperature
W	Molecular weight
q	Heat Flux
M	Mach Number
f	Frequency
L	Length
τ	Shear Stress
σ_1	Hoop stress
σ_2	Longitudinal stress

r	Radius
t	Thickness
F	Force
A	Area
t	Time
V	Volume
$\Re$	Universal gas constant
a_0	Average velocity of sound
S_c	Cross-sectional area of burner
S_b	Burning area of propellant
α	Time exponential coefficient
α_{FT}	Flow-turning coefficient
α_{PD}	Particle damping coefficient
α_{ST}	Structural damping coefficient
R_N	Nozzle response function
I	Acoustic stability integral
C_D	Nozzle discharge coefficient, s / m
c^*	Characteristic velocity, m / s

Subscripts

amb	Ambient
max	Maximum
PC	Pressure coupled

VC	Velocity coupled
QC	Heat flux coupled
b	Propellant burning surface

Superscripts

.	Time Derivative
‘	Fluctuations
-	Mean
r	Real component
i	Imaginary component

CHAPTER 1

INTRODUCTION

1.1. Solid Propellant Rocket Motors

A solid propellant rocket motor is a relatively simple device. It consists of a cylindrical case with propellant bonded to its inner surface, a hollow combustion chamber and a nozzle to direct the flow of gases out of the chamber. Figure 1 shows a schematic of a typical rocket motor. The propellant surface, after reaching its melt temperature forms a liquid layer called the foam layer which contains a mass of bubbling gaseous products and molten propellant. Final combustion gas and metal fuel products are detected in the gas-phase flame region. These products are convected towards the nozzle.

The thrust of the rocket motor can be defined by Equation (1.1) [1]

$$F_{thrust} = \dot{m}_p c \tag{1.1}$$

$$c = u_{ex} + \frac{(P_{ex} - P_{amb}) A_{ex}}{\dot{m}_p} \tag{1.2}$$

where c is the equivalent velocity out of the exit nozzle, A_{ex} is the nozzle exit area, P_{ex} is the nozzle exit pressure and P_{amb} is the ambient pressure.

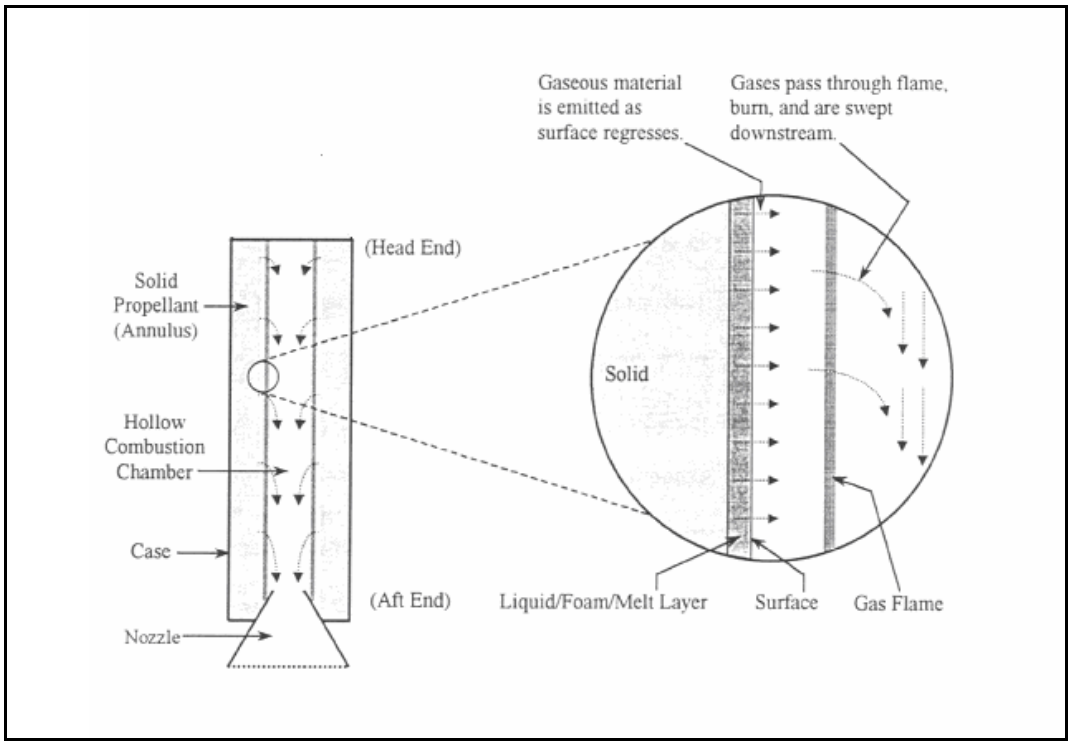

Figure 1. A typical solid rocket motor [1]

1.2. The Unsteady Operational Regimes of Solid Rocket Motors

The designer of a solid rocket motor normally has a design goal stated in terms of thrust level and duration of thrust. The choices of propellant, charge geometry and nozzle throat area are tailored to meet that objective with an acceptable pressure in the motor. To make these choices, the designer uses internal ballistic equations based on the assumption of steady state combustion and flow in the motor.

Nature is no respecter of classical approximations such as the steady state assumption, and the designer is often confronted by nonsteady behavior in the motor. The ignition transient and tail-off transient are the examples of nonsteady behaviors that the designer accepts as obvious design problems. The ignition transition phase is required to join the initial unfired state and the operational state

basic to the usefulness of the motor; and tail-off transition phase is required to join the operational state and the final extinguished state. These three regimes are shown in Figure 2.

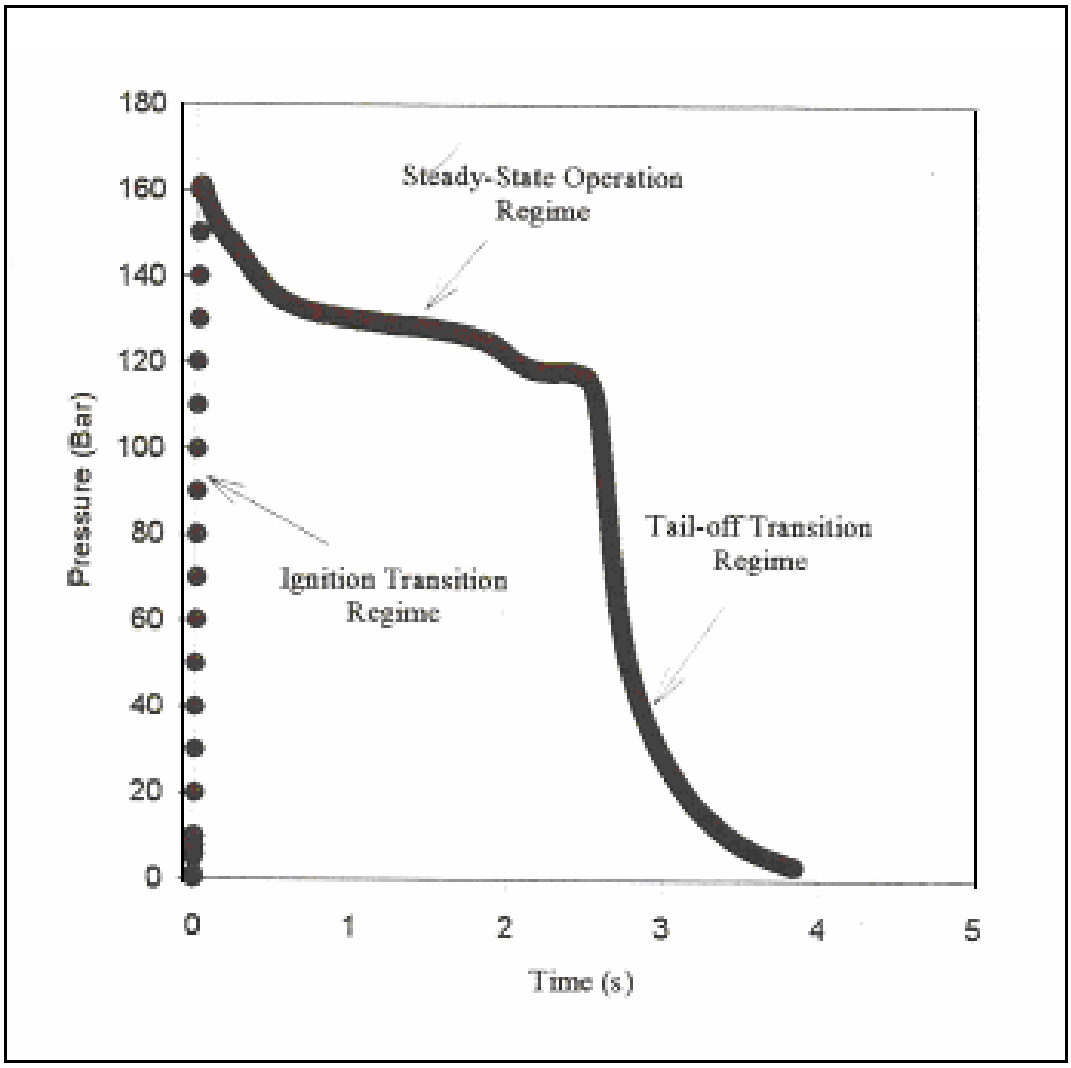

Figure 2. Typical pressure-time curve of a solid rocket motor [2]

Another unexpected problem is an oscillatory mode of operation, in which the pressure oscillates about a time-averaged mean pressure that may, or may not, correspond to the expected mean value. This behavior is illustrated schematically in Figure 3.

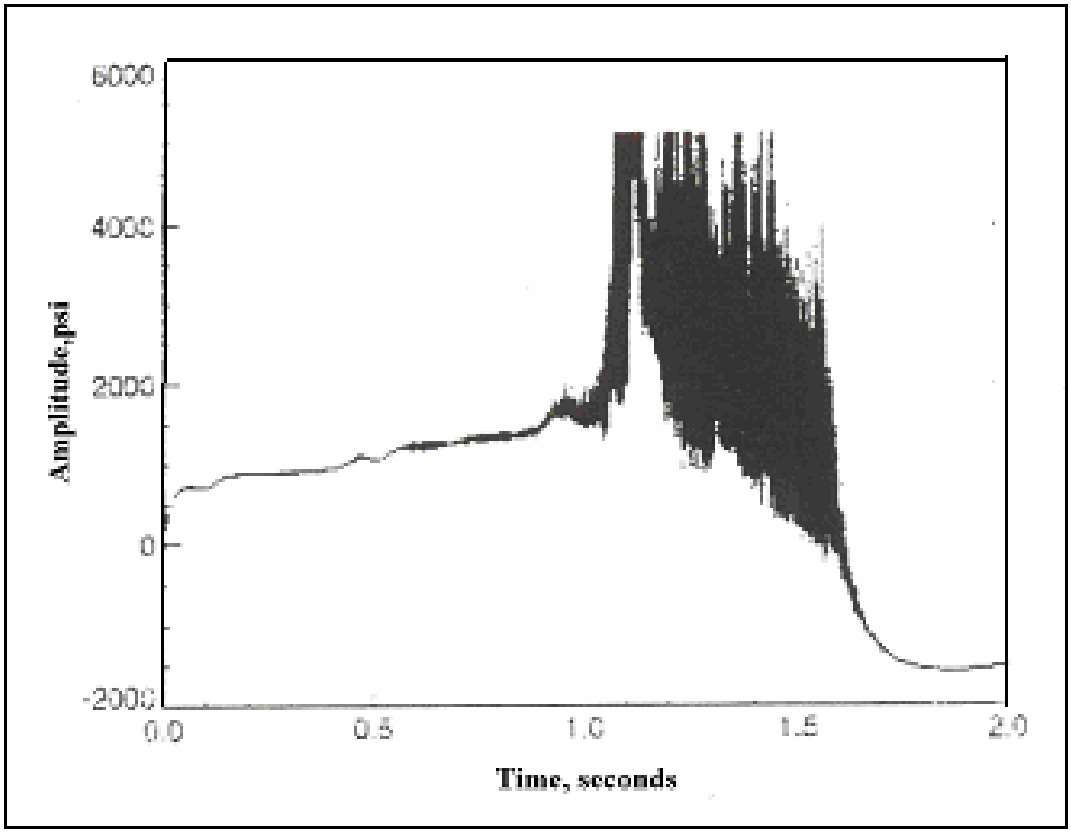

Figure 3. Oscillatory chamber pressure measured during a rocket motor testing [2]

In this illustration, operation starts as expected and, at some time oscillations develop spontaneously and grow to large amplitude. In the example, the mean pressure is seen to rise and remain high until the oscillations decrease. The high mean pressure corresponds to an enhanced mean burning rate and is accompanied by increased thrust, reduced burning time, enhanced heat transfer, and other adverse effects associated with vibrations. The consequences may range from explosion of the motor, or other modes of outright mission failure, to reduced reliability or restriction of service limits. Whenever possible, the motor developer seeks to eliminate oscillatory behavior before a motor goes into service. When oscillatory behavior occurs, it is usually referred to as “combustion instability,” although the oscillations would be more correctly attributed to instability of the entire combustor [2].

1.3. Unsteady Combustion in Rocket Motors

1.3.1. Acoustic Instability

The rocket chamber typically has acoustic waves inside that propagate at resonant frequencies. Frequencies associated with the acoustic waves vary from a few Hertz to several thousand Hertz. Figure 4, Figure 5 and Figure 6 show the acoustic modes for a typical rocket motor [1, 3].

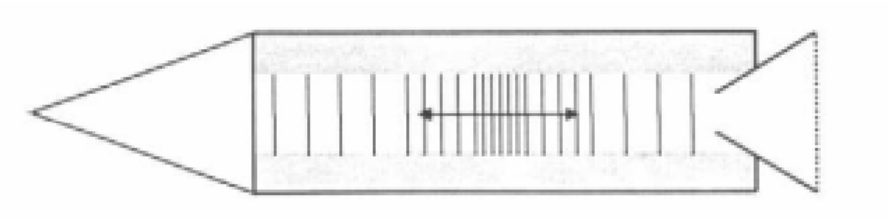

Figure 4. Longitudinal acoustic mode for a typical rocket motor [3]

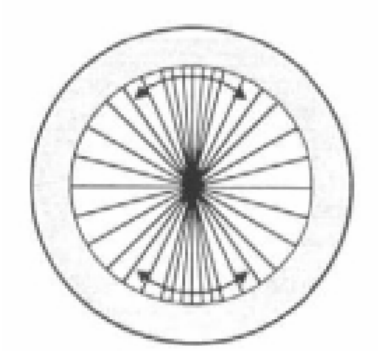

Figure 5. Tangential acoustic mode for a typical rocket motor [3]

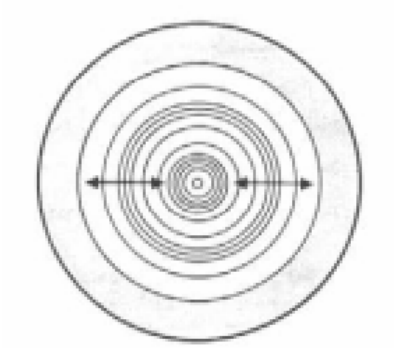

Figure 6. Radial acoustic mode for a typical rocket motor [3]

The lines within the chamber depict pressure waves. Most waves tend to dampen and die out, but if the resonant frequency of the rocket chamber coincides with the resonant frequencies of the propellant, the waves may amplify and acoustic instability may result.

Instability results in large chamber pressure oscillations at the resonant frequencies. Instability can also result in a change in the mean pressure which is extremely undesired in rocket motors. Acoustic waves are driven when fluctuations in acoustic velocity are amplified at an appropriate phase relative to the acoustic pressure. Acoustic velocity changes occur due to either mass or heat addition. Acoustic driving through heat/pressure interactions are described by the Rayleigh criterion. Rayleigh criterion is the cyclic integral of the pressure and heat fluctuations and is expressed by Equation (1.3). A positive value in this equation indicates acoustic driving. Since combustion heat release is often pressure dependent and normally occurs at a higher rate with an increase in pressure, acoustic driving by combustion is a strong possibility.

$$\int Q'P'dt > 0 \tag{1.3}$$

Both means of acoustic driving may be present in a solid rocket motor. The burning rate may vary over the burn period. There is also tremendous heat release during combustion, and if a small amount of this heat varies in-phase with the pressure, acoustic driving may occur by means of the Rayleigh criterion.

The admittance function, A_b, describes the propellant burning surface and its interaction with acoustic waves [4, 5]. The admittance given by Equation (1.4) is a complex number relating the fluctuations in velocity and pressure.

$$A_b = \frac{\left(u'/\bar{a}\right)}{\left(P'/\gamma \cdot \bar{P}\right)} \tag{1.4}$$

where u′ is the fluctuation in burned gas velocity, a is the speed of sound, γ is the ratio of specific heats. A positive $Re(A_b)$ suggests that the acoustic waves will be amplified.

1.3.1.1. Acoustic Damping

Due to viscous damping, two-phase flow effects, and flow turning in the rocket motor, acoustic damping occurs and tends to dampen the unstable effects. Stability in rocket motors is divided into two domains:

a) Linearly stable motors

b) Linearly unstable motors

Small perturbations will decay and eventually damp out in linearly stable motors, while they will grow in linearly unstable motors. However, a large oscillation can occur in a linearly stable motor if the initial amplitude is large

enough (greater than a threshold limit). The oscillations can grow to a limit cycle that is determined by non-linear effects.

1.3.2. Non Acoustic (L) Instability*

Bulk mode instability [6] occurs at conditions where the combustion chamber volume to nozzle throat area ratio (a characteristic length, known as L*) is small. The rocket chamber acts as a Helmholtz resonator and the pressure of the entire chamber rises and falls uniformly. Bulk mode instability is observed mainly during the early stages of burning and is observed only for a narrow band of frequencies. It is believed that bulk mode instability occurs when the burn rate leads the pressure in phase [3]. This is because the chamber acts like a one-way Helmholtz resonator since the throat is choked and does not allow pressure fluctuations to propagate upstream. Therefore, the pressure rise can only be accomplished by increases in mass flow. Hence, the bulk mode instability requires the burn rate fluctuations to lead the pressure fluctuations.

1.4. Response Functions

The rocket designer is well aware that the burning rate of the propellant depends on the pressure and the state of the flow near the burning surface. The "burning rate law", which is described by Equation (1.5), shows the dependence of the rate on pressure (P) and velocity (u) in combustor flow.

$$r_b = CP^n\left(1 + k\frac{u}{a}\right) \tag{1.5}$$

The response functions help isolating the coupling between the various ambient conditions (pressure, velocity) and the combustion characteristics (burning rate) described in previous sections. The use of such sub-models helps isolating the interactions between a given variable and the propellant burning rate. The

propellant response functions listed below describe the effects of pressure, velocity and heat flux on the burning rate. This interaction of propellant combustion with the ambient can be quantified in terms of these response functions, which allow comparisons of different propellants.

1.4.1. Pressure-Coupled Response

Acoustic and non-acoustic oscillatory combustion are thoroughly tied to the dynamic burn rate of the propellant. Propellant burning rate determines the rate of mass injection into the rocket chamber and hence directly affects the mean and fluctuating chamber pressures. The chamber pressure also has a strong effect on the burning rate. This influence of pressure on the burning rate is not instantaneous. This is due to thermal inertia. This dynamic influence of pressure on the burning rate is mathematically expressed as the pressure-coupled response, R_p, and is described by Equation (1.6). The pressure-coupled response is a complex function with an amplitude and phase component and is frequency dependent.

$$R_{PC} = \frac{\left(r_b' \middle/ \overline{r_b} \right)}{\left(P' \middle/ \overline{P} \right)} \tag{1.6}$$

where r_b' is the fluctuation in the burn rate, $\overline{r_b}$ is the mean burn rate. P' is the fluctuation in pressure, and $\overline{P}$ is the mean pressure.

The admittance can also be considered as a response function and is related to the pressure-coupled response function through Equation (1.6) [4, 5]

$$A_b = \gamma \cdot \overline{M} \left(R_{PC} - \frac{\left(\rho' \middle/ \overline{\rho} \right)}{\left(P' \middle/ \overline{P} \right)} \right) = \gamma \cdot \overline{M} \left(\frac{\left(\dot{m}' \middle/ \overline{\dot{m}} \right)}{\left(P' \middle/ \overline{P} \right)} - \frac{\left(\rho' \middle/ \overline{\rho} \right)}{\left(P' \middle/ \overline{P} \right)} \right) \tag{1.7}$$

If the pressure waves are assumed to be isentropic, then P can be taken to be equal to ργ and Equation (1.7) can be expressed as given in Equation (1.8) [4].

$$A_b = \bar{M}\left(\gamma R_{PC} - 1\right) \tag{1.8}$$

The ideal gas law can be used to express admittance in terms of fluctuations in pressure, temperature, and molecular weight fluctuations, as given in Equation (1.9).

$$A_b = \gamma \bar{M}\left(R_{PC} - 1 + \frac{\left(T'/\bar{T}\right)}{\left(P'/\bar{P}\right)} - \frac{\left(W'/\bar{W}\right)}{\left(P'/\bar{P}\right)} \right) \tag{1.9}$$

1.4.2. Velocity-Coupled Response

The velocity-coupled response compares the oscillation in burning rate to the crossflow velocity and its definition is given by Equation (1.10).

$$R_{VC} = \frac{\left(r_b'/\bar{r}_b\right)}{\left(u'/\bar{u}\right)} = \frac{\left(m'/\bar{m}\right)}{\left(u'/\bar{u}\right)} \tag{1.10}$$

where u' is the fluctuating velocity component and $\bar{u}$ is the mean velocity.

The hot gases that flow along the surface of a propellant in a rocket chamber accelerate towards the nozzle. This flow affects the boundary layer and enhances heat transfer from the gas phase to the propellant surface and hence increases the burn rate. This phenomenon is called erosive burning. There is also a fluctuating velocity component that occurs due to the longitudinal or tangential acoustic modes. These fluctuations may also lead to enhanced burning rates. The erosive burning

can link itself to the acoustics in the chamber and result in acoustic growth. This is known as velocity coupling [7].

1.4.3. Heat Flux Coupled Response

The pressure-coupled response is an important parameter in the analysis of combustion instability, but due to limitations and uncertainties in the measurements, heat flux coupled response measurements have become common in recent work. The heat feedback from the oscillating pressure during the pressure-coupled measurements is simulated through an oscillating external heat flux in the heat flux coupled response measurements. The heat flux coupled response is mathematically expressed by Equation (1.11). The response has an amplitude and phase. It is frequency, mean heat flux and pressure dependent.

$$R_{QC} = \frac{\left(r_b' \middle/ \overline{r}_b \right)}{\left(q_{rad}' \middle/ \overline{q}_{rad} \right)} \tag{1.11}$$

1.5. Test Methods for Combustion Stability Properties of Solid Propellant

In the development of any solid-propellant rocket motor, the dynamic combustion stability of the motor design has to be determined. If the motor is stable, any random pressure perturbations that occur will dampen out. On the other hand, if the motor is dynamically unstable, pressure perturbations can grow in amplitude, with potentially disastrous consequences, so that they may exceed the guidance and control limits of the vehicle and may result in the destruction of the rocket motor.

A small pressure disturbance varying sinusoidally in time inside a rocket chamber can be described as the real part of;

$$P = \hat{P} e^{iwt} e^{\alpha t} \tag{1.12}$$

If $\alpha > 0$, the amplitude of the oscillations increases with time and is therefore unstable. If $\alpha < 0$, the amplitude decreases with time, and the oscillations are stable.

The exponential coefficient has been shown to have the general form

$$\alpha = R_{PC}^{(r)} I_{PC} + R_{VC}^{(i)} I_{VC} + \alpha_{FT} + \alpha_{PD} + R_N^{(r)} I_N + \alpha_{ST} \tag{1.13}$$

where, by definition, the response functions relate fluctuations in the linear mass flux rate at the propellant burning surface to fluctuations in pressure (pressure coupling), Equation (1.14) and velocity (velocity coupling),Equation (1.15).

$$R_{PC} = \frac{m_b' / \overline{m}_b}{P' / \overline{P}} \tag{1.14}$$

$$R_{VC} = \frac{m_b' / \overline{m}_b}{u' / \overline{a}} \tag{1.15}$$

The acoustic velocity is 90^0 out of phase with pressure, and so, for velocity coupling, it is the imaginary part of the response function that couples the flow of energy from combustion processes to the acoustic field.

Evaluation of the integrals in the stability prediction requires the distribution of the acoustic pressure and the velocities over the propellant burning surface and throughout the motor chamber. This prediction also requires acoustic frequency, steady-state velocity distribution in the chamber, response functions for the combustion and nozzle, and particle size distribution of condensed phase combustion products. Analytical methods have been developed for estimating the mean flow and acoustic behavior in the rocket chamber, but satisfactory methods

have not yet been developed for predicting either the response of the propellant combustion to pressure and velocity oscillations or particle size distributions. Hence, a series of laboratory test methods have been explored for obtaining the necessary data.

Most of the dynamic response test devices that have been developed are used to determine the acoustic admittance of the propellant burning surface. It is defined as the proportionality relationship between the velocity of the gases leaving the propellant combustion zone and fluctuations in pressure, Equation (1.4) and velocity, Equation (1.16).

$$A_{VC} = \frac{v'/\bar{a}}{u'/\bar{a}} \tag{1.16}$$

The response function and acoustic admittance are related by a mass balance at the propellant burning surface,

$$A_b + \bar{M}_b = \gamma \bar{M}_b R_b \tag{1.17}$$

where $\bar{M}_b$ is the mean Mach number of the gases leaving the burning surface.

Experimental methods for measuring the combustion stability properties of solid propellants (i.e., the propellant acoustic admittance or response function) are categorized by the nature of the exciting disturbance, acoustic velocity oscillations or acoustic pressure oscillations.

1.5.1. Pressure-Coupled Response Measurements

Pressure-coupled admittance measurements are made by using the T-Burner, rotating valve, impedance tube, microwave burner, and magnetic flowmeter. At

higher frequencies (above 3-5 kHz), the slot-vent T-Burner, which is an alternative design for the T-Burner, the magnetic flowmeter, and a modulated throat-acoustic damping burner are used. The following sections present an overview of these methods and their current state of development.

1.5.1.1. T-Burner

The T-Burner was the first of these methods to be evaluated. The very first version of a T-Burner was built 40 years ago, [8]. From that time on, T-Burner has been the most widely used test method. Its simplest form is shown in Figure 7. Propellant disks are mounted at each end of the metal tube, which is typically between 1/3 m to several meters in length and 3 to several centimeters in diameter. The propellant combustion products exhaust through a vent, the leg of the "T". In this configuration which is selected to maximize excitation of the fundamental longitudinal mode, the maximum acoustic pressure is located at the propellant surface.

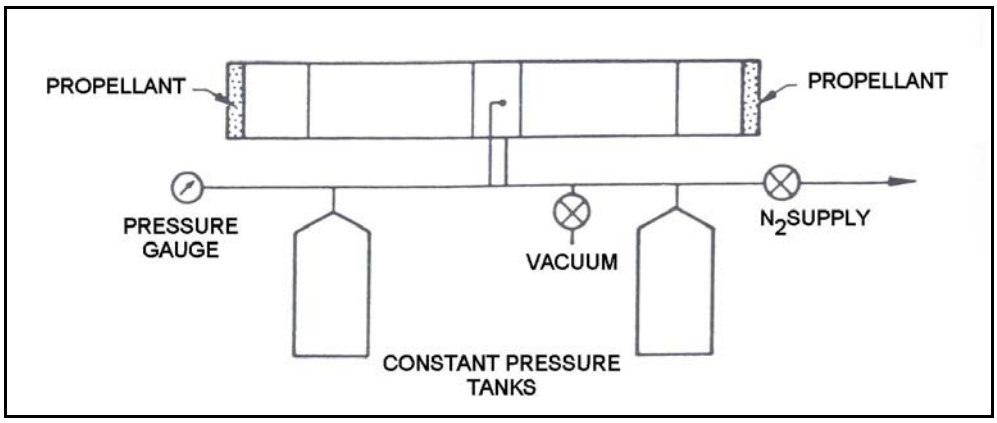

Figure 7. Basic T-Burner [8]

The T-Burner method is the one of the most extensively used method to perform pressure-coupled admittance measurements. It requires relatively simple auxiliary instrumentation for conventional use. Determining the combustion

admittance involves a stability calculation for the burner. The T-Burner is often used in studies of determining the effect of systematic changes in propellant formulation [9, 10, 11]. In such studies, the sources of uncertainty in measured response are often unaffected by the propellant variables, so that comparative results are much more significant than absolute results. The tests can be a good basis for ranking stability of propellants.

1.5.1.2. Rotating Valve

The rotating valve is an alternative laboratory method for measuring the pressure coupled admittance [12, 13]. A schematic drawing of a rotating valve is given in Figure 8. In this method, pressure oscillations are generated by adding a small oscillating component to the nozzle area in a small laboratory motor. The modulations are generated in the low frequency bulk mode, which is much less than the lowest acoustic mode of the burner, so that spatial variations of the acoustic pressure are negligible. The amplitude and phase angle of the pressure oscillations relative to the area oscillations are measured, and the response function is then derived using these parameters in a transient ballistics analysis of the motor.

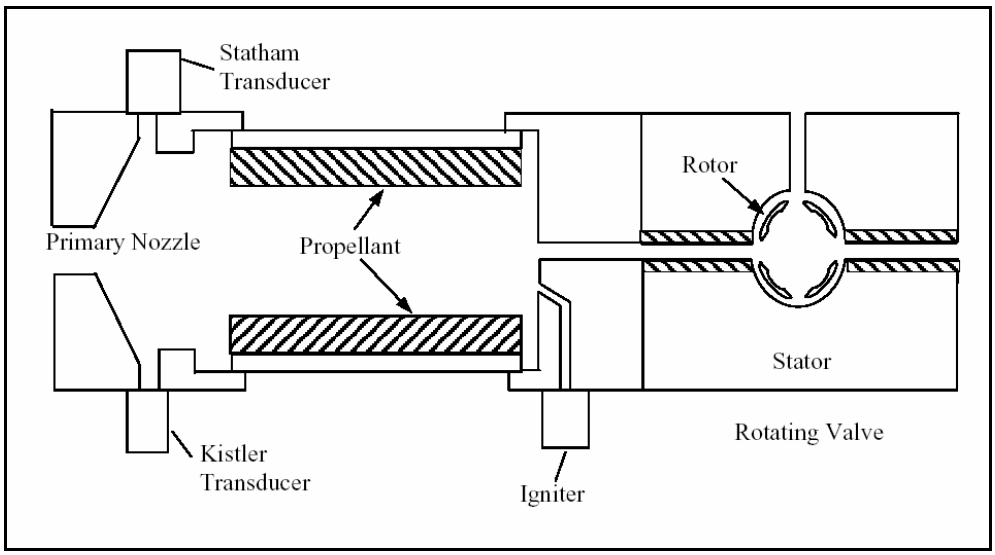

Figure 8. Rotating valve apparatus [13]

1.5.1.3. Impedance Tube

Another approach that has been explored to measure the pressure coupled admittance is the impedance tube (Figure 9). In this method, propellant is placed at one end of a tube, and pressure oscillations are generated by an acoustic driver well downstream of the burning propellant. The amplitude and phase distributions of the acoustic mode are measured using acoustic pressure transducers along the length of the tube. These distributions are then used to determine the propellant admittance, with the aid of a sophisticated computer program specifically developed for this purpose [14, 15].

1.5.1.4. Microwave Burner

Previously described techniques require an analysis of the unsteady gas dynamics during combustion in order to relate the propellant response function to the measured pressure. Consequently, the deduced propellant response is only as accurate as the assumed model of the physical processes occurring within the combustion chamber.

In the microwave burner (Figure 10), a microwave signal propagates through a propellant strand bonded in a circular tube and is reflected from the propellant burning surface (Figure 11). The Doppler phase shift of the reflected signal is continuously measured and, the transient regression rate of the burning propellant surface is obtained from this shift. The propellant filled waveguide is connected to a small burner chamber that is pressurized in an oscillatory manner with nitrogen via a rotary valve. The measured mean and oscillatory components of the propellant regression rate and chamber pressure and the phase relationship between the two oscillatory components yield the real and imaginary components of the pressure coupled response function.

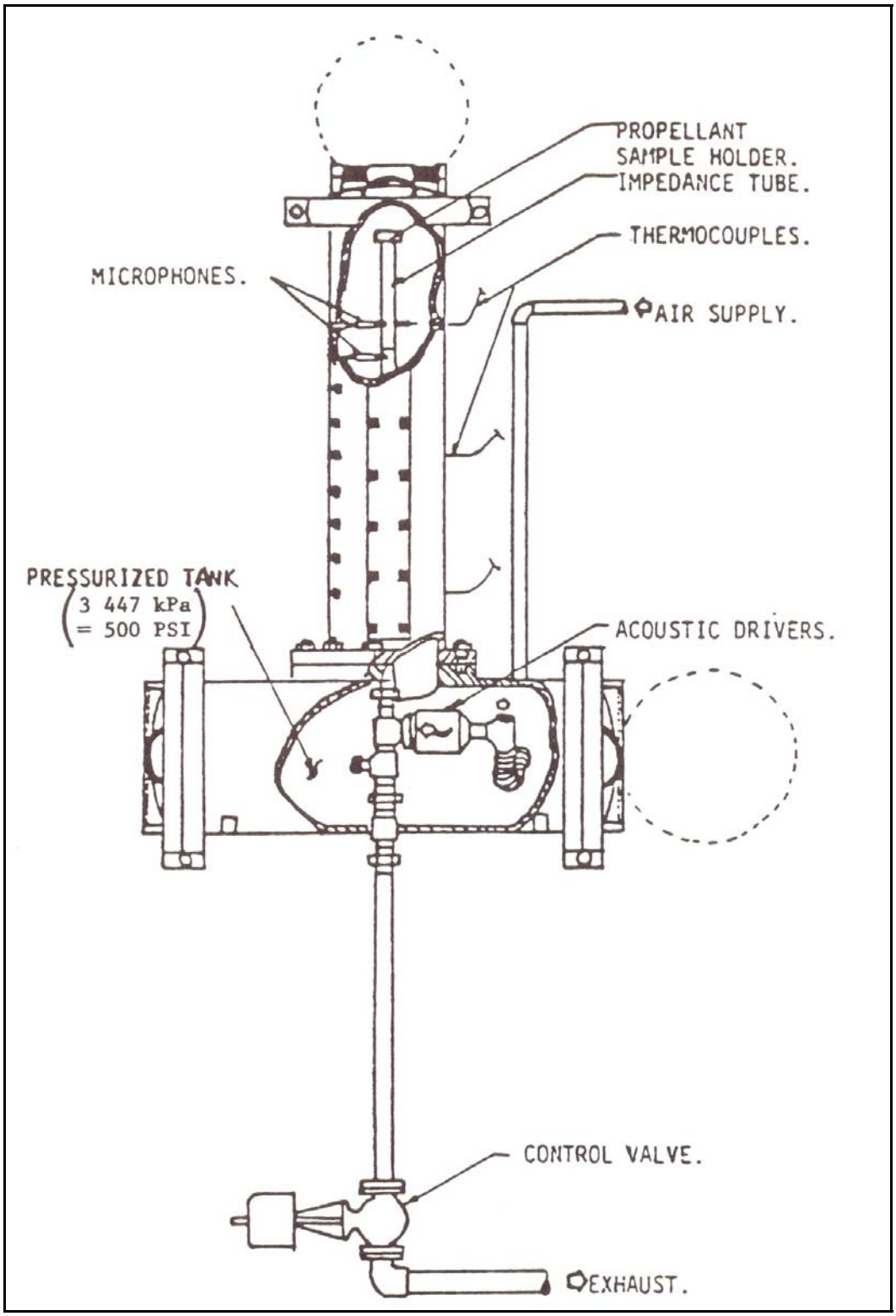

Figure 9. Pressurized impedance tube facility [16]

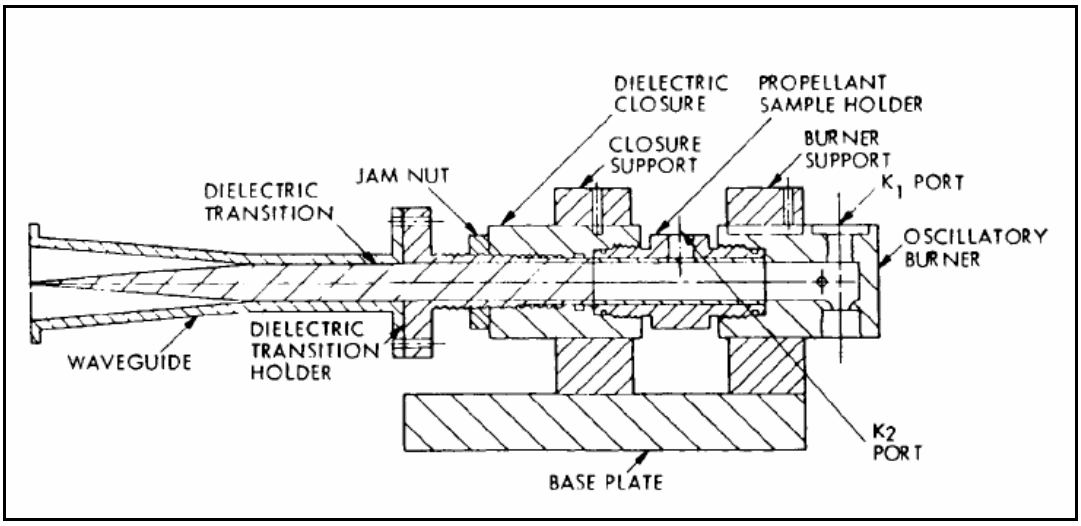

Figure 10. Microwave burner [17]

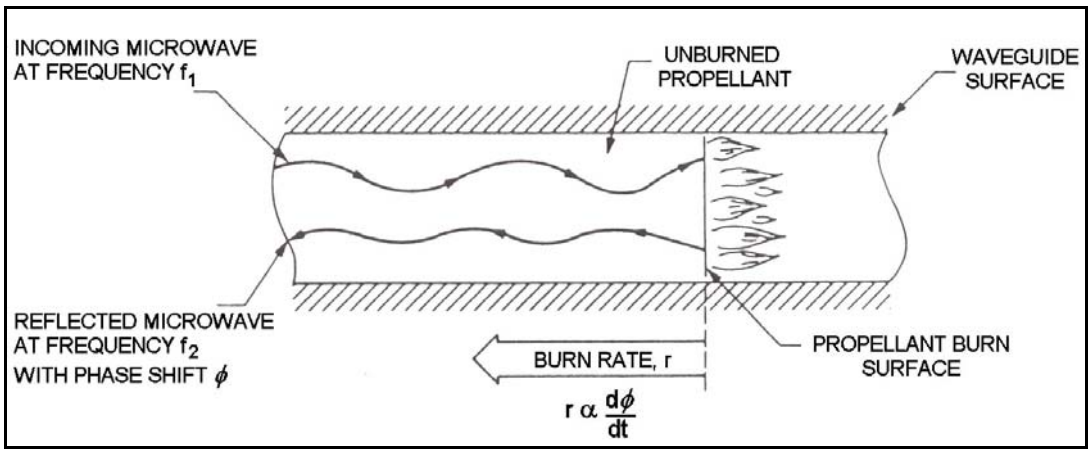

Figure 11. Microwave regression rate measurement technique [17]

1.5.1.5. Magnetic Flowmeter

A second developmental technique for directly measuring the propellant admittance function uses a magnetic flowmeter (Figure 12) to measure the oscillatory velocity of the gases emanating from a burning propellant surface contained within an externally excited combustion chamber. This method is

theoretically capable of having measurements within a high frequency range which is observed in tangential mode motor instability.

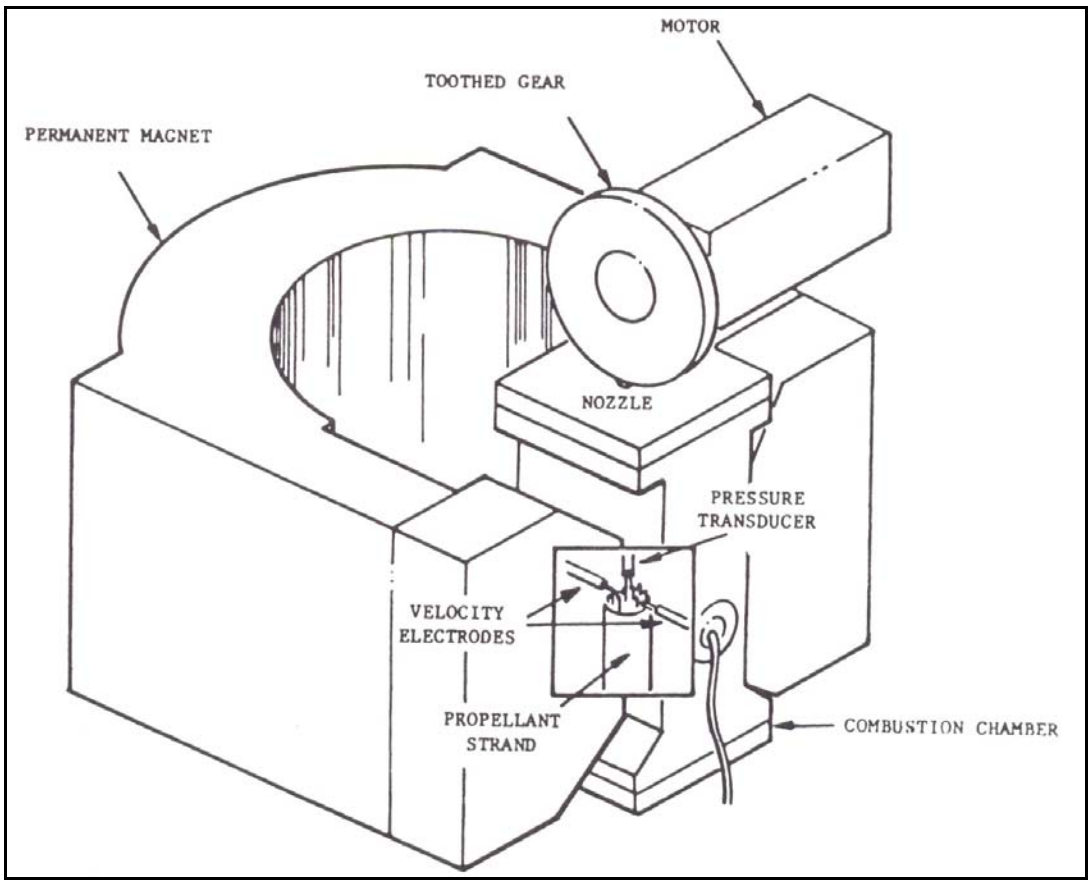

Figure 12. Magnetic flowmeter burner [18]

The magnetic flowmeter utilizes Faraday's law to generate an electrical potential proportional to the flow velocity by moving a conductor relative to a magnetic field. A highly ionized flow can allow magnetohydrodynamic forces to distort the velocity profile.

The combustion chamber is located within the field of a large permanent magnet. Two electrodes within the burner detect the electrical potential produced as the propellant burns between the two probes. The pressure within the burner is modulated by the sonic exhaust through the nozzle with a wheel driven by a

variable-speed motor. The signals from the flowmeter electrodes and pressure transducer are analyzed by a vector voltmeter lock-in amplifier referenced to the pressure signal. The magnitudes of the velocity oscillations in and out of phase with the pressure oscillation yield the real and imaginary parts of the propellant admittance function as a function of height above the propellant surface.

1.5.2. Velocity-Coupled Response Measurements

Dynamic combustion studies have shown that velocity oscillations parallel to the burning surface can also couple with the burning propellant to produce significant acoustic energy gains or losses. Early studies suggested that the acoustic velocity might couple with combustion but did not quantitatively define the processes involved [19]. Velocity-coupled admittance measurements have been attempted using a T-Burner, a dual rotating valve, a velocity-coupled impedance tube, and a magnetic flowmeter. The following sections present an overview of these methods and their current state of development.

1.5.2.1. T-Burner

Several investigations [20, 21, 22] have considered methods for adapting the T-Burner for velocity-coupling measurements (Figure 13). Acoustic analyses suggested that the maximum velocity coupling in T-Burner occurs along $L/4^{th}$ and $3L/4^{th}$ of the length of the burner tubes. Thus, positioning propellant samples at these locations should produce the maximum velocity-coupled responses. The lengths of the propellant samples at the L/4 and 3L/4 positions are varied, and the effect of the propellant surface on the exponential growth or decay rate of oscillations is observed.

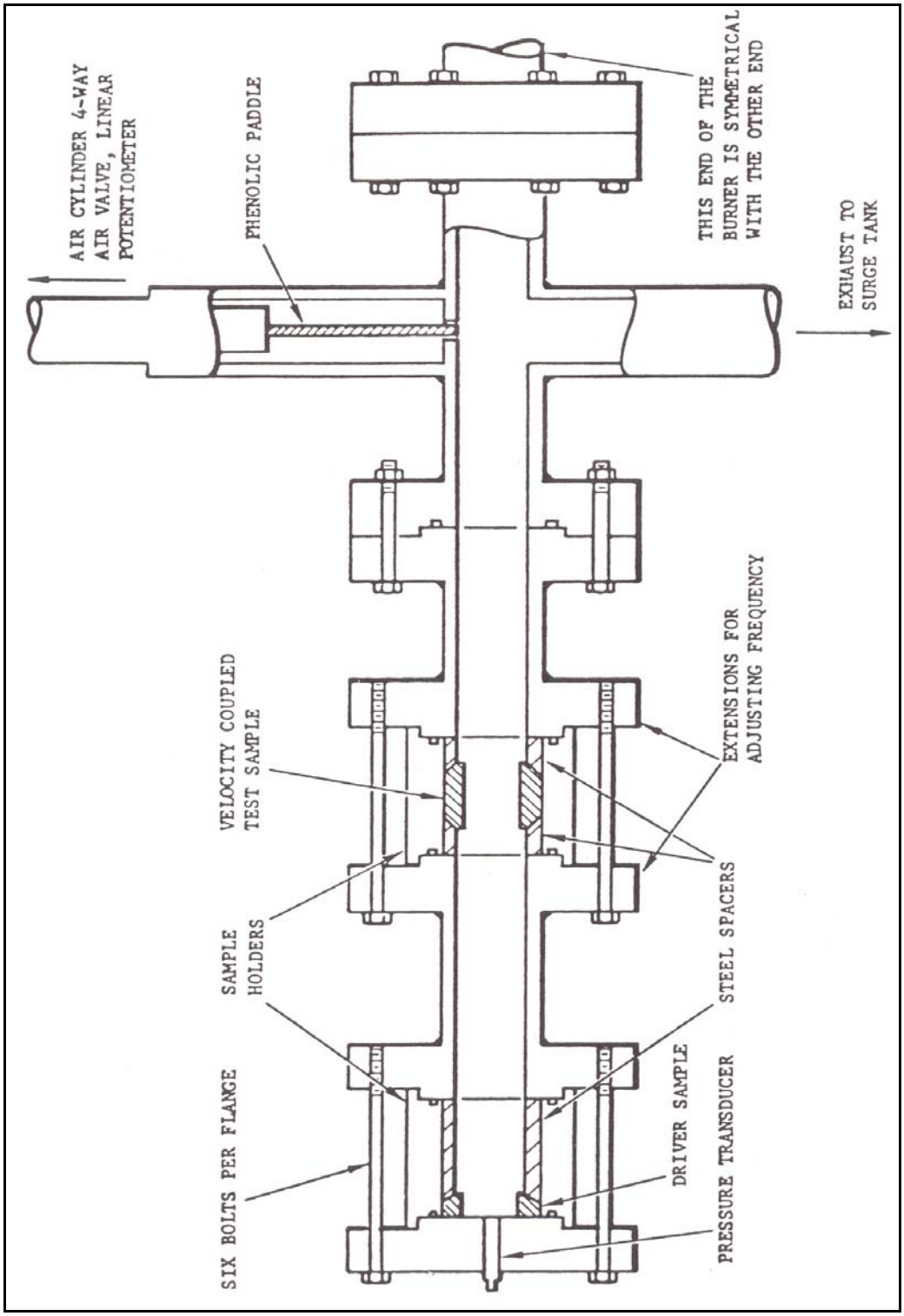

Figure 13. Velocity Coupled T-Burner [20]

Beckstead and Butcher [21] and Micheli [22] have proposed methods of deriving velocity-coupled response functions from test data. These methods are more complicated than the pressure-coupled case because the test samples respond to both pressure and velocity oscillations. Analyses show that these pressure-coupled effects, and possibly other contributions, are significant and must be considered in the data interpretations. Furthermore, additional experimental difficulties were found that are not faced in the pressure-coupled T-Burner. These difficulties result from the generation of harmonic frequencies during the tests.

1.5.2.2. Dual Rotating Valve Apparatus

Consideration has been given to adapt the driver burner approach to measure velocity-coupled response functions [23, 24]. The basic approach (Figure 14) is to attach two valves or drivers to the combustion chamber, one at each end. By operating these two valves 180 deg out of phase, velocity oscillations of controlled amplitude and frequency can be generated.

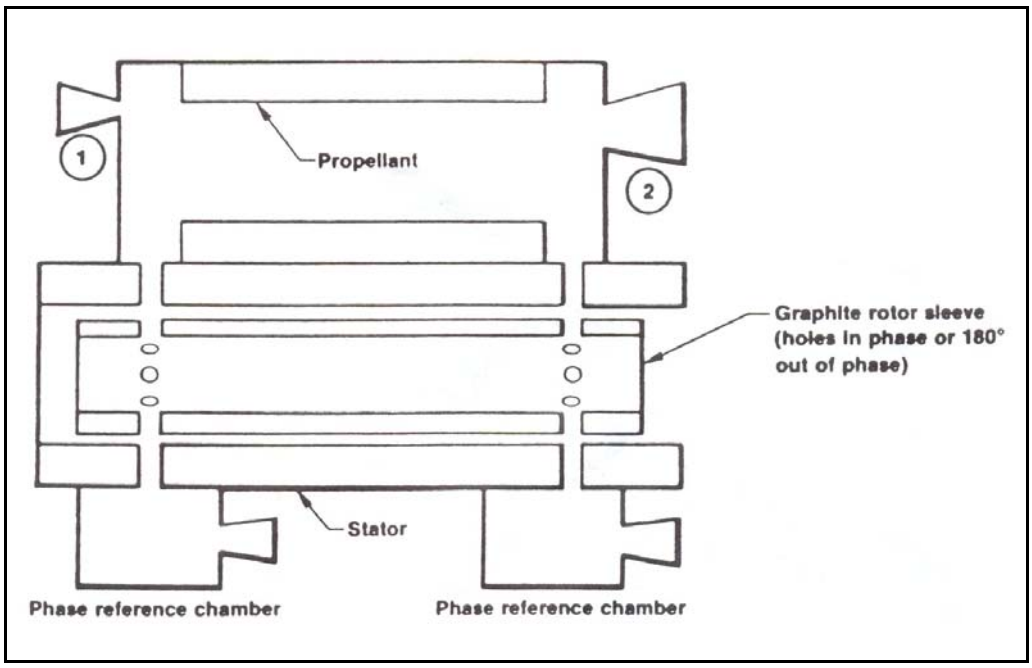

Figure 14. Dual rotating valve apparatus [24]

Early experiments by Eisel and Dehority [25] demonstrated the basic concepts. Radiation measurements were made to explore the qualitative characteristics of the velocity response. More recently, an attempt was made to quantitatively measure the velocity response function [23, 24]. Although some progress was made, further studies are needed to improve the reproducibility of the data. Furthermore, this method, like T-Burner, is an indirect approach and requires a dynamic ballistics model to interpret the data. In view of the large uncertainty in the basic modeling of the velocity-coupling process, further development of this test method must await a better understanding of the basic velocity-coupling mechanisms.

1.5.2.3. Impedance Tube

More recently, the impedance tube has also been modified to determine the velocity-coupled response functions of solid propellants [26, 27]. One propellant sample is placed at one end of the tube, and additional propellant samples are placed along the sidewalls of the tube at some distance downstream of the end sample (Figure 15). A stepper motor advances these latter samples so that they remain flush with the tube walls during the test. As in the pressure-coupled experiment, an acoustic driver is used to excite a standing acoustic oscillation in the tube. The data reduction procedure is based on the assumption that the end propellant sample responds only to pressure oscillations, whereas the sidewall propellant samples respond to both pressure and velocity oscillations. The standing wave phase angles, measured at several axial locations along the length of the tube, are used to determine the velocity-coupled response function of the sidewall samples using a developed data reduction computer program [26,27].

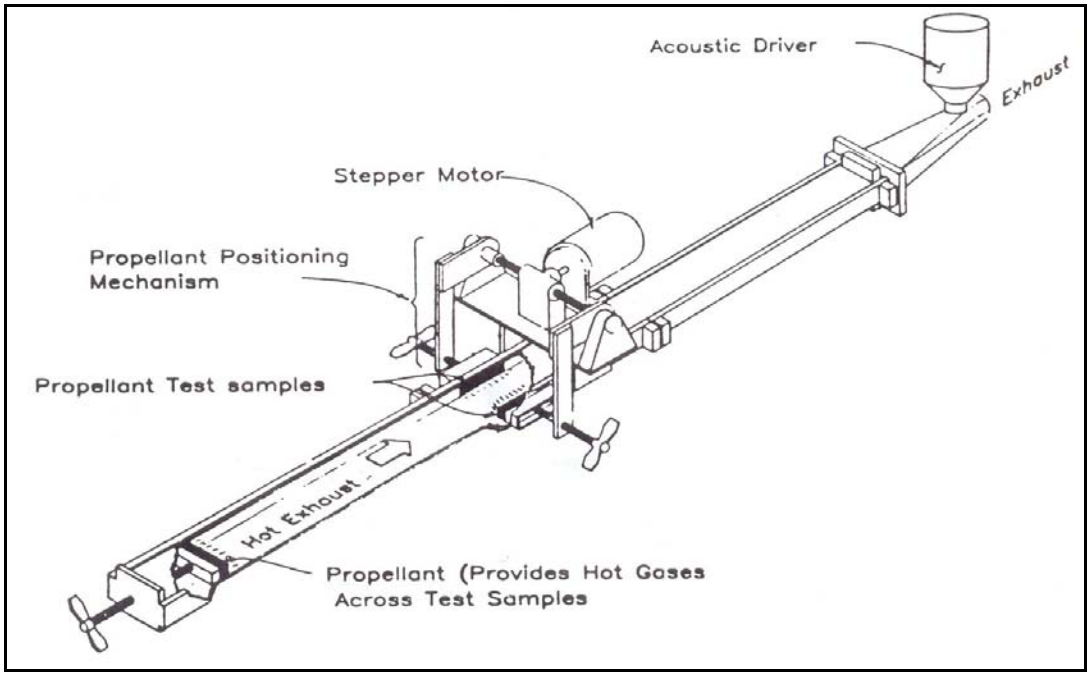

Figure 15. Velocity-coupled impedance tube [26]

Whereas the test results indicated that the propellant burn rate did respond to velocity oscillations parallel to the propellant surface and the data clearly showed that the same propellant samples possess different velocity-coupled response functions when positioned at different locations along a standing acoustic wave. Consequently, it was concluded that the velocity-coupled response function cannot in general, be regarded as a propellant property and, again, the nature of this response is currently not understood.

1.5.2.4. Magnetic Flowmeter

An attempt is being made to measure velocity-coupled response directly by the magnetic flowmeter technique [28, 29], using the experimental apparatus shown schematically in Figure 16, where A is a combustion chamber; B is a permanent magnet; C is an enlarged view of propellant slab orientation and placement of two pairs of velocity measuring electrodes; and D is a nozzle modulation gear. The

combustion chamber (A) is designed to measure simultaneously and directly the cross flow oscillatory velocity and the mass flow oscillatory velocity of the solid propellant combustion at the center of the chamber, the location of the acoustic antinode, where the maximum acoustic velocity and minimum acoustic pressure oscillations are generated by the nozzle modulation gear (D).

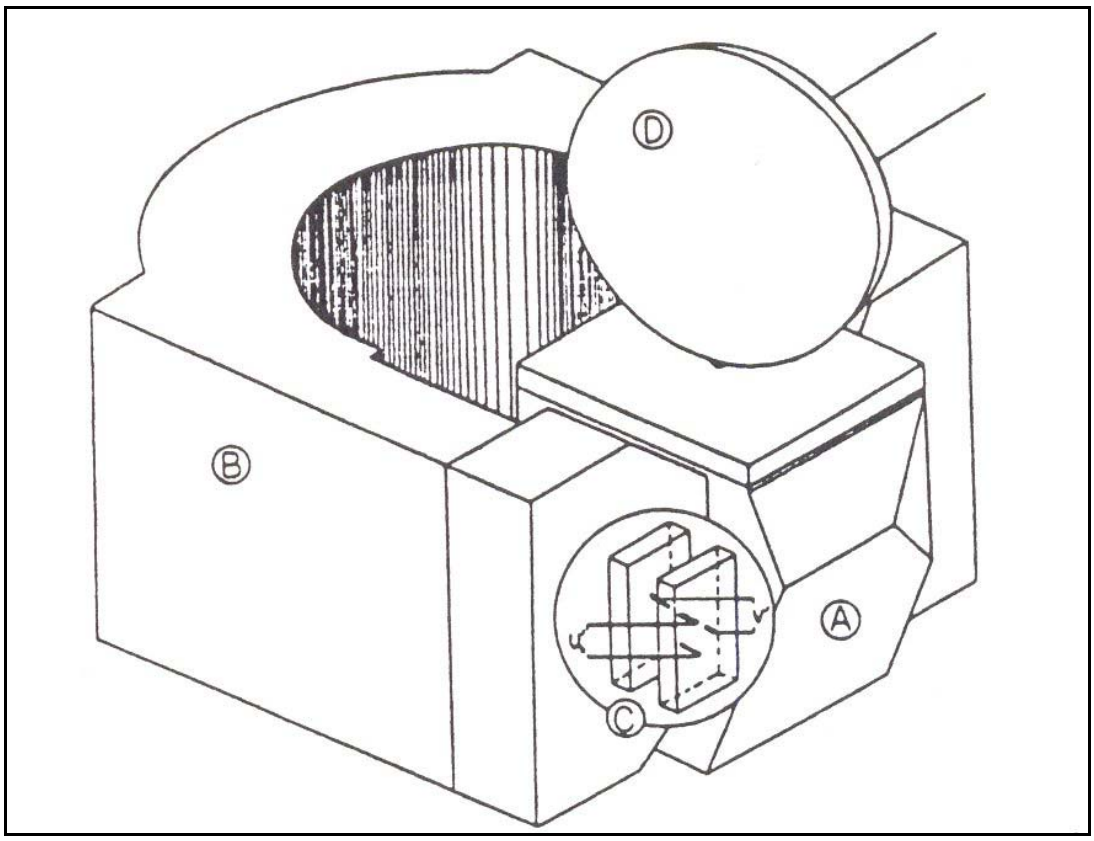

Figure 16. Velocity-coupled magnetic flowmeter [28]

1.5.3. Comparison of the Pressure-Coupled Response Measurement Methods

In this study main motivation is focused on prediction of the combustion instability in solid rocket motors using a pressure-coupled response measurement technique. The measurement of the pressure-coupled response has been attempted

by a variety of methods summarized in Section 1.4.1. A comparison of all these methods is shown in Table 1.

Among these methods, T-Burner system seems advantageous when frequency range, maximum pressure and current technology level are taken into account. As seen in this table, cost per data point for a T-Burner system is stated to be more expensive when compared to other systems. But use of relatively cheaper sub-systems can lower the initial and operational cost of the system which is an aim of this study.

Table 1. Pressure-coupled response measurement [30]

Method	**T-Burner**	**Rotating Valve**	**Impedance Tube**	**Microwave Burner**	**Magnetic Flowmeter Burner**
Frequency Range	200 Hz – 10 kHz	0 - 800 Hz	0 - 2400 Hz	0 - 1 Hz	0 - 20 kHz
Current Maximum Pressure	2000 Psi 14 Mpa	1500 Psi 10.5 Mpa	500 Psi 3.5 Mpa	1000 Psi 7 Mpa	2000 Psi 14 Mpa
Quantity Measured	Real [R_p]	Real [R_p]	Real & Imaginary [A_b]	Real & Imaginary [R_{pc}]	Real & Imaginary [A_b]
Measurement	Indirect	Indirect	Indirect	Direct	Direct
Cost Per Data Point	$450	$325	-	$200	-

1.5.4. Scope of the Study

As for sure, solid propellant rocket motors are generally used for military purposes. So compositions of the solid propellants have a top level secrecy which is procted by international laws (Military Technical Control Regime-MTCR). Also developers of the solid propellant never want to share the information with others. Therefore, in order to develop an original solid propellant, basic specifications of the propellant have to be determined. Actually, determination of the ballistic characteristics of a new developed propellant experimentally is a standart procedure. A full scale rocket motor test can be performed for the evaluation of solid propellant characteristics but it is not appropriate when economical issues are taken into account.

For the analysis of the stability characteristics of a solid-propellant rocket motor, the response functions must be known. With the current limited understanding and knowledge on the extremely complicated subject of combustion instability and limited capabilities, it is not possible to compute these quantities; they have to be evaluated experimentally. For this purpose, an overview of the test methods for combustion-stability properties of solid propellants and comparison of these methods are given in previous sections.

The chamber pressure can be modulated at a determined frequency using a suitable burner. The most extensively used method is a center vented unstable burner, commonly referred as the T-Burner. Not only because of its extensive use, but also its advantages in understanding unstable rocket motors, T-Burner method is selected. The design of a T-Burner is well suited for inducing pressure-coupled combustion response, and design modifications are possible to produce velocity-coupled response.

In this study, it is proposed to construct a T-Burner setup for the quantitative measurements of the response of a burning propellant to unsteady motions. Detailed information about the design, construction and operation are given in the following chapters. Also, the data reduction process for obtaining pressure-coupled response function will be presented.

CHAPTER 2

EXPERIMENTAL SETUP DESIGN AND CONSTRUCTION

In this thesis, a T-Burner with center-vented and end-burning or cylinder propellant charge is designed and constructed. The T-Burner remains as the only test device to yield data for the unsteady burning of solid propellants over abroad ranges of frequency and pressure. Broadly, there are two main uses of the T-Burner; as means of comparing qualitatively the behavior of different propellants, and as a test device for measuring quantitatively the response of a burning propellant to unsteady motions.

The T-Burner, designed by Price et al. [8, 31, 32, 33, 34], is diagrammed in Figure 17. It consists of a cylinder whose length can be changed from test to test, with the propellant at both ends, burning in a cigarette fashion. The nozzle is at the center of the cylinder, and the flow is directed out of the cylinder perpendicular to its axis, into a large reservoir. The heat added by combustion at the bases of the cylindrical combustor cavity is in phase with the pressure fluctuations, in conformity with the Rayleigh's criterion, and can sustain the combustion instabilities in the longitudinal acoustic mode. The frequency is determined by the length of the combustor conduit occupied by the burned gases. A pressure transducer senses the pressure fluctuations.

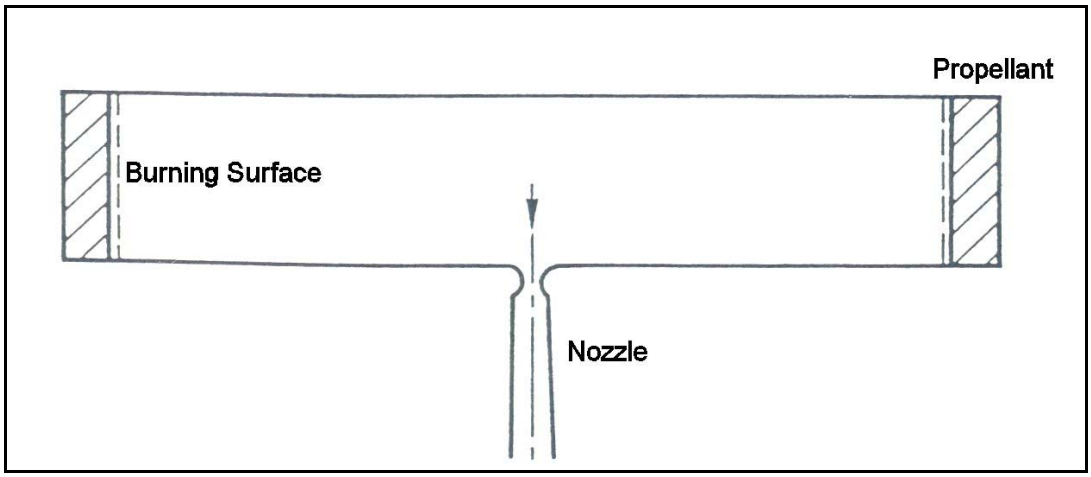

Figure 17. T-configuration rocket motor with center-vented and end-burning propellant charge

The T-Burner is just a special kind of a rocket motor. Thus, the same analyses are applicable to both T-Burner and full-scale motors. Because tests in T-Burner are relatively inexpensive, and data under widely varying conditions are quite easily obtained, the device affords a very convenient means for checking certain features of analytical results.

T-Burner tests can be employed to determine the dependence of propellant response on frequency and pressure. More specifically, the pressure and frequency where the response is maximum can be determined. Based on the data, changes can be made to an unstable motor to minimize the risk of instability.

In Figure 18, the product tree of the T-Burner setup that is designed and constructed in the scope of this study is presented. As seen in Figure 18, T-Burner setup is mainly composed of the base part, the panel and the T-Burner itself. Combustion chamber, pressure stabilization mechanism, pressurization system, measurement instruments and data acquisition systems form the T-Burner.

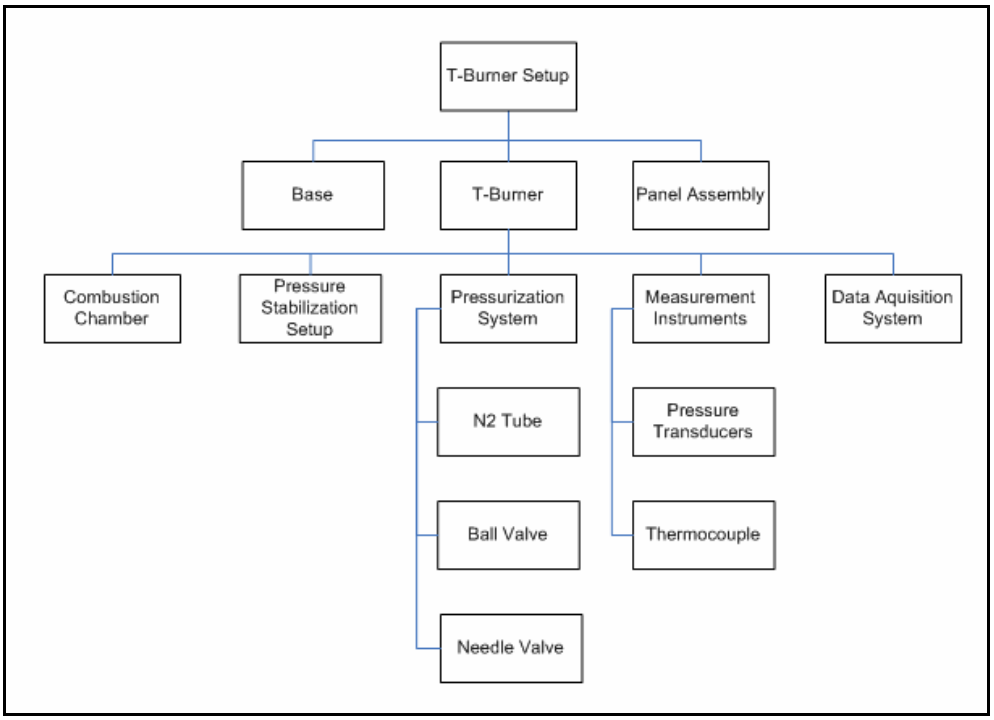

Figure 18. T-Burner setup product tree

In the following sections design considerations, performed analyses and tests and production information about almost every sub system of two of the T-Burner setups that have been built in the scope of this study, are explained in detail. Information about the base part and the control panel assembly are also stated below.

2.1. Combustion Chamber

In Figure 19 detailed product tree of the combustion chamber is presented. Figure 20 shows the solid model of the combustion chamber. In this section, each part of the product tree is investigated separately.

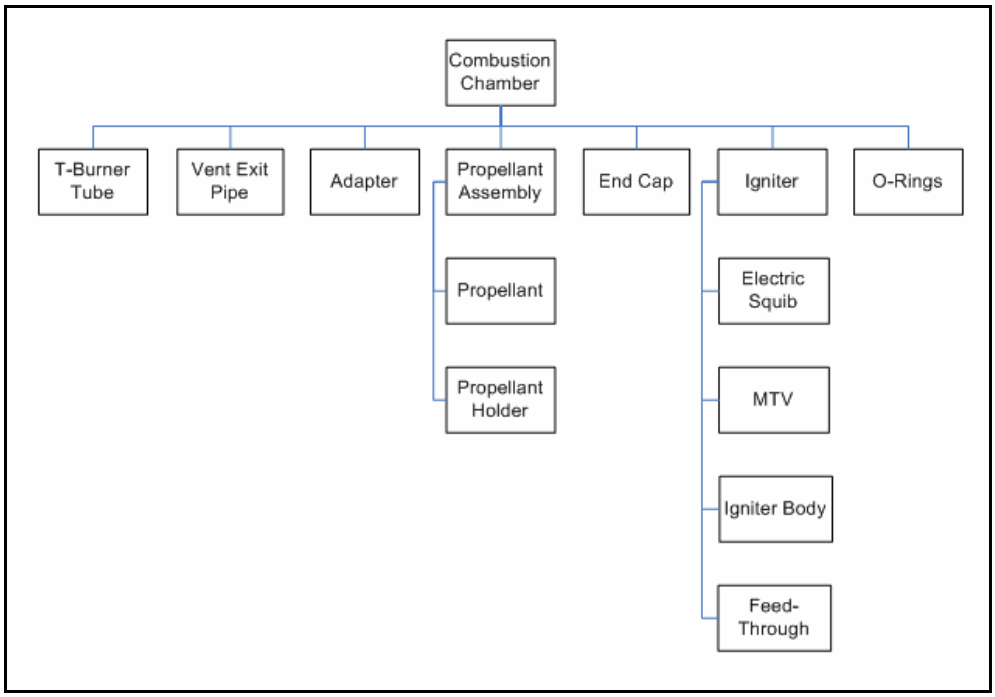

Figure 19. T-Burner combustion chamber product tree

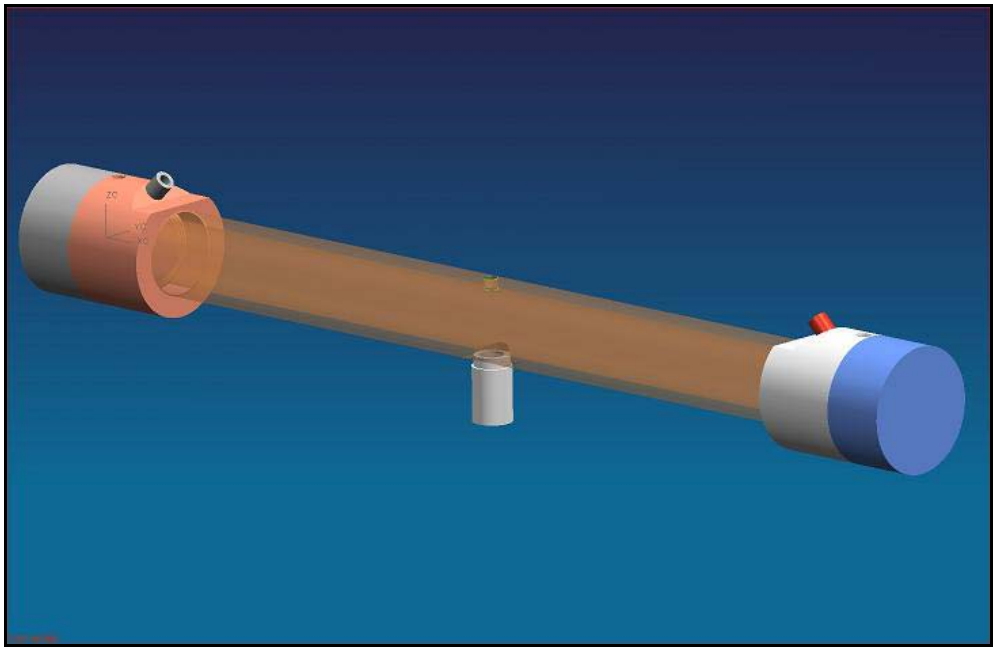

Figure 20. Combustion chamber solid model

2.1.1. T-Burner Tube

The most important element of the combustion chamber is the tube in which combustion occurs. There exist three important criteria that affect the design of the tube. First, the tube is exposed to high pressure and high temperature combustion gases which have corrosive effect. Therefore, structural strength of the tube and its material selection become important design factors. Secondly, mechanical integration of the tube with the adapter parts and the vent exit pipe has an importance, again because of the high loading inside the tube due to high pressure. As a third criterion, which is specific for T-burner setup with surge tank and cavitating venturi, a vent hole has to be designed such that no chocking is allowed as the combustion gases pass through it to the tank.

"Stainless Steel AISI-316L" is selected as the material of the tube. Combustion gases include hydrochloric acid, which has a corrosive effect. This material is known to have a corrosive resistance. [35]

The test frequency for a T-Burner having end discs is determined by the length of the T-Burner, L, and the speed of the sound of the gas particle mixture in the T-Burner, $\overline{a}$;

$$f = \frac{\overline{a}}{2L} \tag{2.1}$$

where the length of the the burner is taken 1 meter for system conformation tests.

T-Burner setup that is constructed in this study will be specificaly used for a confidental propellant. This situation fixed the inside diameter of the tube to be 63 mm.

For the structural strength analysis, T-Burner tube is taken as a simple pressurized vessel. Working pressure of the tube is determined by taking the steady-state operation regime pressure. This value is different for different propellants. A safety factor of 2 is taken and the well known stress determination formulas for a thin vessel, given in Equations (2.2, 2.3, 2.4) [36] are used.

$$\sigma_1 = \frac{\mathrm{Pr}}{t} \tag{2.2}$$

$$\sigma_2 = \frac{\mathrm{Pr}}{2t} \tag{2.3}$$

$$\tau_{\max} = \frac{\mathrm{Pr}}{4t} \tag{2.4}$$

where, σ_1 is the hoop stress, σ_2 is the longitudinal stress and $\tau_{\max}$ is the maximum shearing stress.

Threads at the both ends of the tube are selected using the formula given in Equation 2.5.

$$\sigma = \frac{F}{A} \tag{2.5}$$

Validation of the tube dimensions, the connection threads and O-rings that are used for preventing the leakage is done by a hydrostatic test, which is performed at 150 bars for 10 secs. There occured no failure of the tube and no leakage is observed.

Simple gas dynamics analysis is performed for the design of the vent hole. A control volume, as shown in Figure 21, is taken and mass is conserved inside the control volume. Working pressure of the vessel is taken to be 70 bars. Adiabatic

flame temperature for the specified propellant gas is obtained from internal ballistics simulations as approximately 3000 K. Related Equations (2.6, 2.7, 2.8, and 2.9) are given below. These calculations also determine the diameter of the vent exit pipe. Technical drawing of the vent exit pipe is given in APPENDIX A.

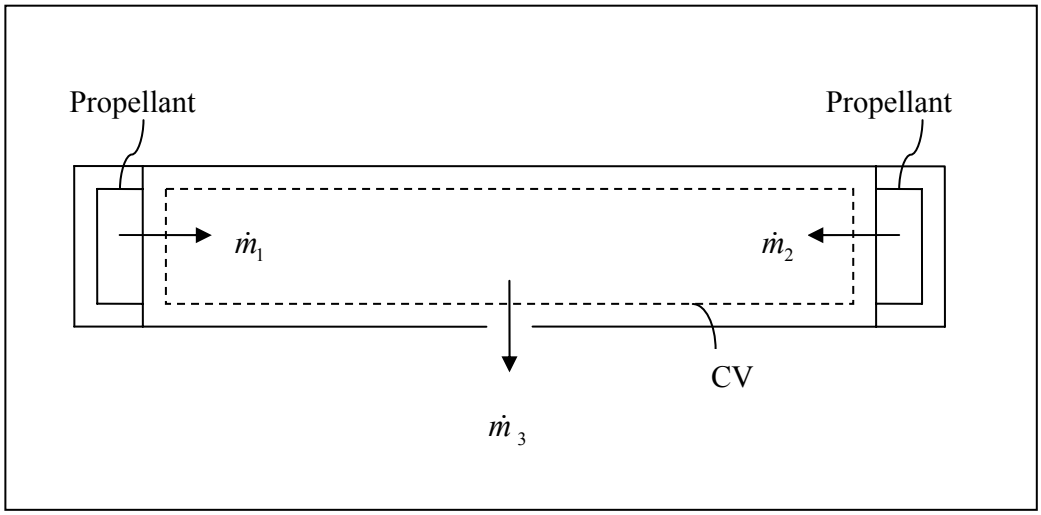

Figure 21. Sketch for T-Burner Tube

$$\frac{Dm}{dt} = 0 \tag{2.6}$$

$$PV = nRT \tag{2.7}$$

$$a = \sqrt{\gamma RT} \tag{2.8}$$

$$M = \frac{v}{a} \tag{2.9}$$

In Figure 22 the solid model of the tube is presented where the picture of the constructed tube is presented in Figure 23. Technical drawing of the tube is given in APPENDIX A. Detailed dimensions of the tube are presented in the technical drawing. Specifications of the T-Burner tube are summarized in Table 2.

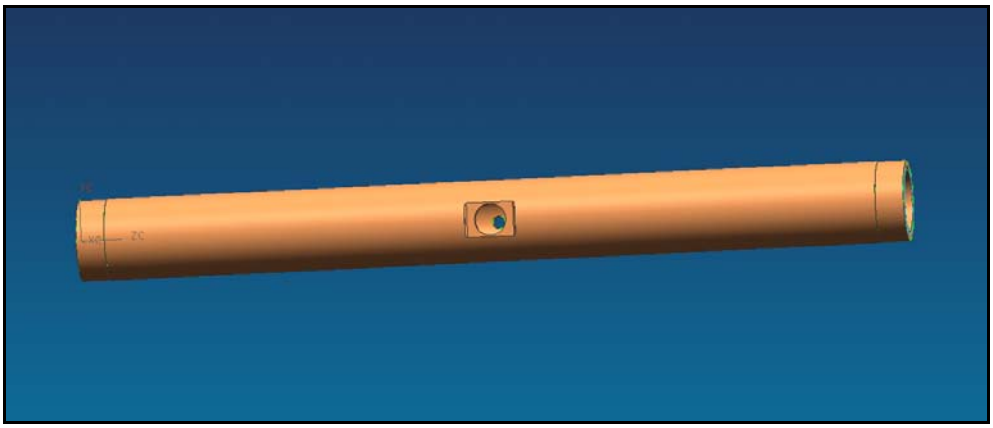

Figure 22. T-Burner tube solid model

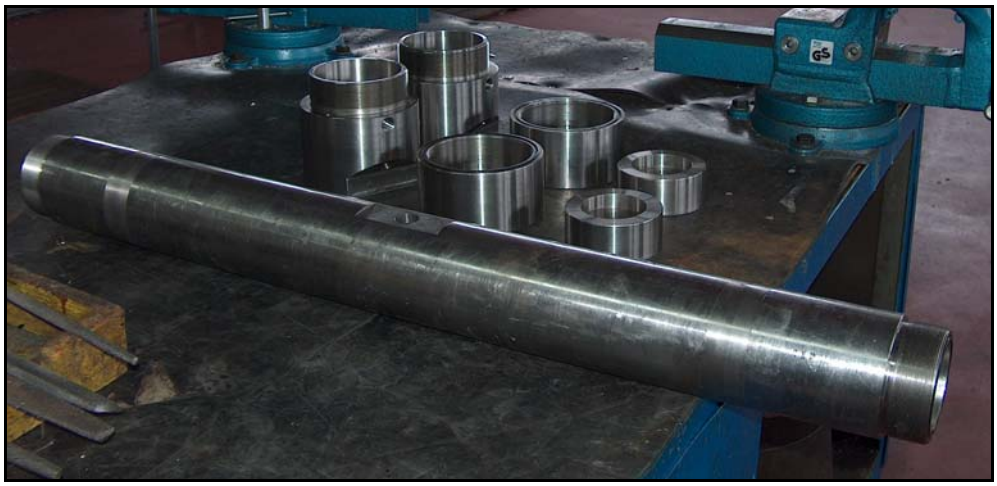

Figure 23. T-Burner tube picture

Table 2. Specifications of the T-Burner tube

Length of the T-Burner Tube	860 mm
Inner Diameter of the T-Burner Tube	63 mm
Thickness of the T-Burner Tube	10.5 mm
Vent Exit Hole Diameter	35 mm

2.1.2. Adapter

The adapter part is also an important element of the combustion chamber. It is mounted to the both ends of the T-Burner tube. There are two ports on the adapter, one of them is used for ignition of the propellant and the other one is used for taking dynamic pressure data. Using an adapter part makes the production of the T-Burner tube easy. Because, unless adapter parts are used, for each test at different frequencies, T-Burner tubes at different lengths have to be drilled for ignition and measurement purpose. Mountable adapter also provides short times between two successive tests, therefore multiple test runs are possible.

The adapter is connected to T-Burner tube and end cap with threads and O-rings are used on both connections for preventing leakage.

In Figure 24, the solid model of the adapter is presented where the picture of the constructed adapter is presented in Figure 25. Technical drawing of the adapter is given in APPENDIX A. Detailed dimensions of the adapter are presented in the technical drawing.

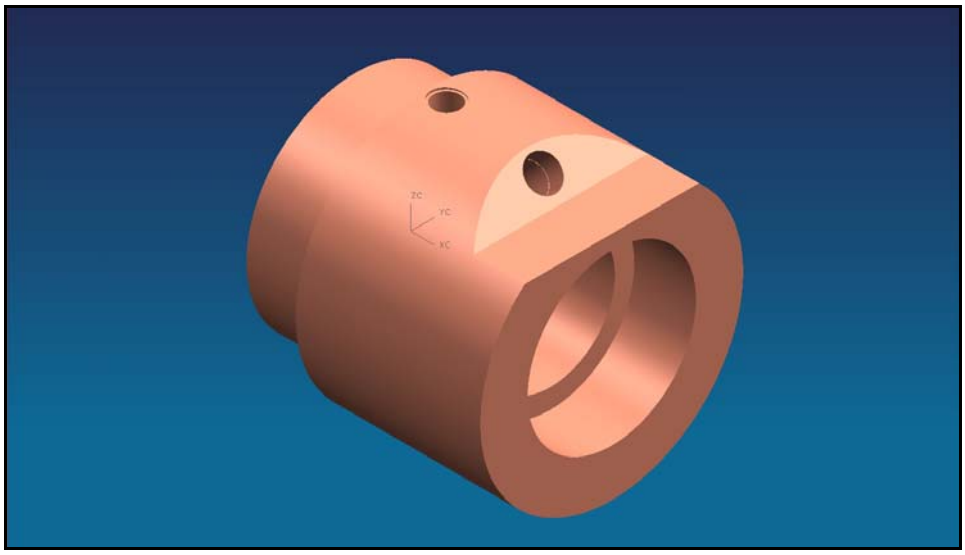

Figure 24. Solid model of the adapter

Figure 25. Adapter Picture

2.1.3. Propellant Assembly

The propellant assembly, which is shown in the product tree, Figure 19, consists of solid propellant and its holder. Propellant assemblies are placed into the adapters and end caps are connected to the adapter by thread connection.

Duration of the test is related to the propellant thickness, which is affected by the propellant burn rate. Two different propellant holders are constructed. The first one permits 1 second test period where the other one permits 1.5 seconds.

In Figure 26 the solid model of the propellant assembly is presented where the picture of the propellant holder is presented in Figure 27. Technical drawing of the propellant holder is given in APPENDIX A. Detailed dimensions of the holder are presented in the technical drawing.

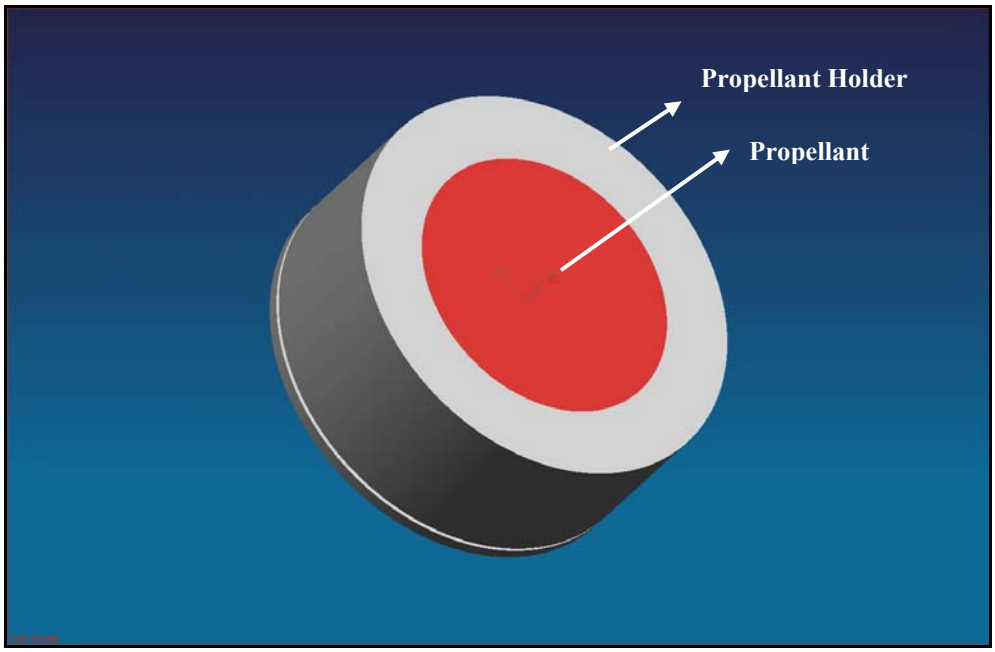

Figure 26. Solid model of the propellant assembly

Figure 27. Propellant holder picture

2.1.4. Igniter

The igniter involves the igniter body, the electric squib, MTV (Magnesium Teflon Viton) and the Feed-through. One igniter is placed at each end of the T-Burner which provides rapid and uniform ignition of propellants. The pyrotechnic igniter includes easily ignitable high-energy charge in the shape of pellets. The electric squib is used as the initiator for the ignition of the pellets. The products of a burning igniter are hot gases and particles which ignite the propellant by conductive, convective, and radiative heat transfer.

In order to have a synchronized ignition in the test setup, ignition cables are connected in parallel. For the sake of security, the control of the igniters is performed by the use of a control panel which is located outside the test room. Ignition cables, come from control panel, are connected to the electric squib that is placed into the igniter body. Feed-through that connects ignition cables is used for preventing the leakage.

“Stainless Steel AISI-316L” is selected as the material of the igniter body for multi purpose usage. This material is known to have a corrosive resistance.

In Figure 28, the solid model of the igniter body is presented where the picture of the igniter body with Feed-through is presented in Figure 29. Technical drawing of the igniter body is given in APPENDIX A. Detailed dimensions of the igniter body are presented in the technical drawing.

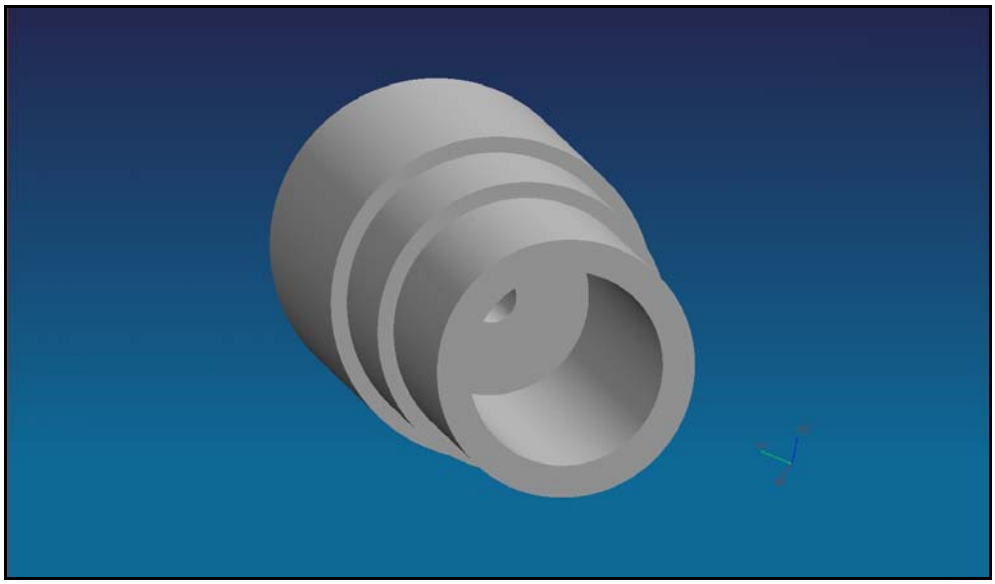

Figure 28. Solid model of the igniter body

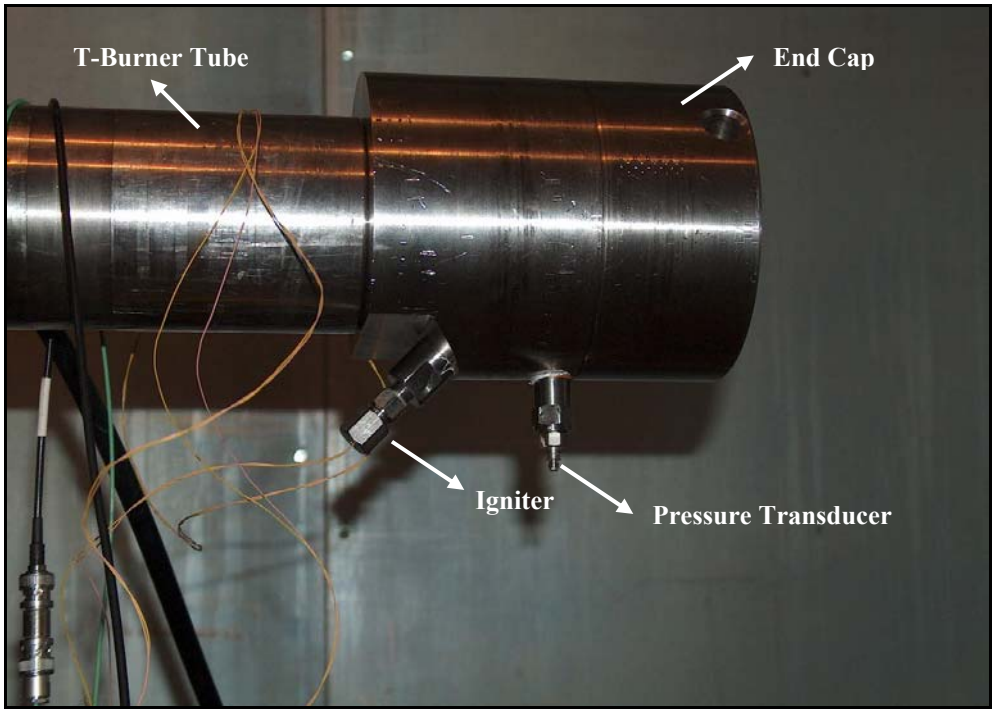

Figure 29. Picture of the igniter body with the Feed-through

2.2. Pressure Stabilization Setup

In literature [37], the pressure in the T-Burner setup can be stabilized using two different methods. First, a sonic orifice can be installed at vent hole of the T-Burner tube. The orifice is designed for a choked flow that results in the desired test pressure. A second approach is to couple the T-Burner vent hole to a large volume surge tank that is pressurized to the desired test pressure. In this mode of operation, the exhaust flow is not choked.

The advantages of the choked nozzle approach are its simplicity in construction and economical feasibility. Since, the additional tankage and plumbing necessary for a surge tank system are not required. However, there are several disadvantages of the choked nozzle that offset these attractions. Firstly, the design of the choked nozzle to provide a desired pressure has the usual complications of a nozzle design. Secondly, the choked nozzle must be fabricated from a material that can withstand corrosive environment.

The advantage of the surge tank approach is that pressure in the T-Burner can be controlled accurately. However, this requires large interior volume of the surge tanks. The manufacturing of high-pressure, large tanks and the plumbing can be very expensive.

In this thesis, a combination of these two approaches is introduced as a first alternative. Pressure stabilization mechanism constructed in this alternative, is composed of a relatively small tank, a discharge pipe, a cavitating venturi and a rupture disc. For economical purposes a small surge tank full of water is used. Instead of a choked nozzle which will directly exhaust the combustion gases to the test room, a cavitating venturi is designed and placed at the exit of the surge tank. Main disadvantage of the choked nozzle, which is its exposure to the corrosive effects, is overcomed by this way. Hot combustion gases are first faced with water

inside the surge tank and then exhausted by use of the venturi which also provides a constant mass flow rate.

In order to see the effect of pressure stabilization system explained above on the overall performance of the T-Burner setup, a second alternative setup is also constructed using a choked nozzle instead of using a surge tank with cavitating venturi. By this way comparison of both systems is performed.

In Figure 30 detailed product tree of the pressure stabilization setups is presented. Each part of the product tree is investigated separately below.

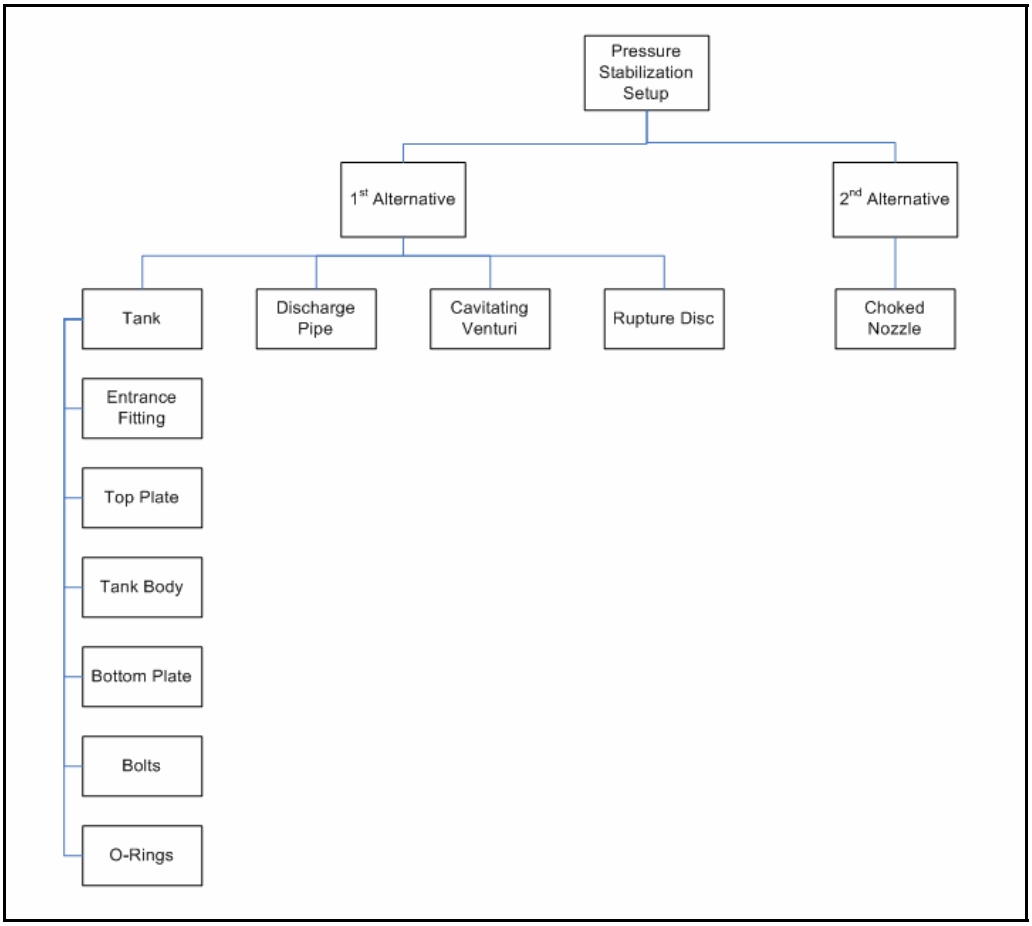

Figure 30. T-Burner pressure stabilization setup product tree

2.2.1. Surge Tank with Cavitating Venturi System (1st Alternative)

2.2.1.1. Tank

Tank is composed of entrance fitting, top plate, tank body, bottom plate, exit fitting, bolts and O-rings. The components of the tank body are exposed to high pressure and high temperature combustion gases which have corrosive effect. Therefore, structural strength of the tank and its material selection become important design factors.

The tank body assembly with plates and bolts are exposed to finite element stress analysis before they are manufactured. The commercially available ANSYS Finite Element software was used for this analysis.

"Stainless Steel AISI-304" is selected as the material of the tank body and plates. This material is known to have a corrosive resistance. [35]

Validation of the tank dimensions, the fasteners and O-rings that are used for preventing the leakage is done by a hydrostatic test which is performed at 150 bars for 10 secs. There occured no failure of the tank and no leakage is observed.

The picture of the constructed tank is presented in Figure 23. Technical drawing of the tank body, top plate and bottom plate are given in APPENDIX A. Detailed dimensions of the components of the tank are presented in the technical drawing.

Figure 31. Picture of the tank

2.2.1.2. Cavitating Venturi

Flow rate of a liquid is mostly controlled by an active flow control system. These systems include a solenoid valve, flow meter, and a control unit. Flow is measured at a high frequency and brought to the desired value playing with the angle of the valve. These systems are expensive and have a slow response time. [38]

In this alternative setup, a cavitating venturi is used as a passive flow control system. The venturi is placed at the exit of the surge tank and it provides constant rate flow which is not affected from the effects of the possible pressure waves inside the tank.

Flow domain can be modeled as a steady one dimensional flow and one can easily derive the basic equations of the flow with some assumptions, [39]. A schematic illustration of cavitating venturi is shown in Figure 32. As a first assumption cavitation region is treated as a fixed, slip boundary which occupies a fixed fraction of the nozzle cross sectional area. The liquid passes through the remaining fraction of the nozzle area "A_c". $A_c = A_{th}\ C_c$. This fraction "C_c" is a function of geometry. Also, constant density of the liquid phase and negligible mass transfer at that interphase can be assumed. Thus the mass flow through the nozzle can be expressed as:

$$\dot{m} = \rho C_c A_{th} V_c \tag{2.10}$$

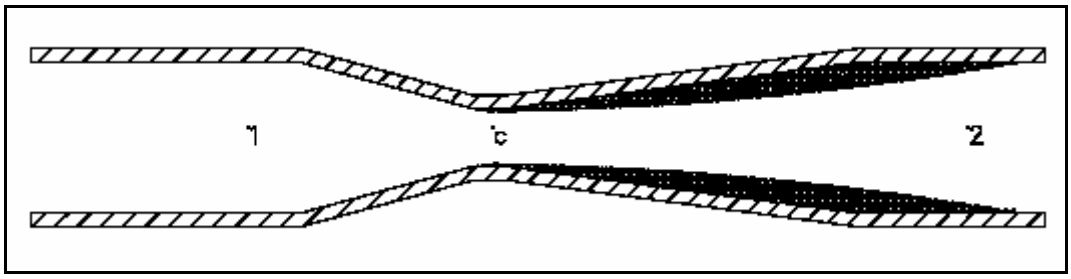

Figure 32. A simplified view of cavitating venture [39]

Another assumption can be made such that there exists no loss in the flow through point 1 to point c. Furthermore, due to the first assumption we can say that the pressure at point c is equal to the vapor pressure. With these assumptions and neglecting the dynamic pressure at inlet, we can write the momentum balance from point 1 to point c using Bernoulli's equation:

$$P_1 = P_v + \frac{1}{2}\rho V_c \tag{2.11}$$

where P_1 is inlet pressure, V_c is average velocity at point c, P_v is the vapor pressure. Combining the Equation (2.10) and Equation (2.11) one can easily calculate the mass flow rate:

$$\dot{m} = A_{th} C_c \sqrt{2\rho(P_1 - P_v)} \tag{2.12}$$

To design cavitating venturi for a specified mass flow rate one can take the area "A_{th}" from Equation (2.12) and calculate the necessary diameter of the throat for a specified inlet pressure.

For the stabilization of the pressure of the T-Burner setup, the cavitating venturi has to be designed for water. Inlet and throat diameters and converging-diverging angles are the parameters of the design. The inlet diameter is equal to the inside diameter of the discharge pipe 22.4 mm. The inlet pressure is taken as 70 bars which is the test pressure of the system. Converging and diverging angles can be found from the literature as 15° and 8° respectively in order to minimize the losses [40]. After substituting the necessary values into Equation (2.12), area "A_{th}" and throat diameter "D_{th}" can be found easily for C_c=1.

To validate the flow rates of the produced cavitating venturi at constant inlet pressure a test setup is used which is available at TÜBİTAK-SAGE. The flow diagram of the experimental setup is given in Figure 33.

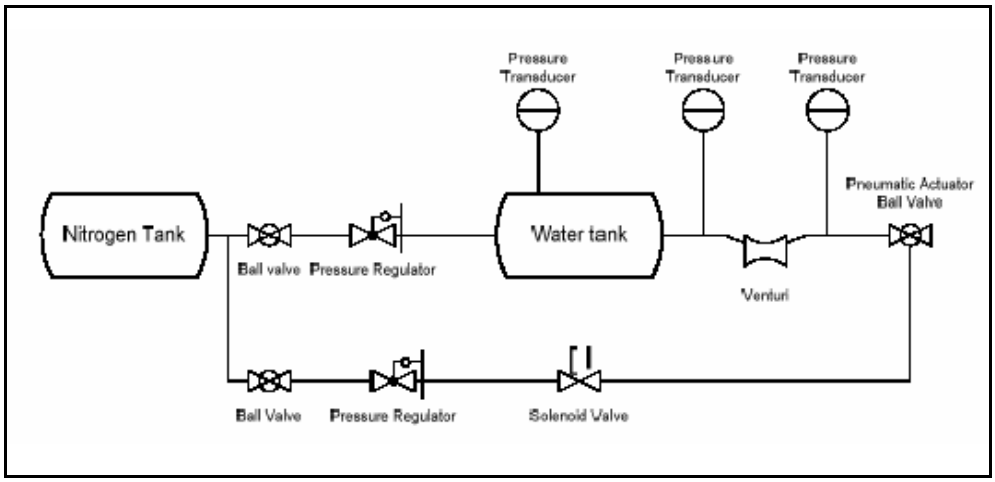

Figure 33. Flow diagram of the experimental setup [38]

In Figure 34 the solid model of the venturi is presented. Technical drawing of the venture is given in APPENDIX A. Detailed dimensions of the venturi are presented in the technical drawing.

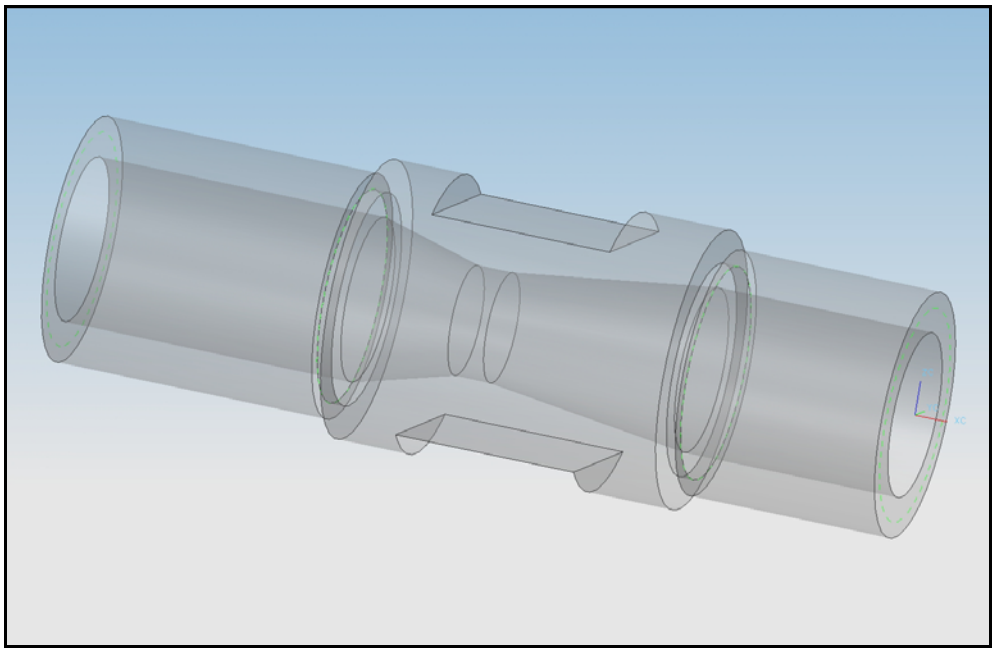

Figure 34. Solid model of the venturi

2.2.1.3. Rupture Disc

The rupture disc is used for pre-presurizing the system and it is mounted at the exit of the venturi by the help of the holder and the lip. The holder and the lip are exposed to high pressure and high temperature combustion gases which have corrosive effect. Therefore, the material selection becomes important design factor. "Stainless Steel AISI-316L" is selected. [35]

Repeatability and precision are two important criteria that affect the design of the rupture disc. For obtaining the required burst pressure, the thickness of the rupture disc is determined using simple mechanical design approaches and analyzed by commercial structural analysis software ANSYS for the validation.

The rapid protyping machine at BİLTİR-METU is used for manufacturing the discs. To validate the burst pressure of the rupture disc a test setup is also designed. The notch thickness was fixed but the thickness of the rupture disc was changed during the tests. For 3 mm, 4 mm and 5 mm thickness values, which are obtained from structural analysis, burst tests are performed. A linear dependence of the burst pressure to the thickness of the rupture disc is obtained from these tests. Using this variation of burst pressure with rupture disc thickness, required thickness for the defined operating pressure is obtained as approximately 3.47 mm. For the validation of this result two sets of extra tests are performed with rupture discs with 3.4 mm and 3.5 mm thicknesses. At the end of these test series sufficient geometric parameters for required burst pressure are reached. The results of the tests are given in APPENDIX C.

The solid model of the constructed rupture disc is presented in Figure 35. Specifications of the material properties of the rupture disc are given in APPENDIX B.

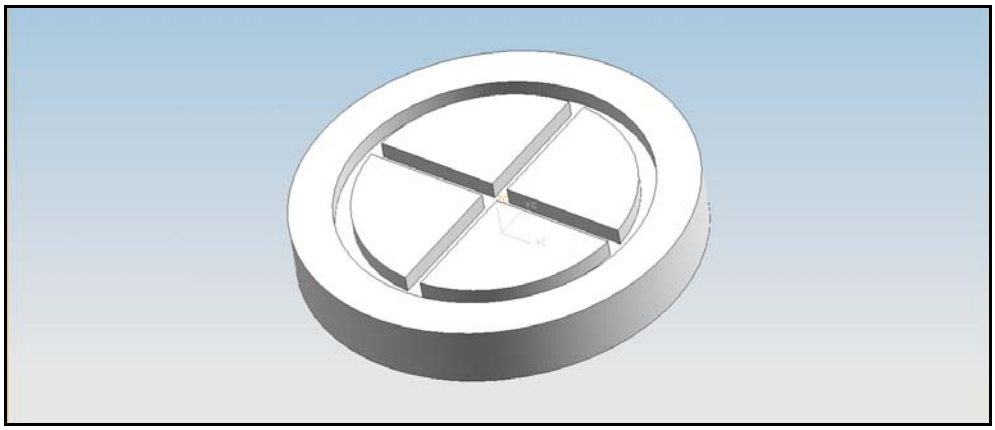

Figure 35. Solid model of the rupture disc

2.2.2. Choked Nozzle (2nd Alternative)

As it is stated in Section 2.2, another way to stabilize the pressure inside the combustion chamber is the use of a choked nozzle instead of a surge tank and cavitating venturi.

Geometric limitations of the T-Burner tube restricted the inlet diameter of the nozzle that will be used. The exit diameter of the nozzle is evaluated easily from internal ballistics analysis if some necessary assumptions are made. The major assumptions taken are listed below.

- The product gas is assumed to be constant property, homogenous ideal gas. ($P=\rho RT$, $Cp=[\gamma/(\gamma-1)R]$)

- The length to diameter ratio ia less than 10 so the pressure and burning rate is assumed to be constant everywhere at a given time.

- Steady state burning is assumed. For each burn step, the given thickness of propellant burns, then the whole chamber pressure stabilizes. The next burn step starts from the stabilized state.

- No frictional or heat transfer losses are assumed along the chamber and the nozzle contour.

- The volume increase inside the motor case due to solid propellant surface regression is neglected.

With the help of these assumptions, simplified zero dimensional internal flow is solved.

The T-Buner is a closed chamber with one opening, the nozzle throat, to the surrounding environment. Therefore the mass balance inside the motor case is given by,

$$\dot{m}_{generated} + \dot{m}_{in} - \dot{m}_{out} = \frac{dm_{motor}}{dt} \cong 0 \Rightarrow \dot{m}_{generated} + \dot{m}_{in} = \dot{m}_{out} \tag{2.13}$$

The net change inside the motor case is zero. And since the motor case has no opening for the inlet, the equation further simplifies to,

$$\dot{m}_{generated} = \dot{m}_{out} \tag{2.14}$$

The generated mass is the product gas of the burning solid propellant. The generation rate is simply the net burning area times the burning rate times the density of the propellant,

$$\dot{m}_{generated} = \dot{r}_b \rho_p A_b \tag{2.15}$$

On the other side, the mass discharged to environment from the nozzle throat is the mass out,

$$\dot{m}_{out} = P_c A_{th} C_d \tag{2.16}$$

If we put these terms into the mass balance,

$$\dot{r}_b \rho_p A_b = P_c A_{th} C_d \tag{2.17}$$

The burning rate of the propellant can be shown as,

$$\dot{r}_b = a P_c^{\,n} \tag{2.18}$$

The above equation is a semi-empirical equation, where the “a” and “n” are obtained from experiments. The “a” and “n” values for the propellant used for this study are given for the pressure unit of bar. But the rest of the equations are all use pressure unit of Pascal. So the burning rate is modified for Pascal unit of pressure.

$$\dot{r}_b = a\left(P_c / 10^5\right)^n \tag{2.19}$$

Introducing the burning rate into the mass balance equation, the below formula for the chamber pressure at a given burning area, propellant properties and nozzle parameters can be achieved.

$$P_c = \left[\frac{a \rho_p A_b c^*}{A_{th} 10^{5n}} \right]^{1/(1-n)} \tag{2.20}$$

The C_d is replaced by 1/c* for harmony with the literature.

The use of a converging nozzle without the diverging part will be sufficent to stabilize the chamber pressure. So a simple converging nozzle geometry is selected.

Computational fluid dynamics analysis is performed in TÜBİTAK-SAGE for the selected nozzle geometry in order to see whether there exists any shock

especially at the entrance of the nozzle. A commercial software, FLUENT is used for this purpose. Axisymmetric computational domain used for CFD analysis is shown in Figure 36. Figure 37 shows the Mach number contours after 0.5 sec. As it can be seen combustion gases fills the chamber and there occurred no shocks inside the nozzle and the flow is choked.

This CFD analysis is only performed to see that the choked nozzle is shock-free. As it will be stated in Section 4, some problems occur especially about the amount of combustion gases mass flow rate. Axisymmteric geometry assumption in this CFD study resulted in higher burn area as for sure.

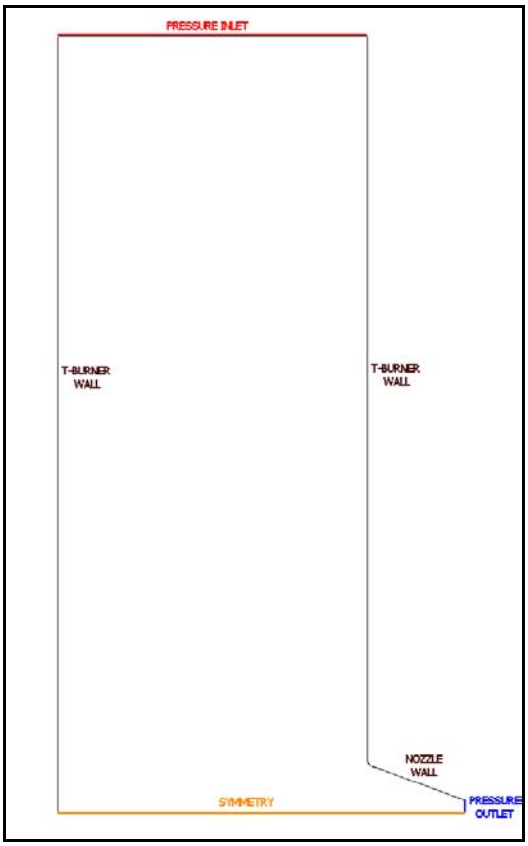

Figure 36. Choked nozzle CFD computational domain.

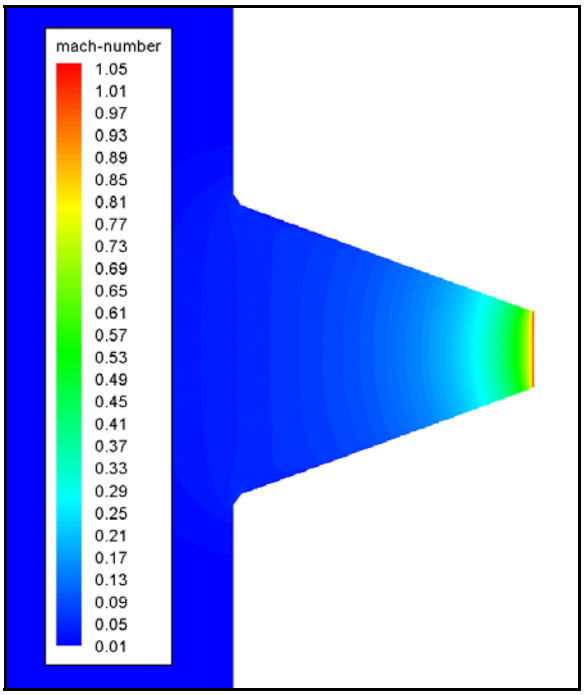

Figure 37. Choked nozzle Mach number contours.

"Stainless Steel AISI-316L" is selected as the material of the choked nozzle body for multi purpose usage. This material is known to have a corrosive resistance.

2.3. Pressurization System

Pressurization system is used for pre-pressurizing the system to the desired pressure with nitrogen gas. The nitrogen gas is supplied from the nitrogen tubes containing 230 bars pressure inside. The ball and needle valves are used to control the pressure of the T-Burner. They are mounted on the control panel.

Pressurization system is not used with the choked nozzle pressure stabilization system.

2.4. Measurement Instruments

The most important considerations in designing and operating instrumentation are to ensure durability, to obtain adequate frequency response capability, to have resolution to reduce intrinsic noise to very low levels and to generate both immediate and permanent records.

High frequency "KISTLER" transducers are mounted on the adapters, behind both of the propellant assemblies. One of them provides redundancy of the data. The high temperature gases do not affect the flush mounted "KISTLER" unit for durations of several seconds, with the use of only a thin film of silicone grease as protection. The coating of grease also protects the transducer from chemical attack by the corrosive products of combustion.

"GEM" pressure transducer and indicator is used to measure the static pressure of the system. The indicator is mounted on the control panel.

Specifications of the measurement instruments are given in APPENDIX B.

2.5. Data Acquisition System

The data acquisition system used during the tests is a DaqBook 2000E data acquisition system integrated to a personal computer. The DBK-01 16 channel BNC input module and DBK-30A power management modules are also used during the tests. The system is capable of acquiring data at 200 kHz maximum. The whole data acquisition system is shown in Figure 38. The software used with the data acquisition system is "DaqView". Both the system and the software are products of IOtech Incorporation, USA.

Figure 38. Data acquisition system

2.6. Base Part and Control Panel Assembly

The base part is used to fix the T-Burner. The base is manufactured from 4mm and 6mm square profiles and beds. Technical drawing of the base is given in APPENDIX A. Detailed dimensions of the base part are presented in the technical drawing.

Another part of the T-Burner setup is a control panel assembly. For the sake of security, the pressurization of the T-Burner and the control of the igniters are performed by the use of a control panel which is located outside the test room. In Figure 39 the picture of the control panel is presented.

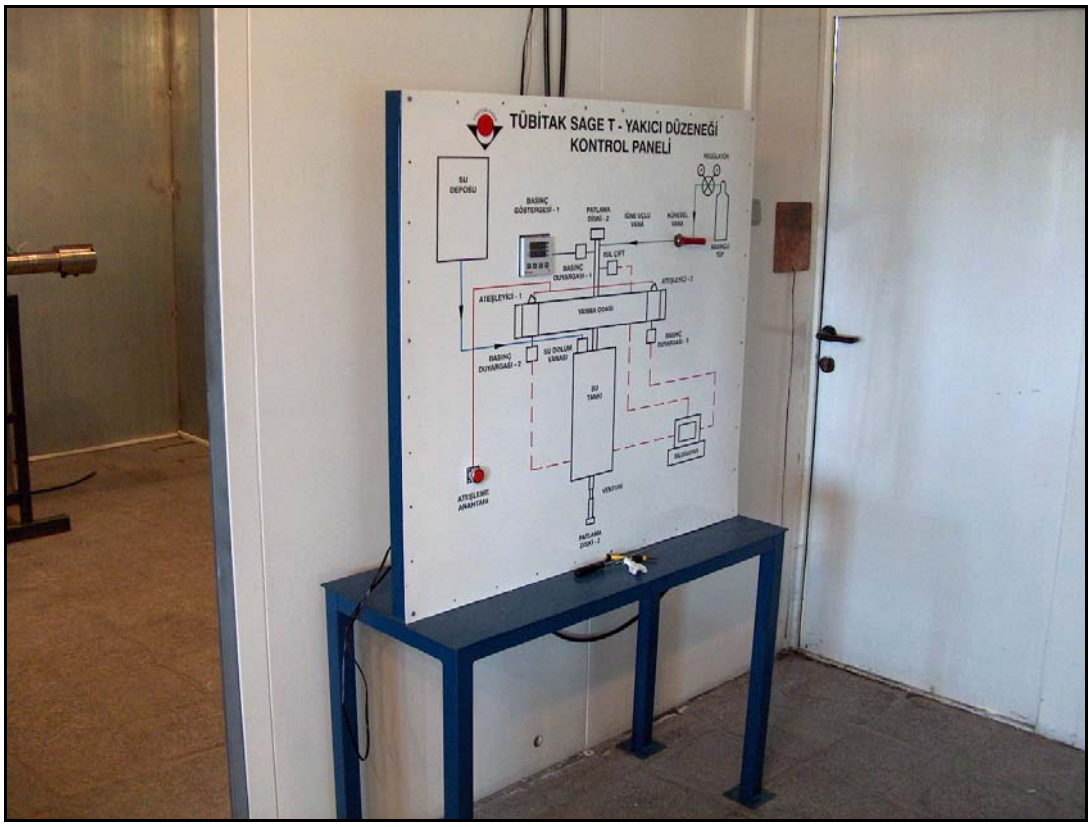

Figure 39. The control panel

Tests with the T-Burner setup that uses choked nozzle as a pressure stabilization system is performed at the test bench facility of TÜBİTAK-SAGE for the sake of safety. Therefore the base part and control assembly of the original system are not used for these tests.

CHAPTER 3

OPERATIONAL SEQUENCES OF T-BURNER TESTS

In this chapter, operational sequences that are followed during T-Burner tests are explained in detail. Two setups which use different pressure stabilization systems that are surge tank with cavitating venturi and choked nozzle are handled separately.

3.1. Operational Sequences of T-Burner with Surge Tank and Cavitating Venturi

The picture of the T-Burner setup that uses a surge tank and a cavitating venturi as pressure stabilization system is given in Figure 40 excluding the control panel which was shown in Figure 39.

In this section detailed explanation about the T-Burner test setup is given. In Figure 41 and Figure 42 the schematic representation of T-Burner and flow diagram of the experimental setup that uses a surge tank and a cavitating venturi as pressure stabilization system are given.

Figure 40. Picture of the T-Burner with surge tank and cavitating venturi

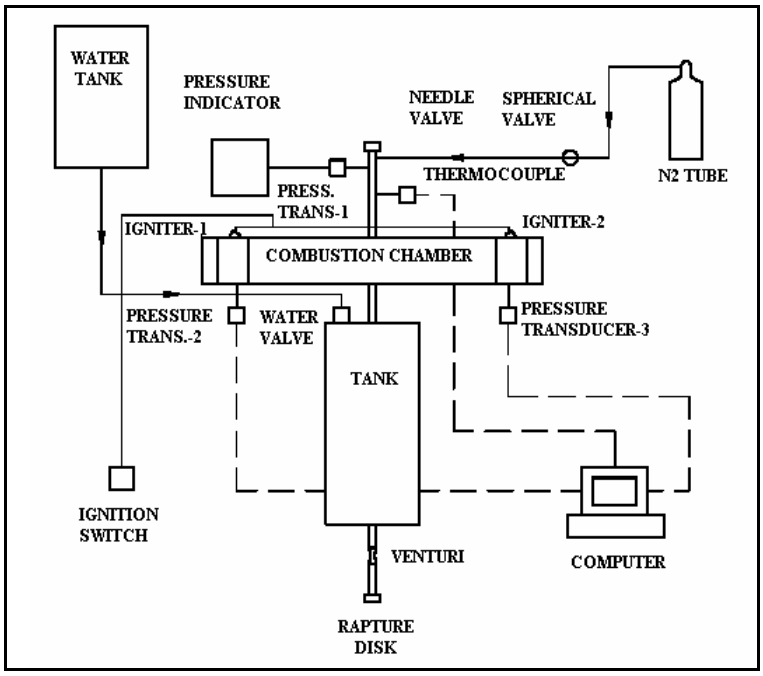

Figure 41. The schematic representation of T-Burner Setup with surge tank and cavitating venturi

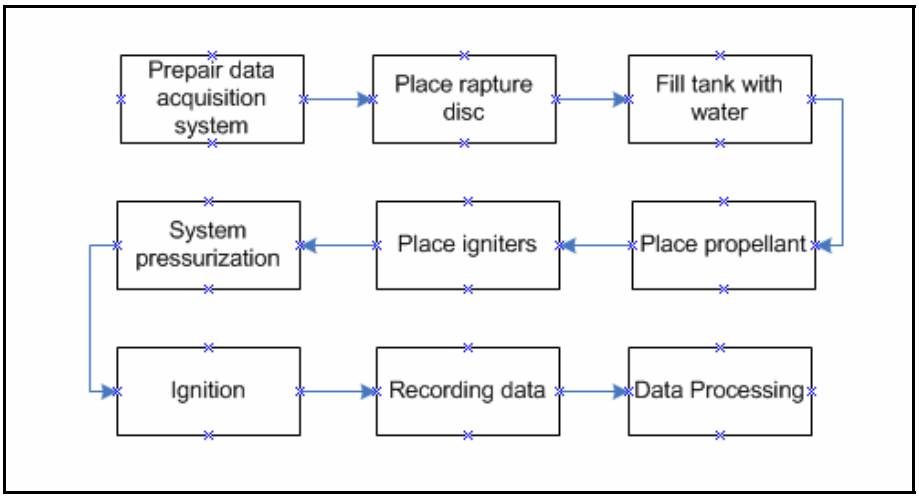

Figure 42. The flow diagram of the T-Burner setup with surge tank and cavitating venturi

Following jobs have to be performed in sequence for a successful T-Burner test:

1. Pressure transducers are attached to necessary locations. One is positioned to the middle of the T-Burner tube to see the system pressure. The second one is positioned to the left side adapter and third one is positioned to the right side adapter.

2. Thermocouple is placed at the middle of the T-Burner tube to see the system temperature.

3. KISTLER pressure transducers which are placed on the adapters are connected to the charge amplifiers.

4. The thermocouple and the charge amplifiers are connected to the data acquisition system. The right side pressure transducer is connected to the 1st channel, the left side transducer is connected to the 2nd channel and the

thermocouple is connected to the 3rd channel of the system. Then the system is integrated to a personal computer.

5. The readings of the amplifiers and the reading of the pressure indicator which is mounted on the control panel are compared with each other.

6. The rupture disc is put between the holder and lip.

7. Water valve located between the water tank and surge tank is opened. The tank is filled with water.

8. Casted and cured solid propellants are put into the left and right side adapters. The O-rings between the adapter and end caps are placed and then the end caps are assembled.

9. Igniters are located into their places and the ignition cables comes from control panel are connected to the cables of electric squibs.

10. Test room is emptied for safety requirements.

11. The system is pressurized with the Nitrogen gas to the desired value. The valve of 230 bar N_2 tank is opened. The system is pressurized with the Nitrogen to the desired value by the help of ball valve and needle valve which are mounted on the control panel.

12. The firing signal is given to the igniters, while acquiring the pressure and temperature data.

13. The data is processed.

3.2. Operational Sequences of T-Burner with Choked Nozzle

The picture of the T-Burner setup that uses a choked nozzle is given in Figure 43.

Figure 43. Picture of the T-Burner with choked nozzle

In this section detailed explanation about the T-Burner test setup that uses choked nozzle is given. In Figure 44 and Figure 45 the schematic representation of T-Burner and flow diagram of the experimental setup that uses a choked nozzle as pressure stabilization system are given.

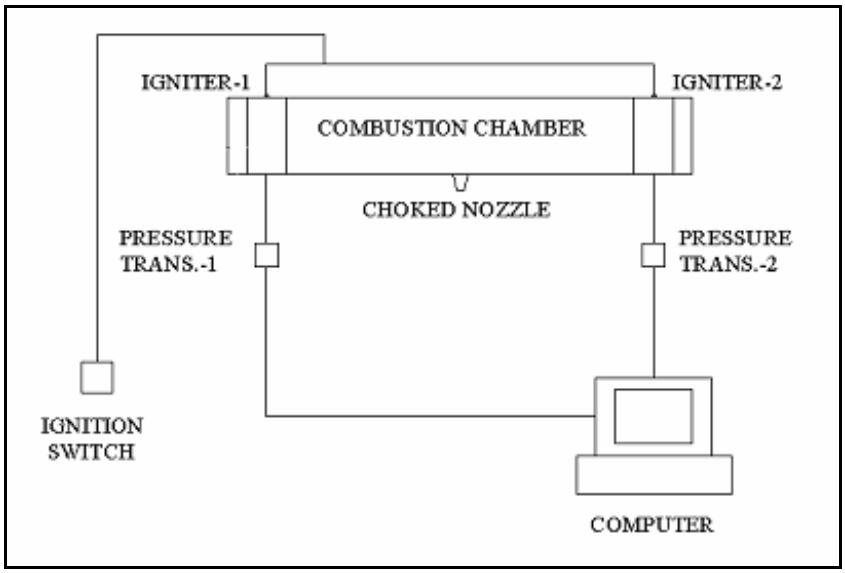

Figure 44. The schematic representation of T-Burner setup with choked nozzle

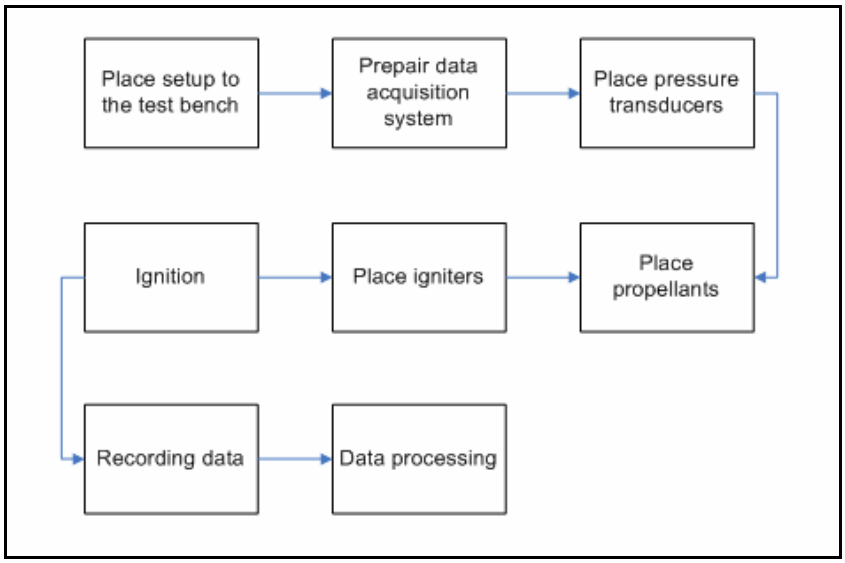

Figure 45. The flow diagram of the T-Burner setup with choked nozzle

Following jobs have to be performed in sequence for a successful T-Burner test with choked nozzle:

1. The T-Burner tube with adapters and choked nozzle is attached to the test bench.

2. Pressure transducers are attached to necessary locations. One is positioned to the left side adapter and the second one is positioned to the right side adapter.

3. KISTLER pressure transducers which are placed on the adapters are connected to the charge amplifiers.

4. The thermocouple and the charge amplifiers are connected to the data acquisition system. The right side pressure transducer is connected to the 1st channel and the left side transducer is connected to the 2nd channel. Then the system is integrated to a personal computer.

5. Casted and cured solid propellants are put into the left and right side adapters. The O-rings between the adapter and end caps are placed and then the end caps are assembled.

6. Igniters are located into their places and they are wired to the firing line.

7. The firing signal is given to the igniters, while acquiring the pressure data.

8. The data is processed.

3.3. Data Processing

When the propellant discs are ignited, the combustion occurs and oscillations develop and grow with exponentially increasing amplitude (Figure 46)

until nonlinear effects limit the amplitude. In Figure 46, upper trades results from filtering out DC component and amplifying pressure signal.

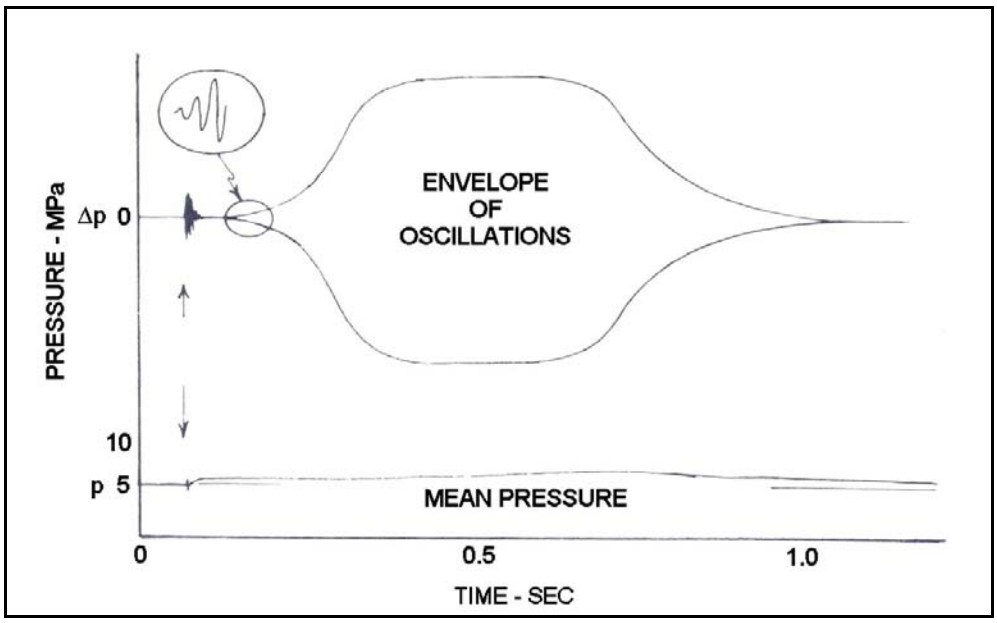

Figure 46. Pressure-time history for a center vented burner test [3]

When the propellant burns out, oscillations decay in a roughly exponential manner. It is assumed that the damping is the same during the period of growing oscillations as the period of decaying oscillations, given by the observed decay rate of oscillations. Then the initial growth rate of oscillations is the sum of a combustion contribution and the measured damping contribution [3]. Hence combustion contribution to oscillations can be stated as:

$$\alpha_c = \alpha_g + \alpha_d \tag{3.1}$$

where α_g and α_d are measured growth rate of oscillations during combusiton and decay rate of oscillations after combustion respectively that are obtained from the test records (Figure 46). Note that α_d has to have a negative value.

The rate of growth or decay of a solid rocket system is expressed in terms of the α in the Equation (3.2) [42].

$$P = \hat{P}e^{\alpha t} \tag{3.2}$$

$$\ln\left(\frac{P}{\hat{P}}\right) = \alpha_c \cdot t \tag{3.3}$$

Approximate evaluation of the growth rate of oscillations and decay rate of oscillations seperately can be performed by taking the ratio of $\ln\left(\frac{P}{\hat{P}}\right)$ with elapsed time in the meausured data.

The quantity α_c reflects the combustion contribution to oscillations and can be determined over a range of frequencies by testing in different length burners. If one is interested in comparing propellants, a direct comparison of α_c vs frequency is often instructive. If one wants the results in motor stability analyses, the equivalent pressure-coupled response functions must be determined. This amounts to construction of a stability analysis of the T-Burner and solving for R_P in terms of the measured quantities of α_g and α_d. An approximate analysis results in the relation, [41]:

$$R_P = \frac{\alpha_c \overline{P}}{4fa\rho_p r_b \left(S_b/S_c\right)}\left[\frac{a_m}{a}\right] \tag{3.4}$$

where

R_P = magnitude of the in-phase component of the oscillatory response of burning rate to pressure oscillation about the mean values

α_c = combustion alpha

$\overline{P}$ = mean pressure

a_m = measured speed of sound ($a_m = 2fL$, L = burner length)

a = theoretical speed of sound of the gases (at the adiabatic flame temperature)

S_c = cross-sectional area of burner

S_b = burning area of propellant

f = frequency of oscillations

ρ_p = propellant density

r_b = mean burning rate

Repeating tests on the same propellant in different burner lengths provide R_P vs frequency and further tests can provide such functions over a range of pressures [41], as shown in Figure 47.

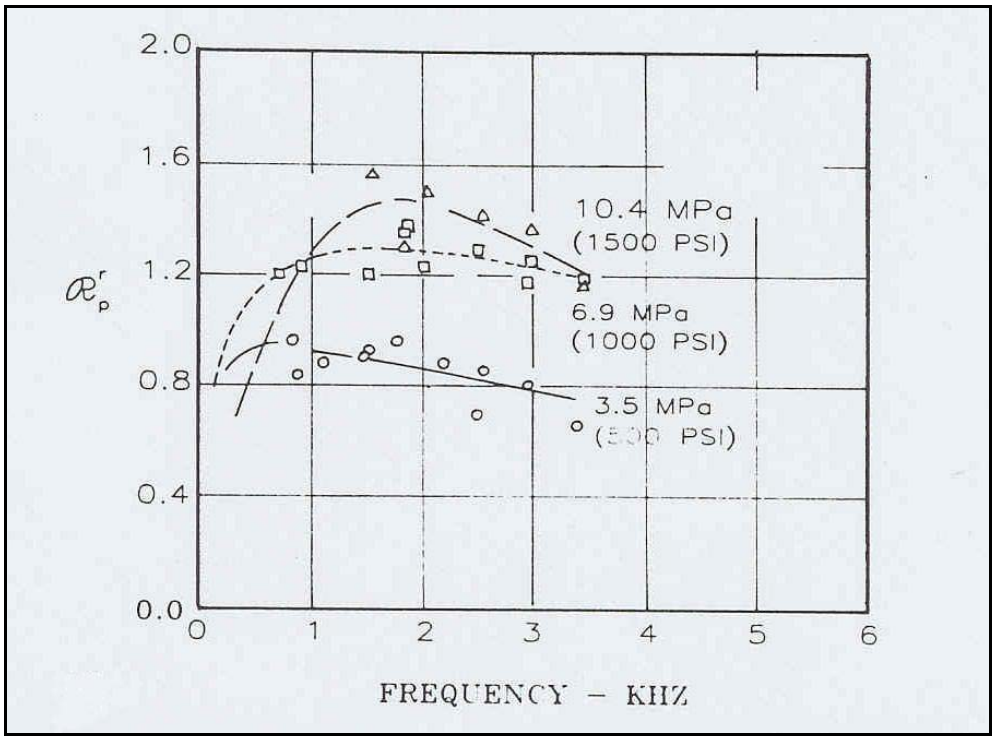

Figure 47. Response functions as measured by the T-Burner method [3]

CHAPTER 4

EXPERIMENTS AND RESULTS

4.1. Determination of the Resonance Frequencies of the System

Developed T-Burner test setup has two alternatives for pressure stabilization as mentioned in previous chapters. This alternative structure yields different setup characteristics for each pressure stabilization mechanisms. To find out resonance behaviours of setup characteristics, a test set of two experiments per each alternative is introduced. Each alternative is tested both with a pressurized and nonpressurized test scheme. In pressurized scheme, the setup is pressurized with nitrogen and is pulsed the T burner cavity with the help of pyrotechnic cartridge and pressure data are recorded. Unpressurized test scheme is similar with the absence of nitrogen pressurization. Obtained results are given in the following sections in graphical form. The FFT of the test data yields the frequency content of the oscillations. All of the test data which are presented below are taken at 50 kHz.

4.1.1. Resonance Frequencies of T-Burner Setup with Surge Tank and Cavitating Venturi

In Figure 48, Figure 50 and Figure 52 pressure-time histories for three T-burner tests with tank and cavitating venturi are given. Tests at the same conditions are repeated in order to have a reliable overall result. In these tests the system is not initially pressurized. Figure 49, Figure 51 and Figure 53 show the FFTs of the measured data of three seperate tests respectively. It can be concluded from these figures that the pulsing generated shock waves are eventually died out by

dissipation inside the tube. The peak which occurs around 180 Hz is due to oscillations in the first longitudinal mode (assume a=300 m/s, L=1 m; f=a/2L=150 Hz). The maximum pulse amplitude is around 2 atm.

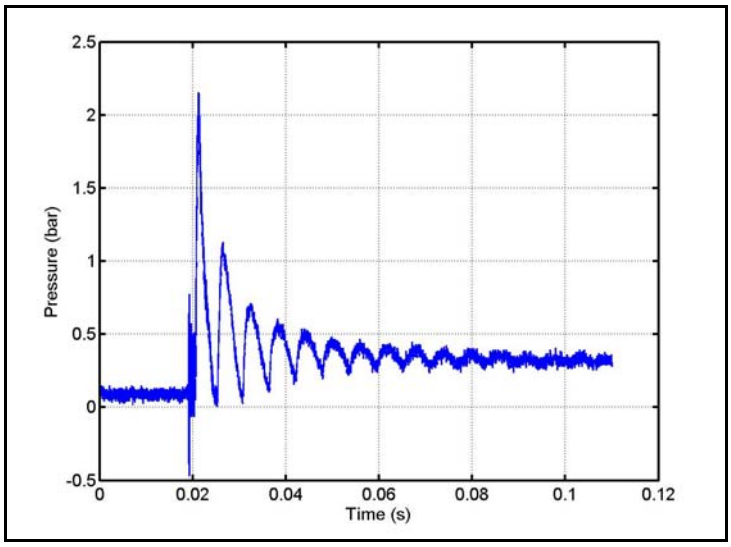

Figure 48. Pressure-time history for the T-Burner test with tank and cavitating venturi (with no initial-pressure)

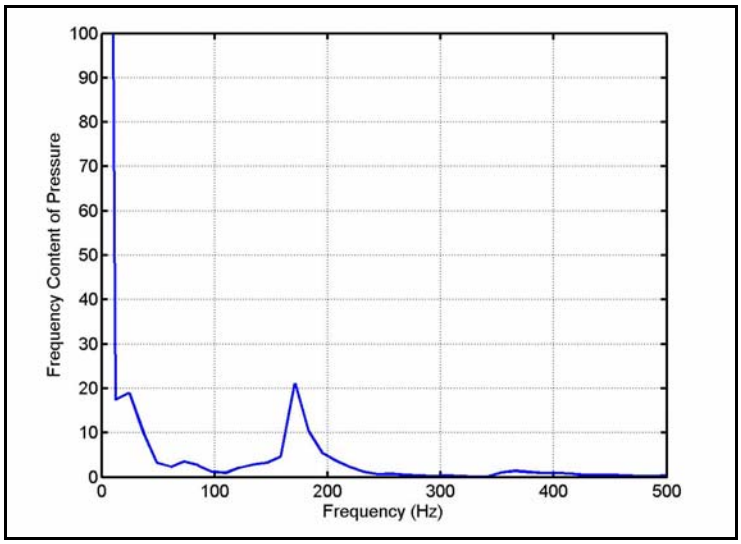

Figure 49. FFT for the T-Burner test with tank and cavitating venturi (with no initial-pressure)

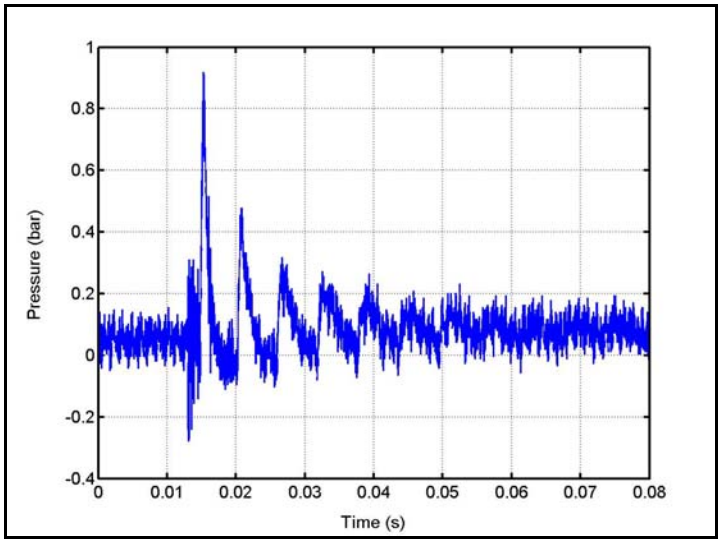

Figure 50. Pressure-time history for the T-Burner test with tank and cavitating venturi (with no initial-pressure)

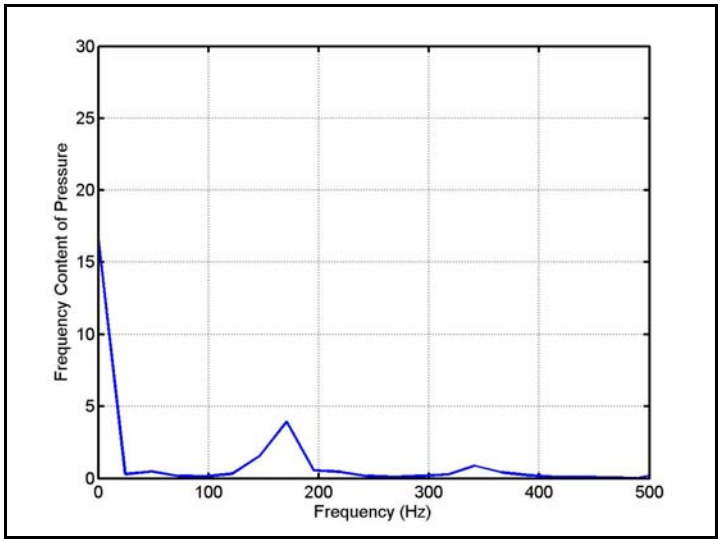

Figure 51. FFT for the T-Burner test with tank and cavitating venturi (with no initial-pressure)

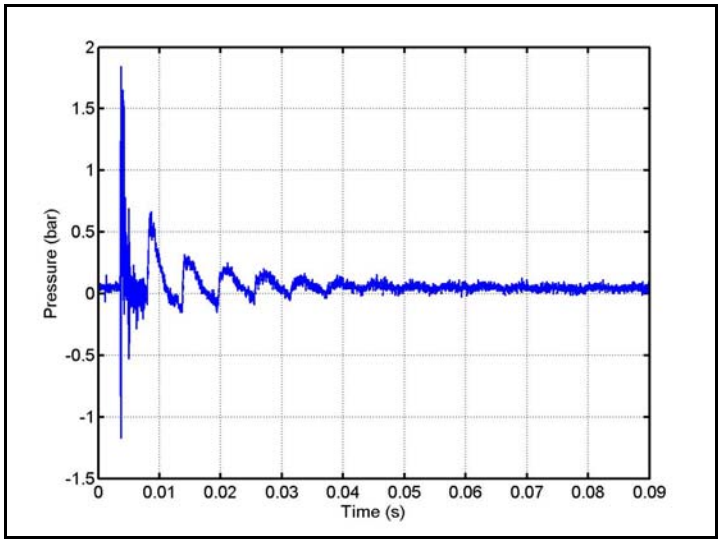

Figure 52. Pressure-time history for the T-Burner test with tank and cavitating venturi (with no initial-pressure)

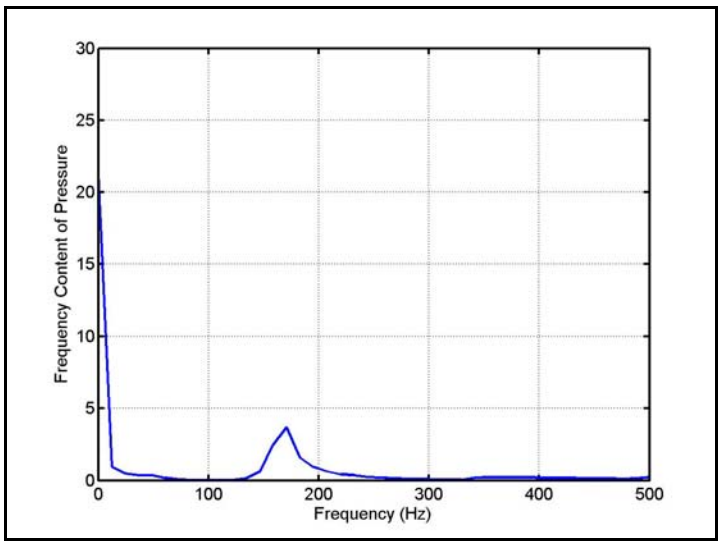

Figure 53. FFT for the T-Burner test with tank and cavitating venturi (with no initial-pressure)

In Figure 54 and Figure 56 pressure-time histories for two T-burner tests with tank and cavitating venturi, which are initially pressurized to 65 bars and 67 bars respectively, are given. Figure 55 and Figure 57 show the FFTs of the measured data of two seperate tests respectively. It can be seen from these figures that for these tests higher harmonics exist. The higher harmonics are multiple of first longitudinal mode. The maximum pulse amplitude is between 5 and 20 atm. The existence of higher harmonics may be due to the pulse strength. Pulse strength is a function of burn rate of pyrotechnic and burn rate is a strong function of pressure. Higher acoustic energy inside the burner may feed the higher harmonics with nonlinear energy transfer.

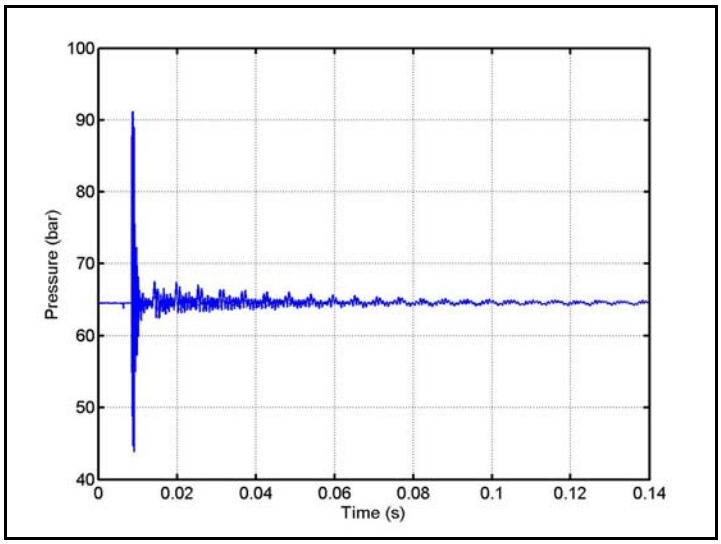

Figure 54. Pressure-time history for the T-Burner test with tank and cavitating venturi (with initial-pressure of 65 bars)

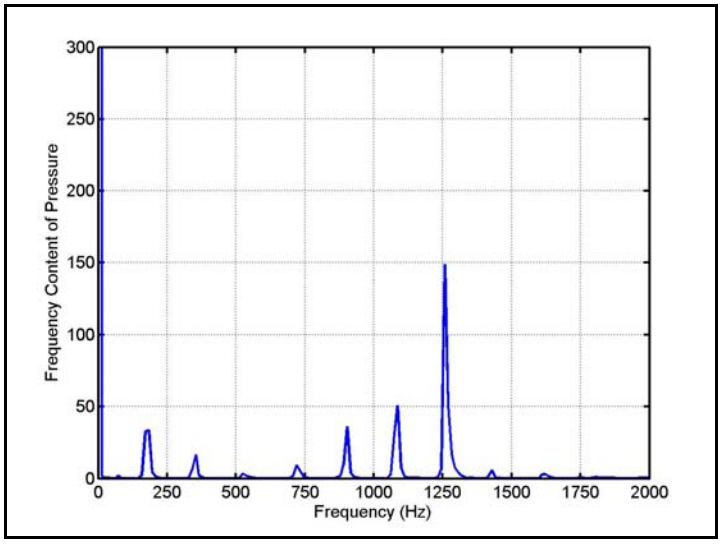

Figure 55. FFT for the T-Burner test with tank and cavitating venturi with (with initial-pressure of 65 bars)

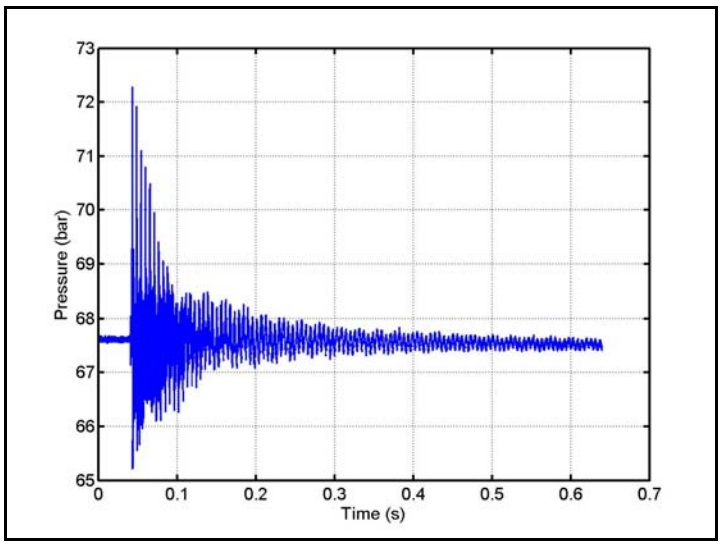

Figure 56. Pressure-time history for the T-Burner test with tank and cavitating venturi (with initial-pressure of 67 bars)

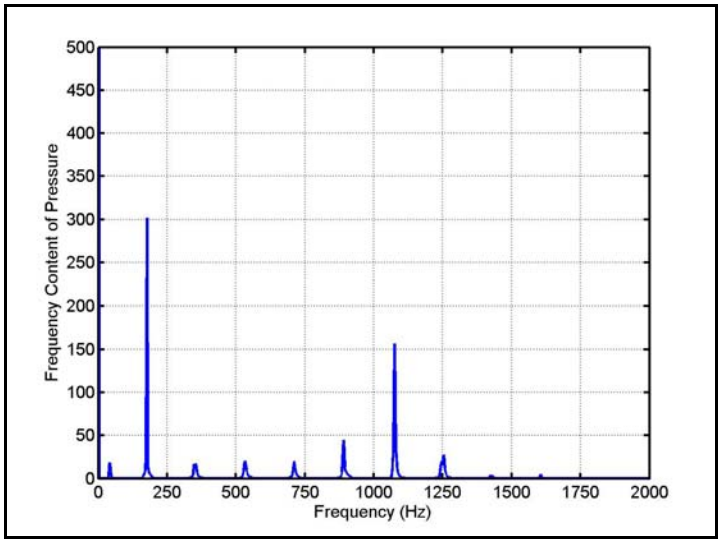

Figure 57. FFT for the T-Burner test with tank and cavitating venturi (with initial-pressure of 67 bars)

4.1.2. Response Frequencies of T-Burner Setup with Choked Nozzle

In Figure 58 and Figure 60 pressure-time histories for three T-burner tests with choked nozzle are given. In these tests the system is not initially pressurized. Figure 59 and Figure 61 show the FFTs of the measured data of two seperate tests respectively. It can be seen from these figures that results came out to be similar to the results of tests with tank and cavitating venturi. The pulsing generated shock waves are eventually died out by dissipation inside the tube. The peak occurs again around 180 Hz. The maximum pulse amplitude is around 2 atm.

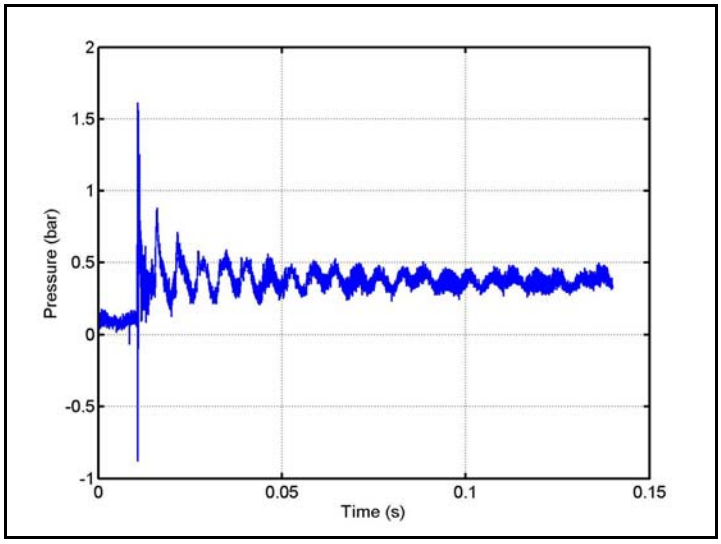

Figure 58. Pressure-time history for the T-Burner test with choked nozzle (with no initial-pressure)

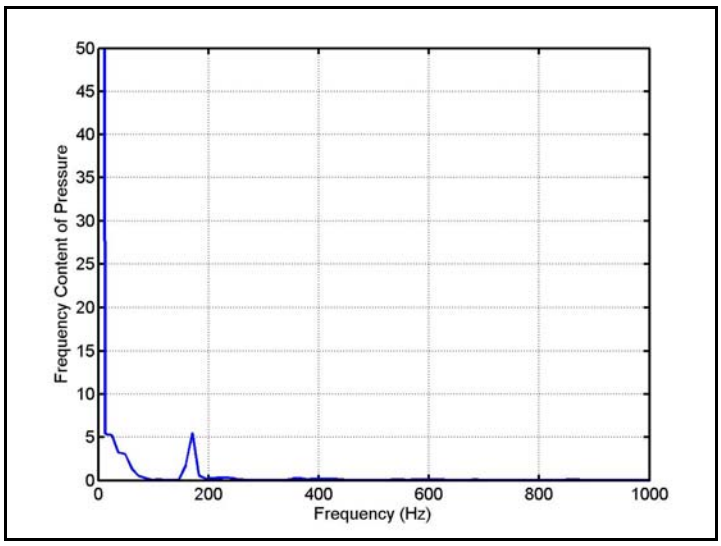

Figure 59. FFT for the T-Burner test with choked nozzle (with no initial-pressure)

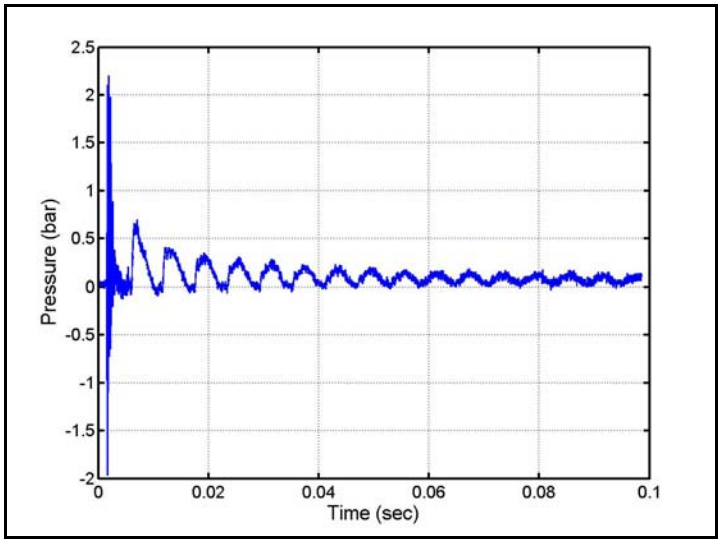

Figure 60. Pressure-time history for the T-Burner test with choked nozzle (with no initial-pressure)

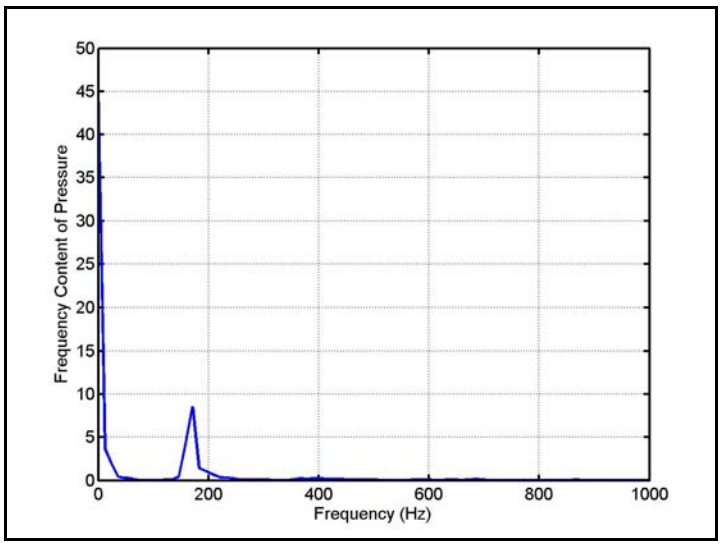

Figure 61. FFT for the T-Burner test with choked nozzle (with no initial-pressure)

In Figure 62 and Figure 64 pressure-time histories for two T-burner tests with choked nozzle, which are initially pressurized to 71 bars and 69 bars respectively, are given. Figure 63 and Figure 65 show the FFTs of the measured

data of two seperate tests respectively. Results again show similar behaviour to the test data obtained from T-burner setup with tank and cavitating venturi. There exists higher harmonics.

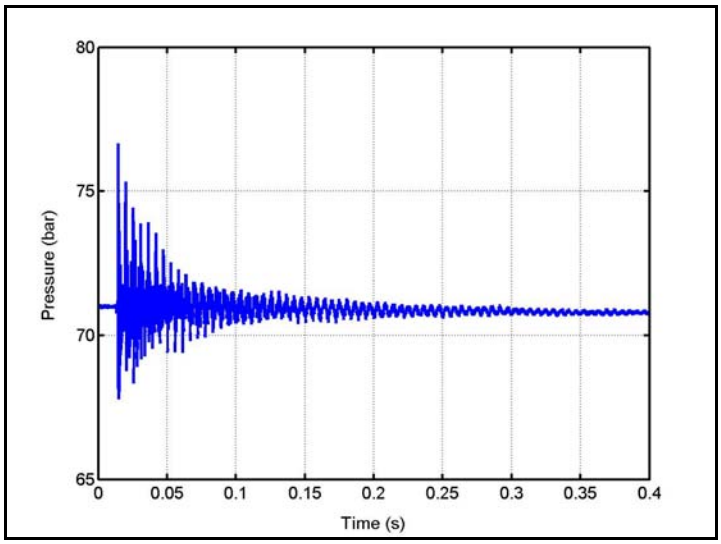

Figure 62. Pressure-time history for the T-Burner test with choked nozzle (with initial-pressure of 71 bars)

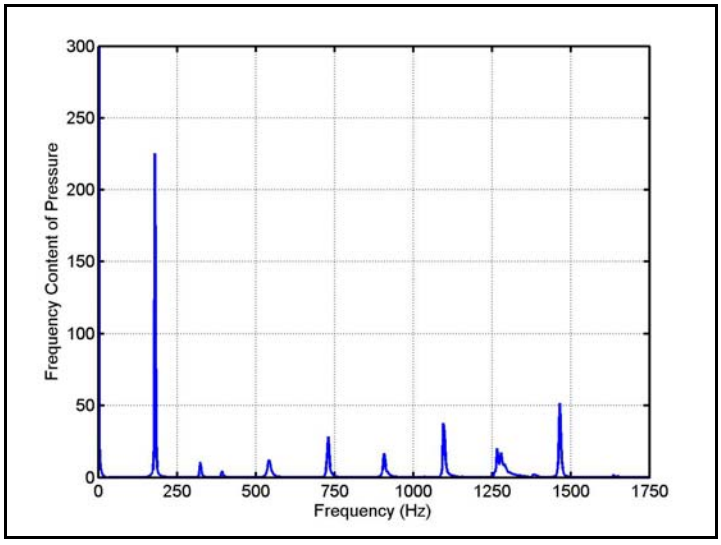

Figure 63. FFT for the T-Burner test with choked nozzle (with initial-pressure of 71 bars)

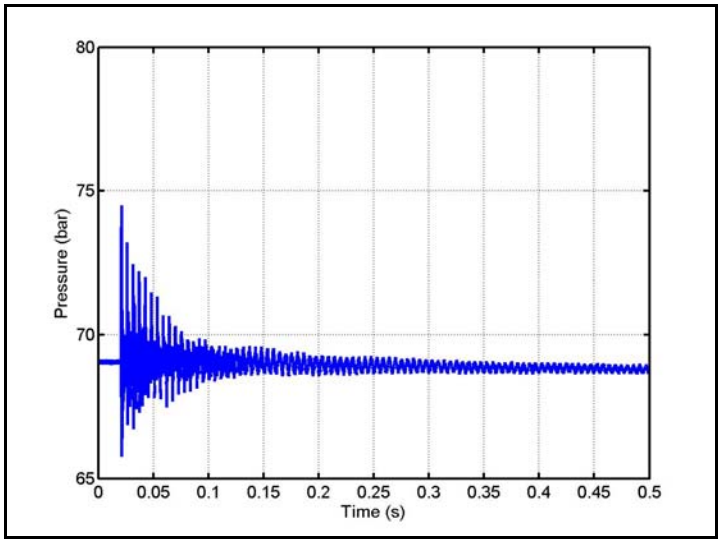

Figure 64. Pressure-time history for the T-Burner test with choked nozzle (with initial-pressure of 69 bars)

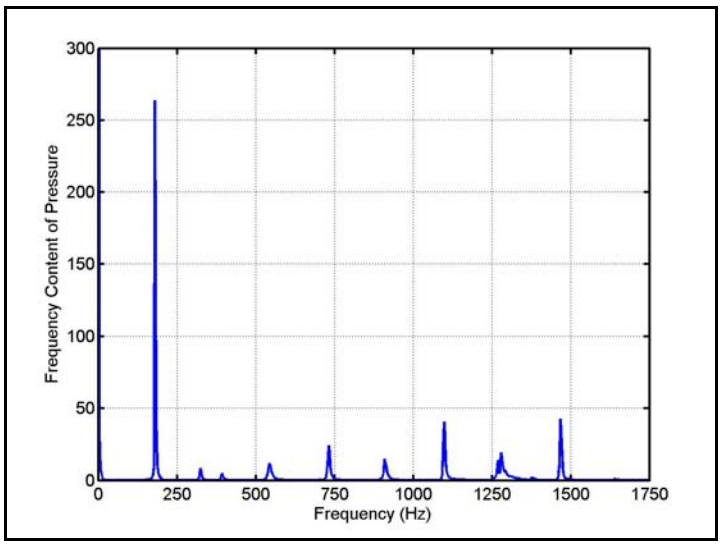

Figure 65. FFT for the T-Burner test with choked nozzle with (with initial-pressure of 69 bars)

As an overall conclusion from these set of experiments it can be said that choked nozzle configuration and venturi configuration yield the same harmonic structure inside the tube. Therefore it can be concluded that the acoustic modes are not affected by the purging mechanisms.

4.2. System Check-out Tests with T-Burner Setup with Surge Tank and Cavitating Venturi

In this section application of the T-Burner tests, following the procedures described in detail in section 3.1 is presented. For these tests, a specific solid propellant of TÜBİTAK-SAGE, which is used in a solid rocket motor, is used. This propellant is chosen because there exits huge amount of data about its burning characteristics. Another reason is about the manufacturing techniques used at TÜBİTAK-SAGE.

4.2.1. Test 1

As a first demonstration of the setup with tank and cavitating venturi, the system is pressurized to 30 bars with Nitrogen gas instead of 70 bars. Actual tests will be performed for a propellant with working pressure of 70 bars. In this test, the data is recorded at 10 kHz.

Recorded pressure data from two pressure transducers with respect to time is given in Figure 66. This graph proves that the ignition of the propellant is occurred. It shows that the T-Burner setup is working but neutral burning could not be achieved in this experiment.

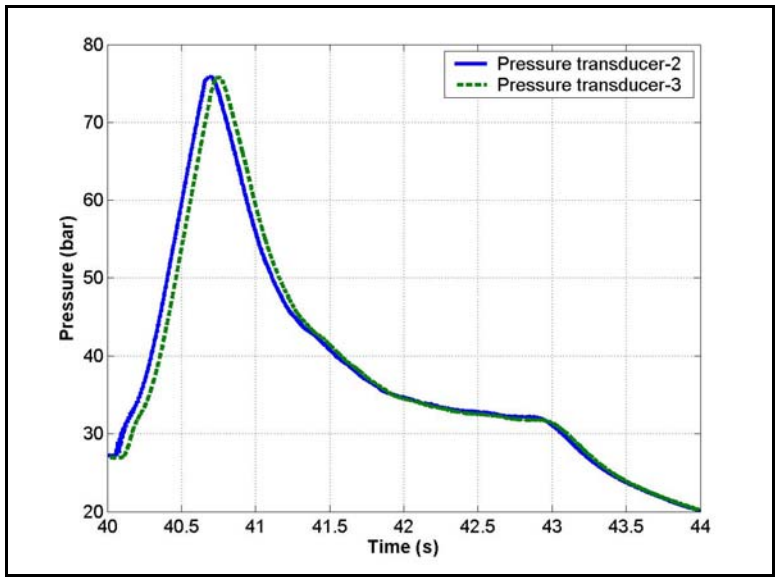

Figure 66. Pressure-time history for the T-Burner test with tank and cavitating venturi

It can also be seen from this figure that there exists no oscillations in the pressure data. This means that for this specific experiment a clear unstable behaviour can not be observed. Therefore, data processing of these data is not performed since it will not give any meaningfull result as for sure.

As it can be seen in Figure 66, a sharp ignition transition regime is observed which may be a remark of excessive usage of igniter content. In this first test, use of 2 grams of MTV as a part of igniter content which itself includes metal particles is thought to be the reason of not seeing any pressure oscillations. In order to prevent this problem for the next tests the amount of MTV is minimized and black powder is used as the main part of the igniter content.

The ignition transition regime obtained in this test also verified the working of the rupture disc. It can be seen that, the system is pressurized up to approximately 75 bars and after that value the rupture disc is burst out.

Figure 67 shows the temperature variation with time inside the combustion chamber. This measurement is necessary for the evaluation of the velocity of sound which requires the adiabatic flame temperature. It can be observed from this figure that the response of the thermocouple used is not sufficient enough. Analysis of solid propellant combustion results in higher temperature values, which is about 3000 K. It is sure that a thermocouple with higher response time is required especially when it is thought that a solid propellant with higher working pressure will be used for the tests. But it must be taken into account that even if a thermocouple with an appropriate response time is used it will burn out at these temperatures. On the other hand, adiabatic flame temperature of the solid propellant can also be obtained from some programs used for the simulation of solid propellant combustion which are originally developed in TÜBİTAK-SAGE. So, from this point forward no temperature data is measured in the tests.

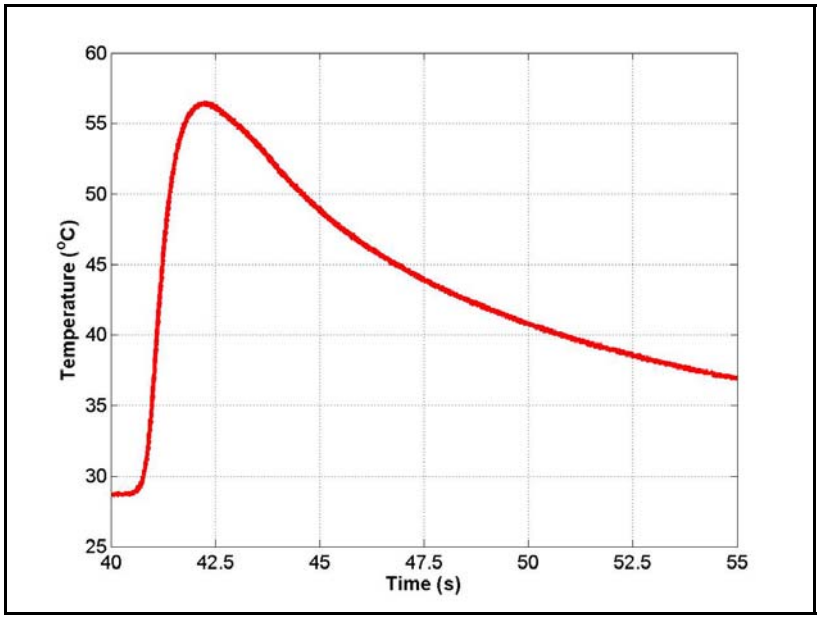

Figure 67. Temperature vs. time graph of T-Burner test with tank and cavitating venturi

4.2.2. Test2

In order to see the effect of the amount of MTV in the igniter content a second demonstration of the setup with tank and cavitating venturi is performed. System is pressurized to 45 bars with Nitrogen gas. In this test, the data is recorded at 50 kHz.

In this test amount of MTV inside the igniter is reduced to 0.2 gram. 1 gram of black powder is added to the igniter content. Recorded pressure data from two pressure transducers with respect to time is given in Figure 68 and Figure 69 respectively.

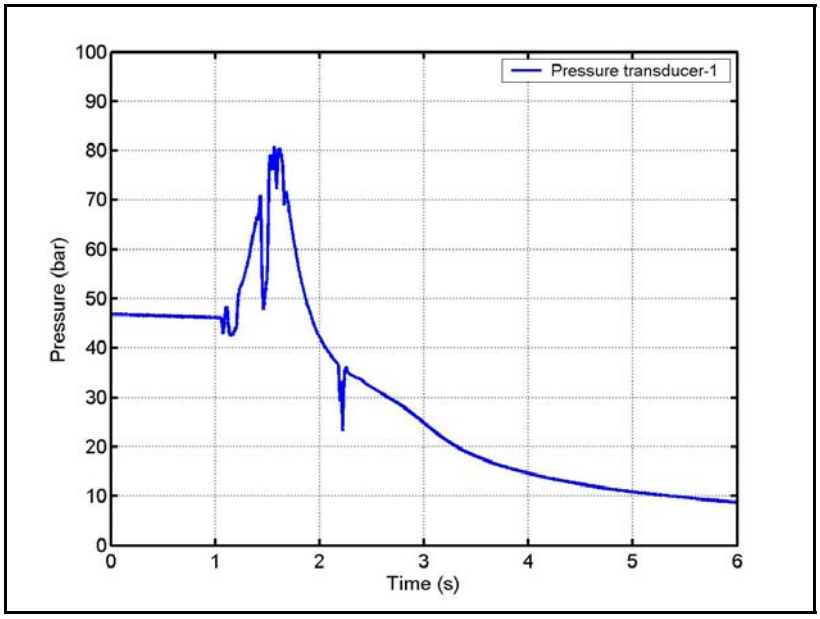

Figure 68. Pressure-time history for the T-Burner test with tank and cavitating venturi (1st pressure transducer)

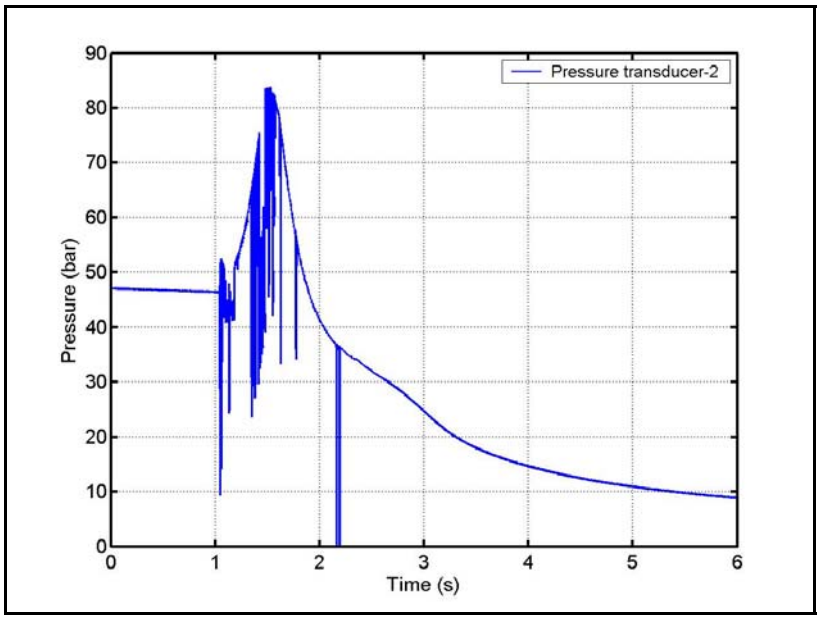

Figure 69. Pressure-time history for the T-Burner test with tank and cavitating venturi (2nd pressure transducer)

As it can be seen from both of the figures no oscillations could be obtained again. Also a mean constant pressure, which is a must of neutral burning, is not observed. For this specific test some unexplainable peaks of the pressure data is observed especially at the moment when the rupture disc is burst out.

This test shows that the content of the igniter does not play an important role for this setup which uses a surge tank and a cavitating venturi. It is thought that main reason for not observing oscillations may be the existence of the rupture disc and the cavitating venturi. Cavitating venturi seems not working properly and burst of the rupture disc seems to damp out the oscillations.

For these reasons, in order to see the effect of the pressure stabilization system which is used for the first alternative T-Burner setup, further tests are performed with the setup which uses a choked nozzle as the pressure stabilization system.

4.3. System Check-out Tests with T-Burner Setup with Choked Nozzle

In this section application of the T-Burner tests, following the procedures described in detail in section 3.2 is presented. For these tests, a specific solid propellant of TÜBİTAK-SAGE, which is used in a solid rocket motor, is used. This propellant is chosen because there exits huge amount of data exist about its burning characteristics. Another reason is about the manufacturing techniques used at TÜBİTAK-SAGE. Different from first alternative T-Burner tests which are described in Section 4.2 cylinder charged propellant is also used.

4.3.1. Test 1

In order to make a comparison between two T-Burner setups which uses different pressure stabilization systems, same test that is described in Section 4.2.2 is repeated without initial pressurization. The data is recorded at 50 kHz again. The igniter content and used propellant (end burning) are all the same with Section 4.2.2.

Recorded pressure data from two pressure transducers with respect to time is given in Figure 70. As it can be seen from this figure, the peaks that are thought to be a result of the burst of rupture disc and cavitating venturi are not observed in this setup. But still no oscillations and neutral burning could be observed.

It is thought that there exist two different causes for this situation. One is about the propellant burn area. Side burning, instead of a full end burning, may be happening because of the absence of liner.

Another reason may be the large interior volume of the T-burner tube. As it can be seen from Figure 70, maximum pressure obtained is approximately 50 bars instead of the design pressure 70 bars. It seems that the volume of the combustion

chamber is too large to be filled with this amount of mass flow rate generated by the end-burning propellants used.

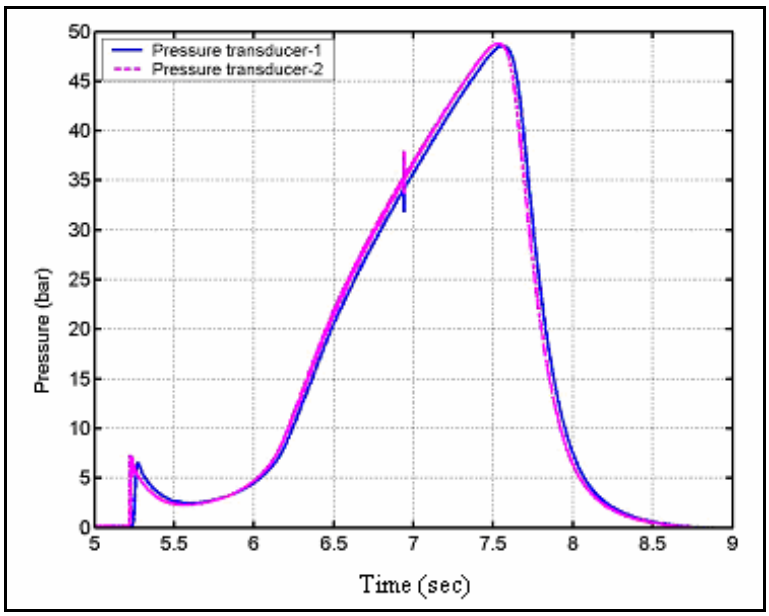

Figure 70. Pressure-time history for the T-Burner test with choked nozzle

4.3.2. Test 2

In order to fix the situation encountered in the previous experiment this time a propellant which will burn longer, 1.5 sec instead of 1 sec is used in the following tests.

Three tests are performed with the same configuration in order to see the repeatability. Recorded pressure data from two pressure transducers with respect to time are given in Figure 71, Figure 72 and Figure 73 respectively. As it can be seen from these figures, results did not change a lot except a little increase in the maximum pressure. Still no oscillations and neutral burning could be observed.

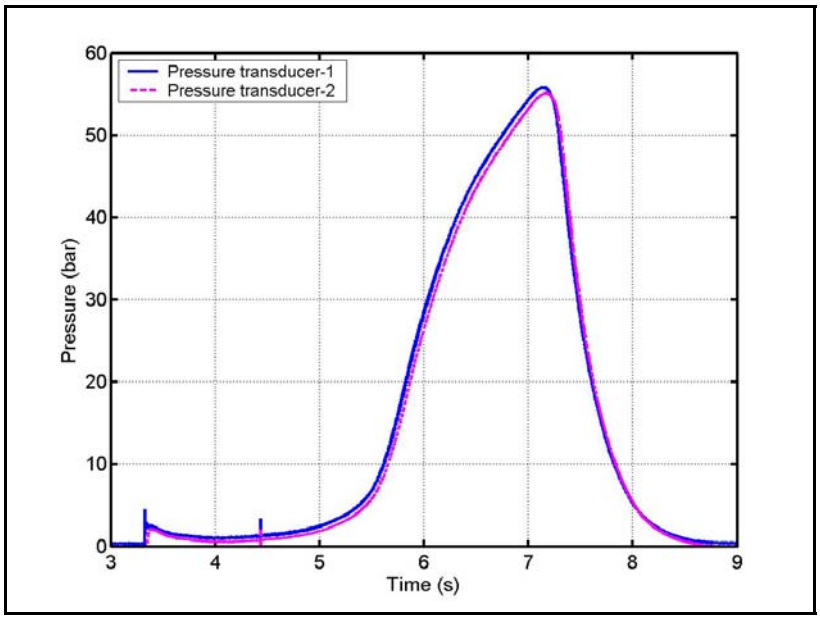

Figure 71. Pressure-time history for the T-Burner test with choked nozzle

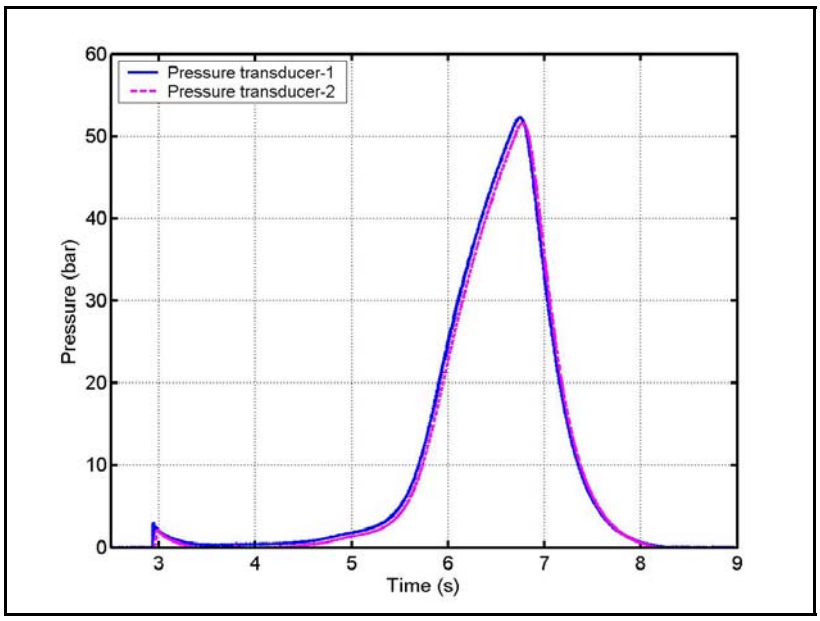

Figure 72. Pressure-time history for the T-Burner test with choked nozzle

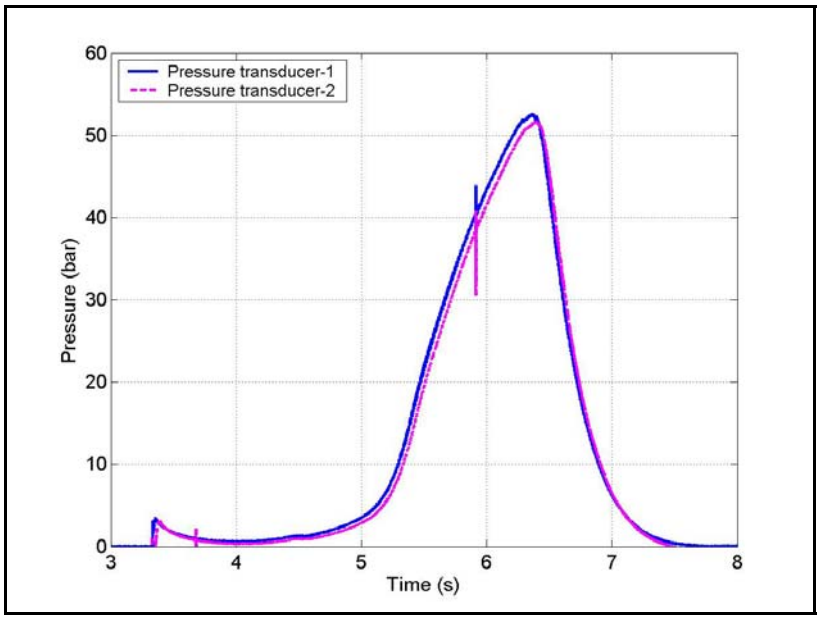

Figure 73. Pressure-time history for the T-Burner test with choked nozzle

A similar result is observed by Villela, [43] (Figure 74). In their study they have studied four different types of propellants. The T-Burner setup they have used is very similar to the first alternative used in this study, which has a surge tank and cavitating venturi. Main difference between their setup and the setup used in this study is that they are using a large surge tank which itself provides a stable pressure without the usage of a passive control element such as cavitating venturi.

When the results of Villela are investigated, it can be observed that although they are using a large surge tank, they could not be able to achieve neutral burning. Their system is for variable tube length, but for approximately 200 tests, they could not obtain any oscillations.

Both in Villela's study and in this study up to now, end burning propellants are used to obtain neutral burning. In this thesis, it is decided that use of a cylinder charged propellant which will provide more mass flow rate to the combustion

chamber may be the solution of the common problem encountered both in this study and Villela's study.

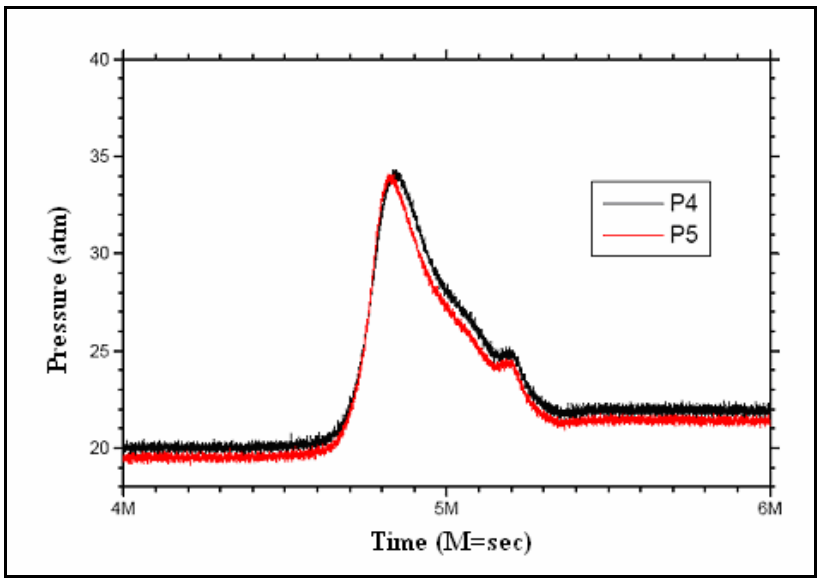

Figure 74. Pressure-time history of Villela's T-Burner [43]

4.3.3. Test 3

In order to validate the decision mentioned above a 1-D internal ballistics simulation is performed by the experts in TÜBİTAK-SAGE for the T-Burner setup constructed. In order to simulate the pressurization period, 1-D unsteady Euler equations (conservation of mass, momentum and energy) were solved numerically by employing 2nd order space and time accurate Roe's approximate Riemann solver. The wall boundary conditions were applied at the left and right end of the T burner. Combustion products were modeled as mass, momentum and energy sources in the conservation equations. The choked nozzle mass, energy and momentum fluxes were also modeled as source terms. The initial chamber filling period was calculated above 2 seconds which is consistent with the experimental observations.

In Figure 75, pressure versus time graph obtained from this simulation is presented. As it can be seen from this figure, with the setup constructed there is no possibility of obtaining a constant pressure that means neutral burning, with the use of the end burning propellant. Figure came out to be very similar to the experimental measurements. It can be concluded from this figure that the present propellant geometry and amount is not sufficient to obtain a neutral burning inside the combustion chamber. It can be concluded that absence of sufficient amount of mass flow rate inside the tube does not allow generation of oscillations. What is generated inside is damped out.

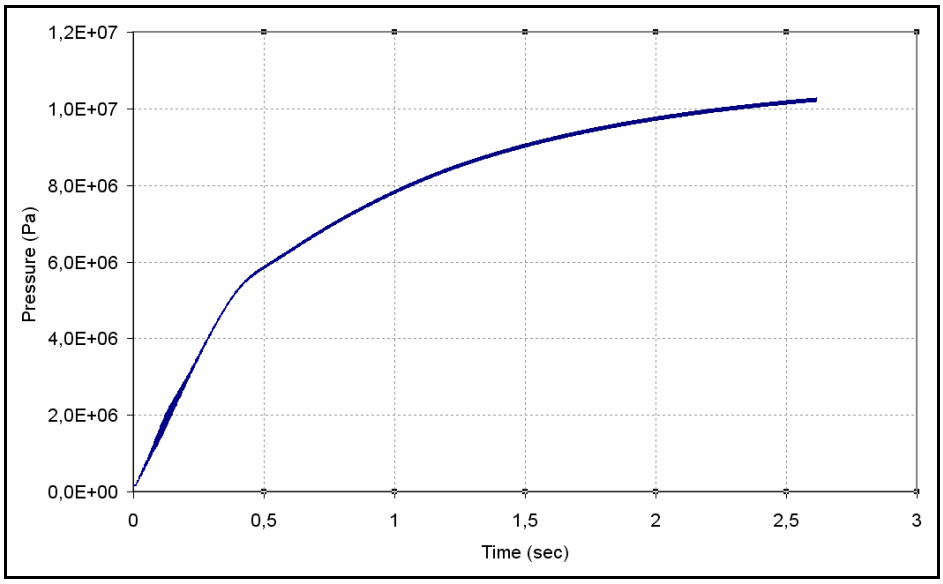

Figure 75. Pressurization simulation of the chamber with circular end burning propellant configuration

In order to obtain more mass flow rate from the combustion, burning area of the propellant has to be increased. With the present end burning propellant it is not possible to increase the burn area due to the geometric limitations of the T-Burner tube. So, a cylinder charged propellant that provides neutral burning, which is previously proven with ground tests, is adapted to the T-Burner setup. Since the burn area is higher it is essential to re-design the choked nozzle exit diameter.

Such a propellant was previously manufactured for ground test purposes. In order to accelerate the experiment, one side of the T-Burner tube is closed and one propellant charge is installed to the other side by appropriate adapters. It is expected that the pressure waves will reflect from the closed part and return back to give a similar result which is expected from an original T-Burner setup.

Recorded pressure data from two pressure transducers with respect to time is given in Figure 76. As it can be seen from this figure, from one of the pressure transducers, oscillations in pressure data are obtained. These sinusoidal oscillations can be observed more clearly in the close-up view of the data, Figure 77. As it can be seen the other pressure transducer does not show any oscillation. This is most possibly because of the dynamic calibration of the transducers. All of the transducers used in this study are statically calibrated but dynamic behaviours of them are unfortunately unknown. This test showed that such a dynamic calibration is necessary for these types of T-Burner experiments.

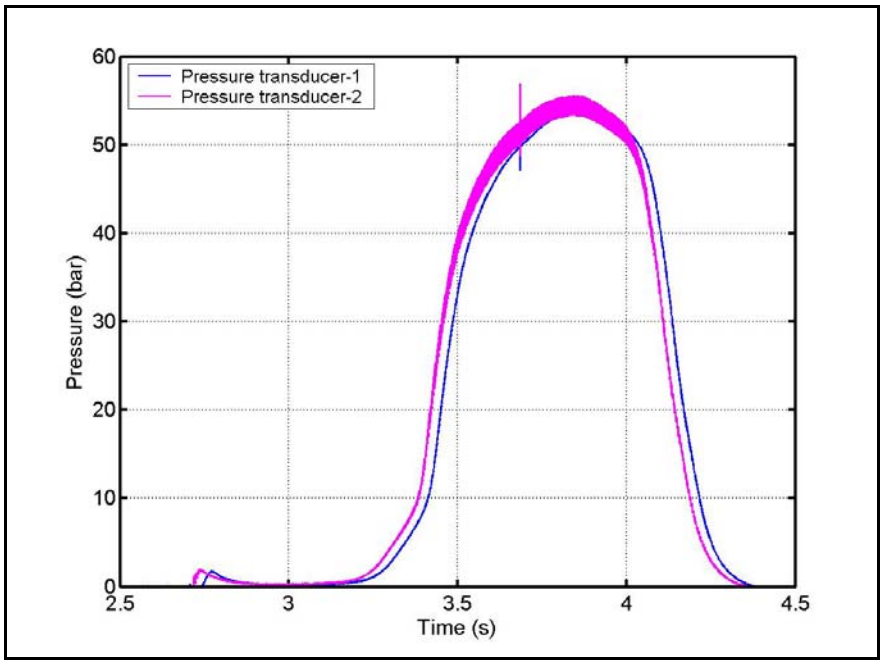

Figure 76. Pressure-time history for the T-Burner test with choked nozzle

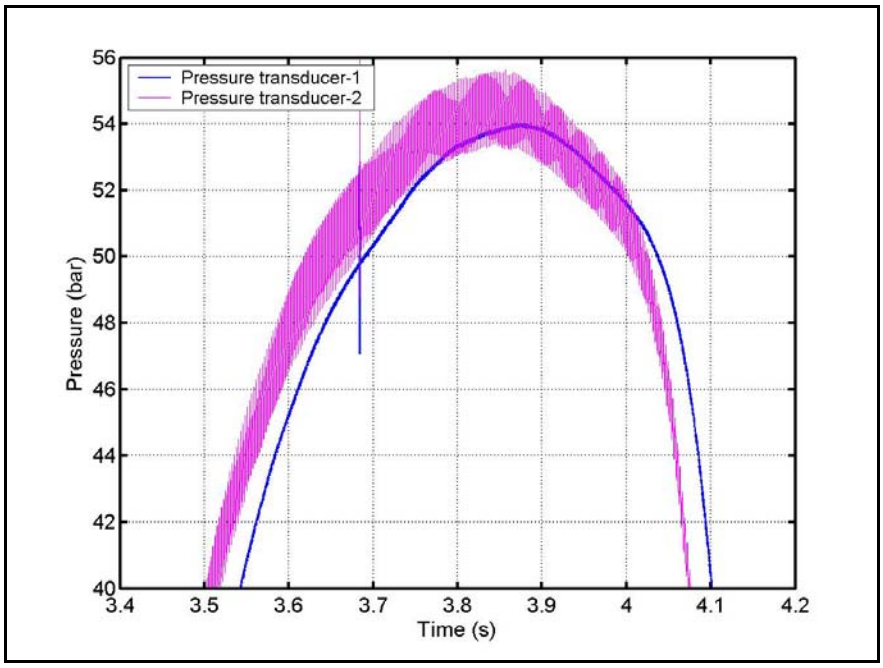

Figure 77. Close-up view of the pressure-time history for the T-Burner test with choked nozzle

An approximately neutral burning behaviour is obtained but it is hard to take a mean pressure from these figures. For this purpose, in order to apply data reduction techniques described in Section 3, a data fit of the evaluated data is performed and data is subtracted from this equation, Figure 79. By this way it is possible to observe the growth and decay rates of the oscillations which are necessary for the evaluation of pressure response of the propellant.

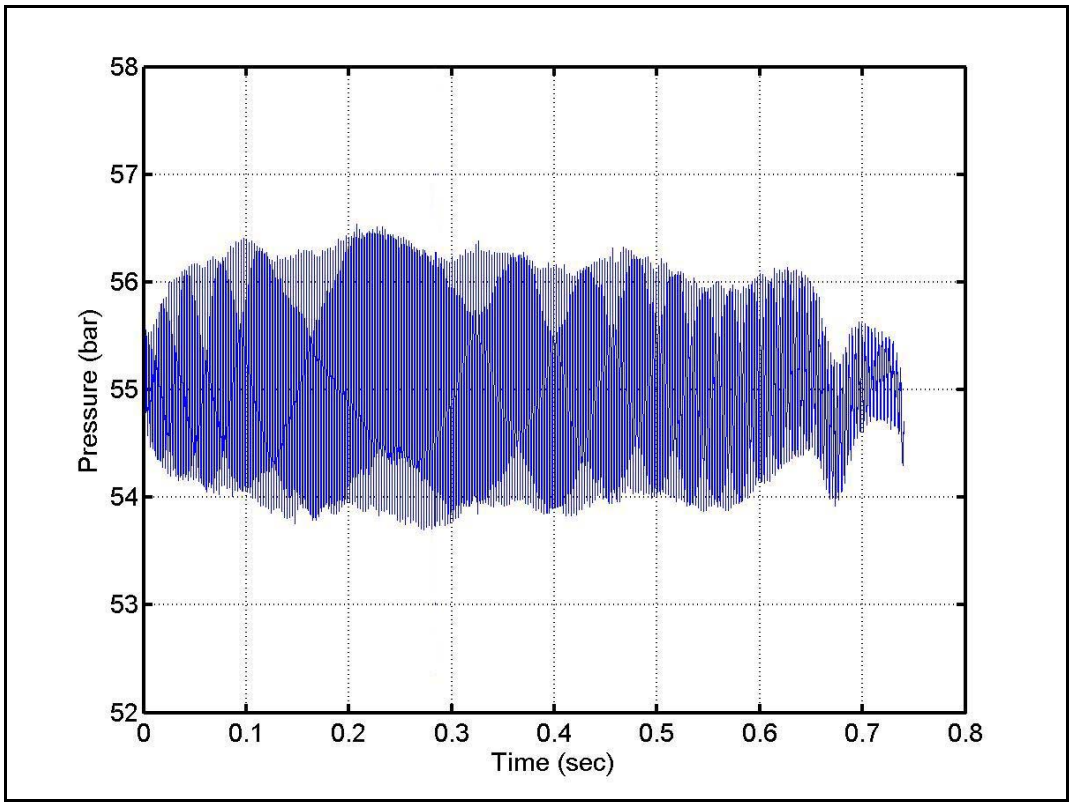

Figure 78. Evaluated pressure-time history for the T-Burner test with choked nozzle

Figure 79 and Figure 80 shows the growth and decay rates of the oscillations. Mean pressure of the test is taken as approximately 55 bars. Approximate evaluation of the growth rate of oscillations and decay rate of oscillations seperately can be performed by taking the ratio of $\ln\left(\frac{P}{\hat{P}}\right)$ with elapsed time in the measured data. From Figure 79 and Figure 80, growth and decay rate of oscillations are computed to be 0.52 sec^{-1} and -0.63 sec^{-1}.

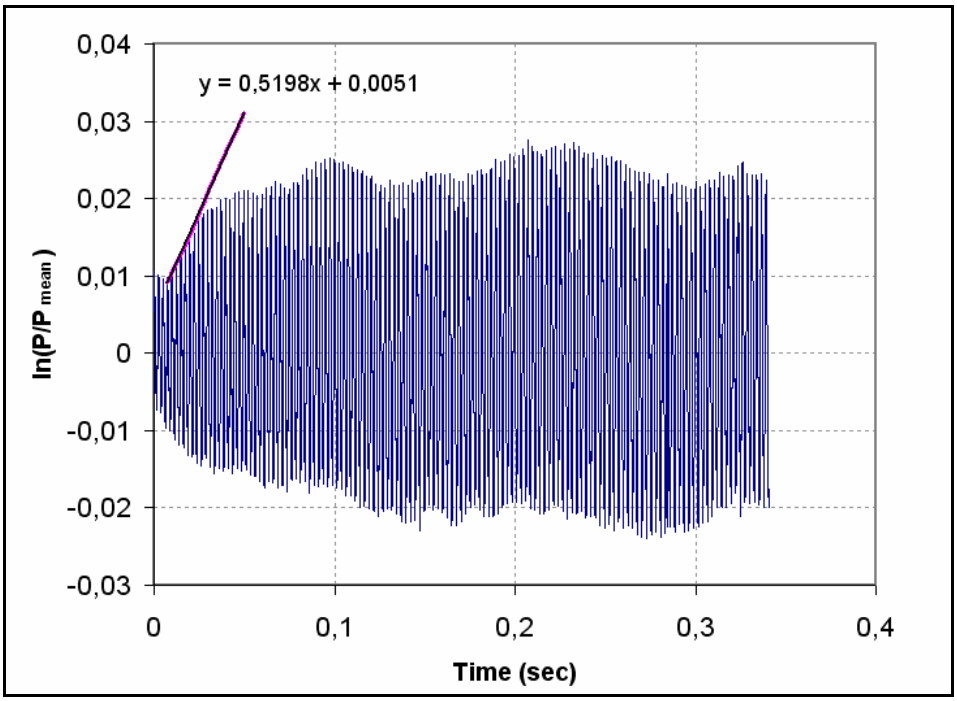

Figure 79. Growth rate of the pressure oscillations

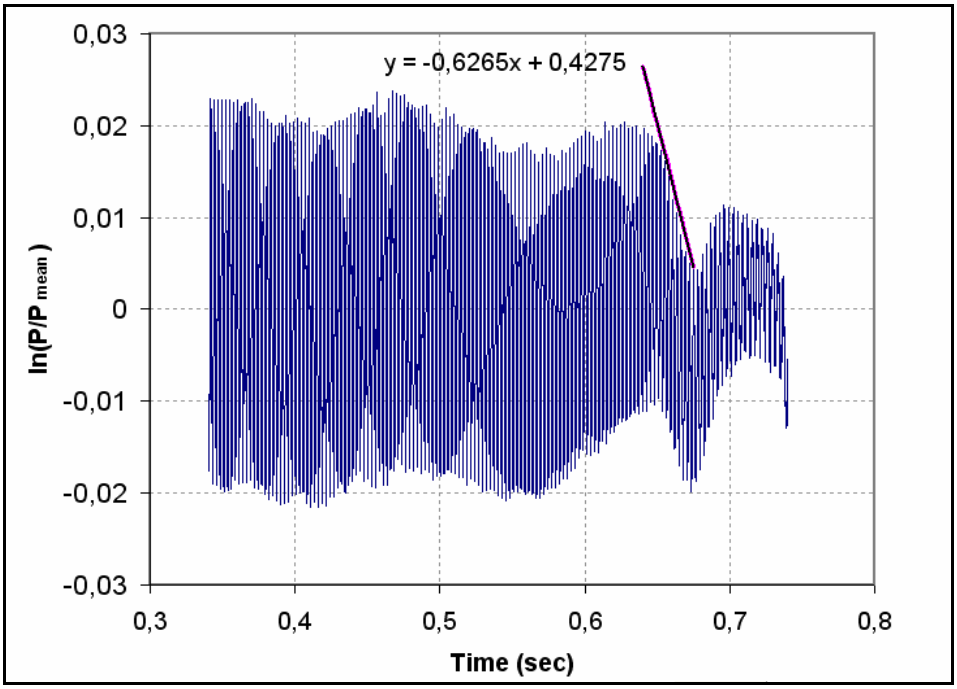

Figure 80. Decay rate of the pressure oscillations

The frequency spectrum of the test is shown in Figure 81. The burner length is 1m as it mentioned before. Then, the average velocity of sound in the burner as indicated by the frequency (a_m) is computed as 768 m/sec ($a_m = 2fL$). The adiabatic flame temperature and mean burning rate of the solid propellant are evaluated form internal ballistics analysis as 3000 K and 12.2 mm/s respectively. After substituting the necessary values in to Equation (3.4), the pressure response of the propellant is calculated as 0.02.

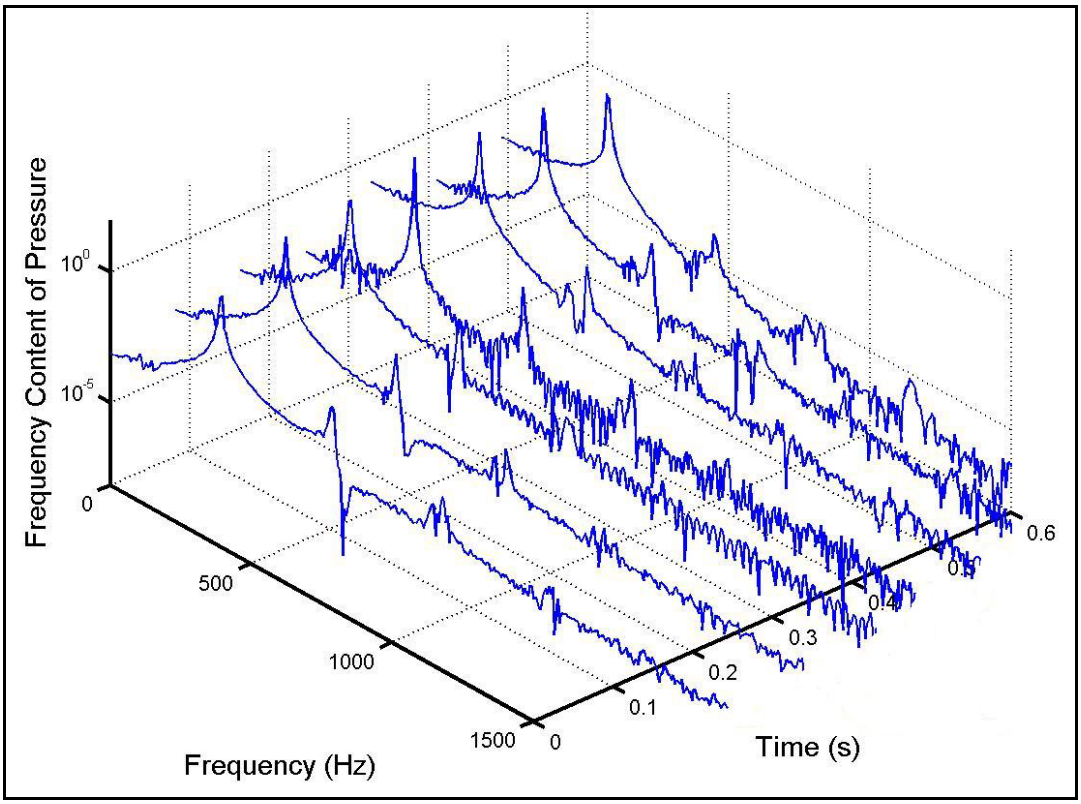

Figure 81. Frequency spectrum of T-Burner, waterfall diagram

4.4. Helmholtz Instability Investigation

Helmholtz resonator (HR) is named after Hermann Ludwig Ferdinand von Helmholtz (1821-1894), the German scientist who worked out the design equation

for the resonator. Essentially, a Helmholtz resonator consists of two parts, a rigid-walled cavity of volume V, and a neck or an opening with area S and length L. The classical formula for calculation of the resonance frequency of the Helmholtz resonator is as shown the following, which can be found in every standard acoustic text book:

$$f = \frac{c}{2\pi}\sqrt{\frac{S}{VL}} \tag{3.4}$$

where c is the speed of sound.

Helmholtz frequency of the T-burner in the current study is calculated as 88 Hz utilizing the given formulation. As it can be seen from the FFT of previous test data, no Helmholtz instability is observed. As a result, it can be stated that the acoustic design of the T-Burner is correct.

CHAPTER 5

DISCUSSION AND CONCLUSION

In this study, experimental investigation of solid propellant combustion instability using an end burning T-Burner setup is performed. For this purpose, a T-Burner setup is designed, analyzed, constructed and tested with all its sub components.

T-Burner setup is mainly composed of a base part, a control panel and the T-Burner itself. Combustion chamber, pressure stabilization mechanism, pressurization system, measurement instruments and data acquisition systems form the T-Burner.

Pressure stabilization mechanism is utilized in two different alternatives, first of which is by the use of nitrogen gas and a small surge tank with a cavitating venturi. This is a brand new approach for this kind of system. The second alternative was to introduce a choked nozzle for pressure stabilization

The main usage of a T-Burner setup is to compare the behavior of different propellants qualitatively. Evaluation of the response function of a specified solid propellant is also another usage.

All necessary design, analysis and test efforts are carried out for all sub components of the T-Burner and a system design is also performed. Appropriate materials for all parts are selected. Production of sub systems and system assembly are performed. Measurement instruments and data acquisition system are coupled

with the T-Burner. All of these efforts resulted in a T-Burner test setup which can be used for the areas stated above.

Constructed T-Burner setup is the first and only one in Turkey for these types of applications. All of the sub components except the measurement instruments and data acquision system are manufactured in Turkey. Use of a cavitating venturi in such an application for the stabilization of the pressure is a brand new approach.

T-Burner setup with tank and cavitating venturi is tested for a specific solid propellant. This solid propellant is used for a rocket motor which was statically tested previously. No oscillations could be obtained using tank with cavitating venturi scheme. Also a mean constant pressure, which is a must of neutral burning, is not observed. For this specific test some unexplainable peaks of the pressure data is observed especially at the moment when the rupture disc is burst out. The shocks generated during the disc rupture and cavitating flow, could inversely affect the burning rate oscillations.

For these reasons, in order to see the effect of the pressure stabilization system which is used for the first alternative T-Burner setup, further tests are performed with the setup which uses a choked nozzle as the pressure stabilization system.

In order to make a comparison between two T-Burner setups which uses different pressure stabilization systems, same test that is described in Section 4.2.2 is repeated without initial pressurization. Unfortunately, still no oscillations and neutral burning could be observed.

It is thought that there exist two different causes for this situation. One is about the propellant burn area. Side burning, instead of a full end burning, may be happening because of the absence of liner.

Another reason may be the amount of the propellant gases that fills the T-Burner tube. It seems that the volume of the combustion chamber is too large to be filled with this amount of mass flow rate generated by the end-burning propellants used.

To understand the real reason behind the absence of neutral burning and oscillations, 1-D internal ballistics simulation is performed by TÜBİTAK-SAGE for the T-Burner setup constructed. It is concluded that, with the setup constructed there is no possibility of obtaining a constant pressure that means neutral burning, with the use of the end burning propellant. The present propellant geometry and amount is not sufficient to obtain a neutral burning inside the combustion chamber. It can also be concluded that absence of sufficient amount of mass flow rate inside the tube does not allow generation of oscillations. What is generated inside is damped out.

In order to obtain more mass flow rate from the combustion, burning area of the propellant has to be increased. With the present end burning propellant it is not possible to increase the burn area due to the geometric limitations of the T-Burner tube. So, a cylinder charged propellant that provides neutral burning, which is previously proven with ground tests, is adapted to the T-Burner setup. Since the burn area was higher it was essential to re-design the choked nozzle exit diameter.

Such a propellant was previously manufactured for ground test purposes. In order to accelerate the experiment, one side of the T-Burner tube is closed and one propellant charge is installed to the other side by appropriate adapters. It is expected that the pressure waves will reflect from the closed part and return back to give a similar result which is expected from an original T-Burner setup.

In Figure 76 oscillations in pressure data were shown. However one of the pressure transducers did not show any oscillation. This is most possibly because of the dynamic calibration of the transducers. All of the transducers used in this study

are statically calibrated but dynamic behaviours of them are unfortunately unknown. This test showed that such a dynamic calibration is necessary for these types of T-Burner experiments.

Since oscillations are observed, growth and decay rate and frequency of oscillations are calculated together with data processing to evaluate response function.

In the upcoming studies including the T-Burner setup with choked nozzle, experimenting with twin propellant scheme has the priority. Pressurizing the system and pressurized testing will be of the next importance.

For the setup with surge tank and the cavitating venturi, future works will include cylindrical charged propellant tests to see if neutral burning and oscillations can be seen. Cavitating venturi and rupture disc designs will be re-evaluated to overcome any design flows.

For both of these mentioned setups, a constant length of burning chamber is used. To form a dataset, different lengths of burning chambers, which corresponds to different frequency values will be tested. Finally these dataset will be utilized to construct the frequency – pressure response characteristics of the propellant. Constructed T-burner may well be utilized for many different cases of propellants leading to an effective and easy to use tool for combustion instability studies.

REFERENCES

1. Sutton, G. P., Rocket Propulsion Elements, Sixth Edition, John Wiley and Sons, 1992.

2. Ak, M. A., *"Analysis of Transient Regimes in Solid Rocket Propulsion,"* Ph.D. Thesis in Mechanical Engineering, METU, 2001.

3. Price, E. W., *"Experimental Observations of Combustion Instability,"* Fundamentals of Solid-Propellant Combustion, Kuo, K. K., and Summerfield, M., Progress in Astronautics and Aeronautics, Vol. 90, AIAA Inc., New York, 1984, pp. 733-790.

4. Culick, F. E. C., *"Calculation of the Admittance Function for a Burning Surface,"* Astronautica Acta, Vol. 13, 1967, pp. 221 – 237.

5. Culick, F. E. C., *"A Review of Calculations for Unsteady Burning of a Solid Propellant,"* AIAA Journal, Vol. 6, 1968, pp. 2241-2255.

6. Price, E. W., *"L* Instability,"* Fundamentals of Solid-Propellant Combustion, Kuo, K. K., and Summerfield, M., Progress in Astronautics and Aeronautics, Vol. 90, AIAA Inc., New York, 1984, pp. 325-362.

7. Razdan, M. K., and Kuo, K. K. *"Erosive Burning of Solid Propellants,"* Fundamentals of Solid-Propellant Combustion, Kuo, K. K., and Summerfield, M., Progress in Astronautics and Aeronautics, Vol. 90, AIAA Inc., New York, 1984, pp.515-598.

8. Price E. W., and Sofferis, J. W., *"Combustion Instability in Solid Propellant Rocket Motors,"* Jet Propulsion, Vol. 28, March 1958, pp. 190-192.

9. Mihlfeith, C. M., and Sayer, L., *"Combustion Instability of Low Smoke Propellants in Ballistic Test Motors and in the T-Burner,"* AIAA Paper 74-202, Washington, DC, Jan. 1974.

10. Miller, R. R., Donohue, M.T., Yount, R. A., and Martin, J. R., *"Control of Solids Distributions in HTPB Propellants,"* Hercules Inc. Allegany Ballistics Lab., AFRPL TR-78-14, April 1978.

11. Strand, L. D., and Cohen, N. S., *"Effect of HMX on the Combustion Response Function,"* Journal of Spacecraft and Rockets, Vol. 17, No. 6, 1980, pp. 566-568.

12. Brown, R. S., Erickson, J. E., and Babcock, W. R., *"Combustion Instability Study of Solid Propellants,"* United Technologies Corp., United Technology Center, AFRPL TR-73-42, June 1973.

13. Brown, R. S., Erickson, J. E., and Babcock, W. R., *"Combustion Response Function Measurements by the Rotating Valve Method,"* AIAA Journal, Vol. 12, No. 11, 1974, pp. 1502-1510.

14. Baum, J. D., Daniel, B. R., and Zinn, B. T., *"Determination of Solid Propellant Admittances by the Impedance Tube Method,"* AIAA Paper 80-0281, Pasadena, CA, Jan. 1980.

15. Zinn, B. T., and Narayanaswami, L. L., *"Application of the Impedance Tube Technique in the Measurement of the Driving Provided by Solid Propellants Using Combustion Instabilities,"* Acta Astronautica, Vol. 9, No. 5, pp. 305-313.

16. Zinn, B. T., Salikuddin, M., Daniel, B. R., and Bell, W. A., *"Solid Propellant Admittance Measurement by the Driven Tube Method,"* Georgia Institute of Technology, AFOSR TR-76-1211, Atlanta, GA, Aug. 1976.

17. Strand, L. D., Magiawala, K. R., and MacNamara, R. P., *"Microwave Measurement of the Solid Propellant Pressure-Coupled ResponseFunction,"* Journal of Spacecraft and Rockets, Vol. 17, No. 6, 1980, pp. 483-488.

18. Wilson, J. R., and Micci, M. M., *"Direct Measurement of High Frequency Solid Propellant Pressure-Coupled Responses,"* Journal of Propulsion and Power, Vol. 3, No. 4, 1987, pp. 296-302.

19. Strand, L. D., Brown, R. S., *"Laboratory Test Methods for Combustion-Stability Properties of solid Propellants,"* Nonsteady Burning and Combustion Stability of Solid Propellants, AIAA Inc., Vol. 143, 1990.

20. Stepp, E. E., *"Effect of Pressure and Velocity Coupling on Low-Frequency Instability,"* AIAA Journal, Vol. 5, No. 5, 1967, pp. 945-948.

21. Beckstead, M. W., and Butcher, A. G., *"The Velocity Coupled T-Burner,"* AIAA Paper 74-200, Washington, DC, Jan. 1974.

22. Micheli, P. L., *"Investigation of Velocity Coupled Combustion Instability,"* Aerojet Solid Propulsion Co., AFRPL TR 76-100, Jan 1977.

23. Brown, R. C., Willoughby, P. G., and Kelly, V. L., *"Rotating Valve for Velocity Coupled Combustion Response Studies,"* AIAA Paper 77-975, Orlando, FL, July 1977.

24. Brown, R. S., Waugh, R. C., and Kelly, V. L., *"Rotating Valve for Velocity Coupled Combustion Response Measurements,"* Journal of Spacecraft and Rockets, Vol. 19, No. 5, 1982, pp. 437-444.

25. Eisel, J. L., and Dehority, G. L., *"A Technique for Investigating Low Frequency Velocity-Coupled Combustion Instability,"* Chemical Propulsion Information Agency Publication 105, May 1966, pp. 703-712.

26. Narayanaswami, L. L., *"Investigation of the Pressure- and Velocity-Coupled Responses of Solid Propellants Using the Impedance Tube Technique,"* Ph.D. Dissertation, Georgia Institute of Technology, Atlanta, GA, 1984.

27. Narayanaswami, L. L., Zinn, B. T., and Daniel, R. B., *"Experimental Investigation of Characteristics of Solid Propellant, Velocity-coupled Response Functions,"* AIAA Journal, Vol. 25, No. 4, 1987, pp. 584-591.

28. Micci, M. M., Taylor, R. D., Chung, I., and Colozza, A., *"Magnetic Flowmeter Measurement of Solid Propellant Pressure-Coupled and Velocity-Coupled Rsponses,"* Pennsylvania State Univ., AFAL-TR 88-075, University Park, PA, Nov. 1988.

29. Crump, J. E., Mathes, H. B., Clark, W. H., and Beckstead, M. W., *"Motor Test Data Comparisons with Laboratory Data and Stability Predictions,"* Chemical Propulsion Information Agency Publication 476, Vol. I, Laurel, MD, Oct. 1987, pp. 101-114.

30. Micci, M. M., *"Workshop Report: Methods for Measuring Solid Propellant Combustion Response,"* Chemical Propulsion Information Agency Publication 457, Vol. I, Laurel, MD, Oct. 1986, pp. 51-57.

31. Price, E. W., *"Combustion Instability in Solid Propellant Rocket Motors,"* Astronautica Acta, Vol. 5, No.1, 1959, pp. 63-72.

32. Price, E. W., *"Review of Experimental Research on Combustion Instability of Solid Propellants,"* Solid Propellant Rocket Research, Vol. 1, edited by M. Summerfield, ARS Progress in Astronautics and Rocketry, Academic, New York, 1960, pp. 561-602.

33. Price, E. W., Mathes, H. B., Crump, J. E., and McGie, M. R., *"Experimental Research in Combustion Instability of Solid Propellants,"* Combustion and Flame, Vol. 5, June 1961, p. 149.

34. Price, E. W., *"Review of the Combustion Instability Characteristics of Solid Propellants,"* AGARD Proceedings No. 1, 1968, pp. 141-194.

35. *"Corrosion Chart,"*HOKE Incorporated, Spartanburg, USA.

36. Beer, F. P. and Johnston, E. R., *"Mechanics of Materials,"* McGraw-Hill Ryerson Limited, SI Metric Edition, 1987.

37. Cullick, F. E. C., *"T-Burner Testing of Metalized Solid Propellants,"* California Institute of Technology, October 1974.

38. Yazıcı, B., Gündüz, D. E., Püskülcü, G., Yıldırım, C., Sümer, B., Orhan, F. E., Gönç, L. O., and Ak, M. A., *"Passive Flow Rate Control of the Fuel and the Oxidizer in Liquid Fuelled Rocket Motors,"* TÜBİTAK SAGE, Ankara.

39. Schmidt, D. P., and Corradini, M. L., *"One-Dimensional Analysis Of Cavitating Orifices,"* Engine Research Center, University of Wisconsin Madison, WI 53706.

40. Fox Venturi Products, *"Bulletin 052"*, www.foxvalve.com, Last Accessed Date: November 2005.

41. Aerochemistry Division, Research Department, U.S. Naval Weapons Center, *"Experimental Studies on the Oscillatory Combustion of Solid Propellants,"* Rept. NWC TP 4393, March 1969.

42. Blomshield, F. S., *"T-Burner Response Analysis Using the SPP/SSP Code,"* Naval Air Warfare Center, China Lake, CA 93555.

43. Villela, T. E. A., *"Emprego Do Queimador T ("T-Burner") Para a Pesquisa de Instabilidades de combustão em Propelentes Sólidos,"* INPE, São José dos Campos, 2004.

APPENDICES

A. TECHNICAL DRAWINGS

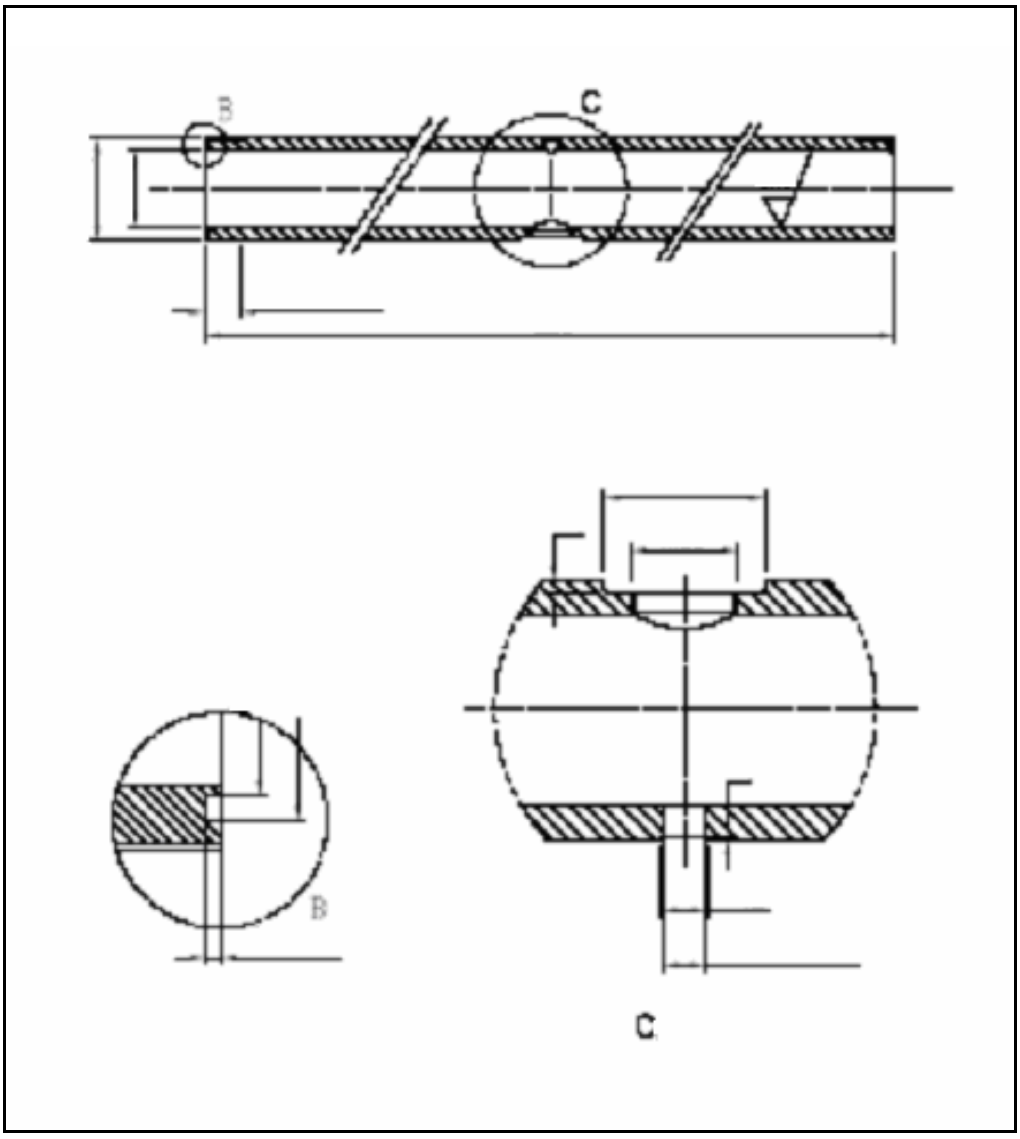

Figure 82. Technical drawing of T-Burner Tube

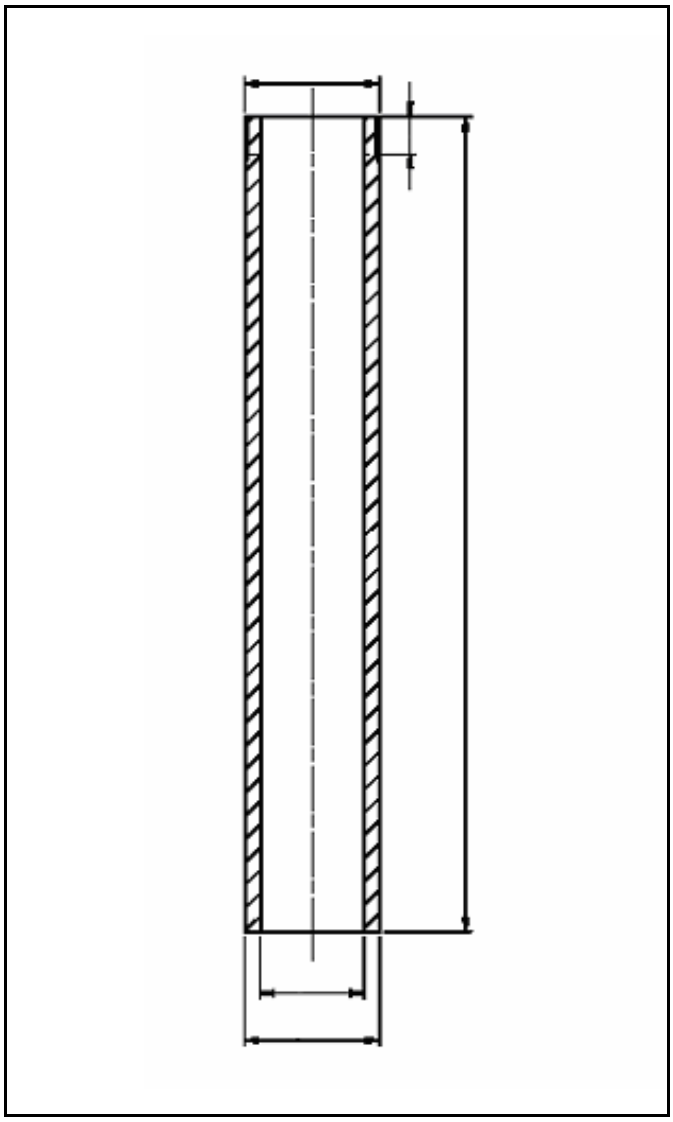

Figure 83. Technical drawing of Vent Exit Pipe

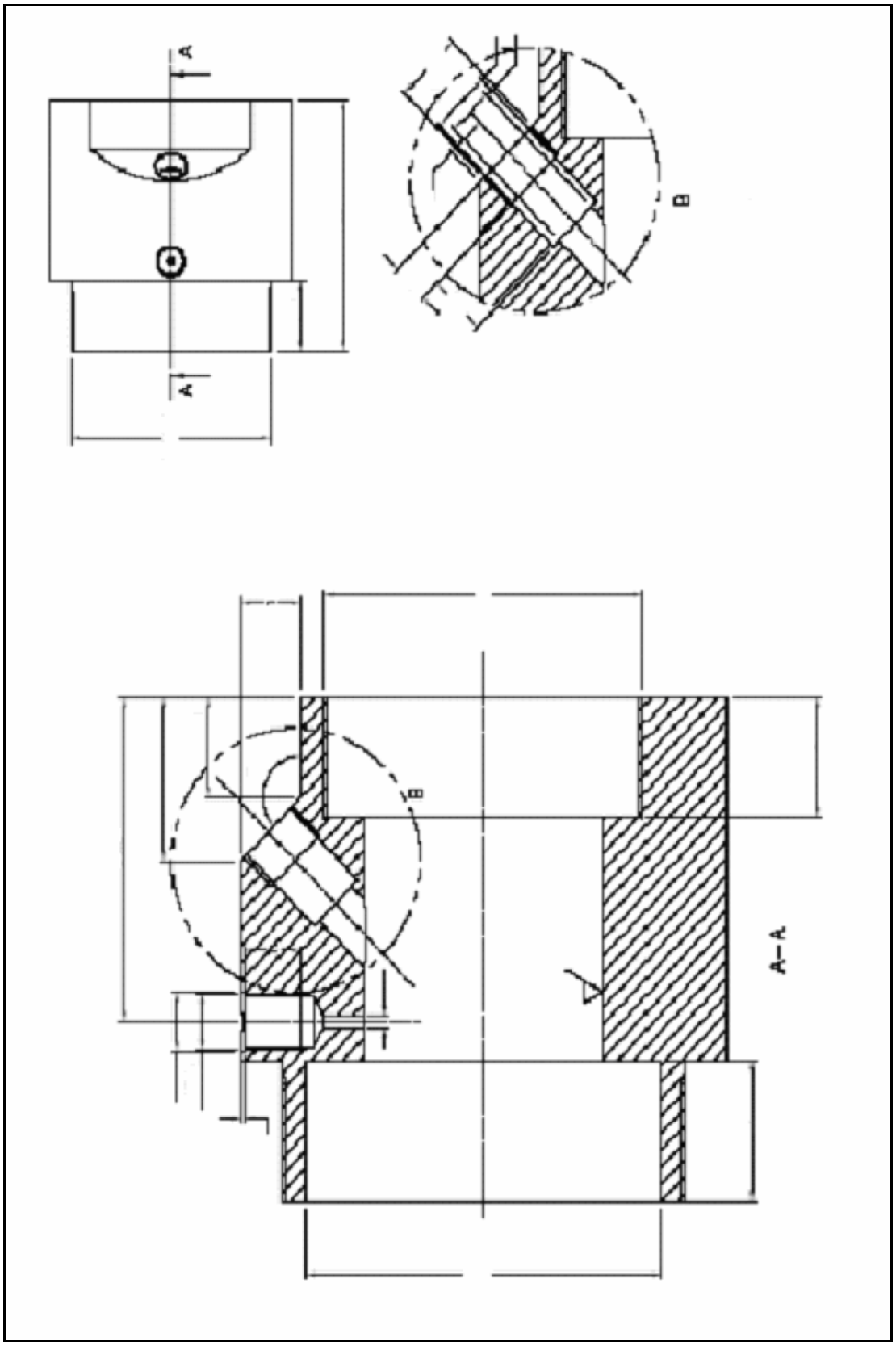

Figure 84. Technical drawing of Adapter

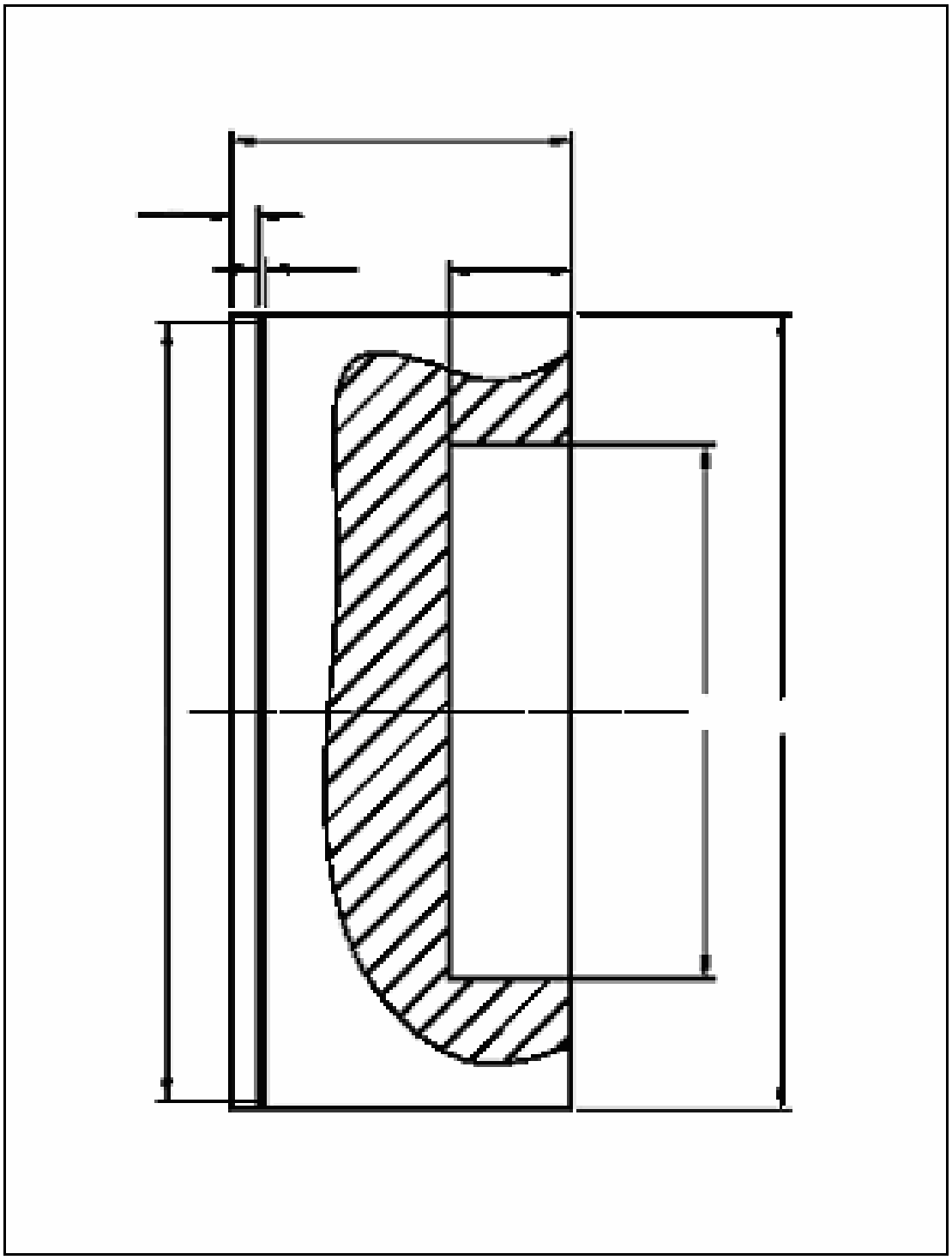

Figure 85. Technical drawing of Propellant Holder

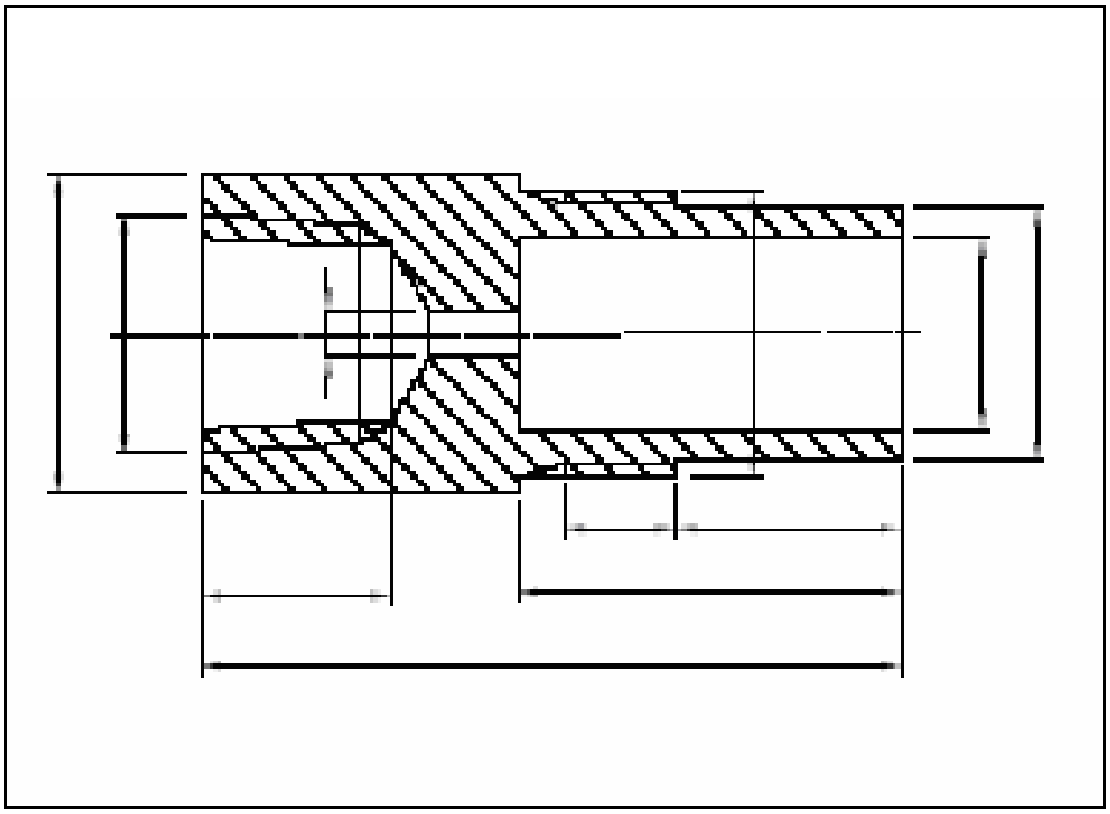

Figure 86. Technical drawing of Igniter Body

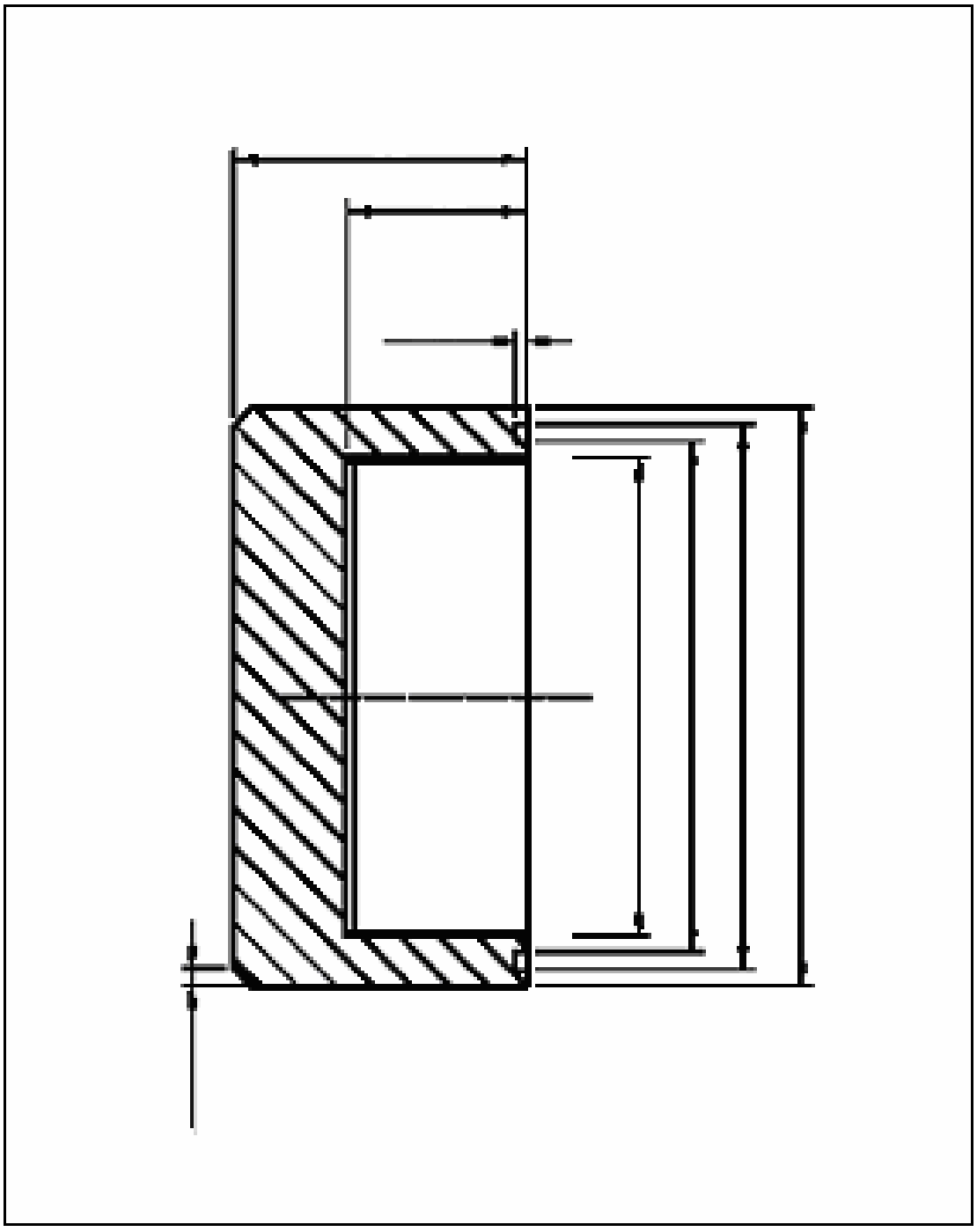

Figure 87. Technical drawing of End Cap

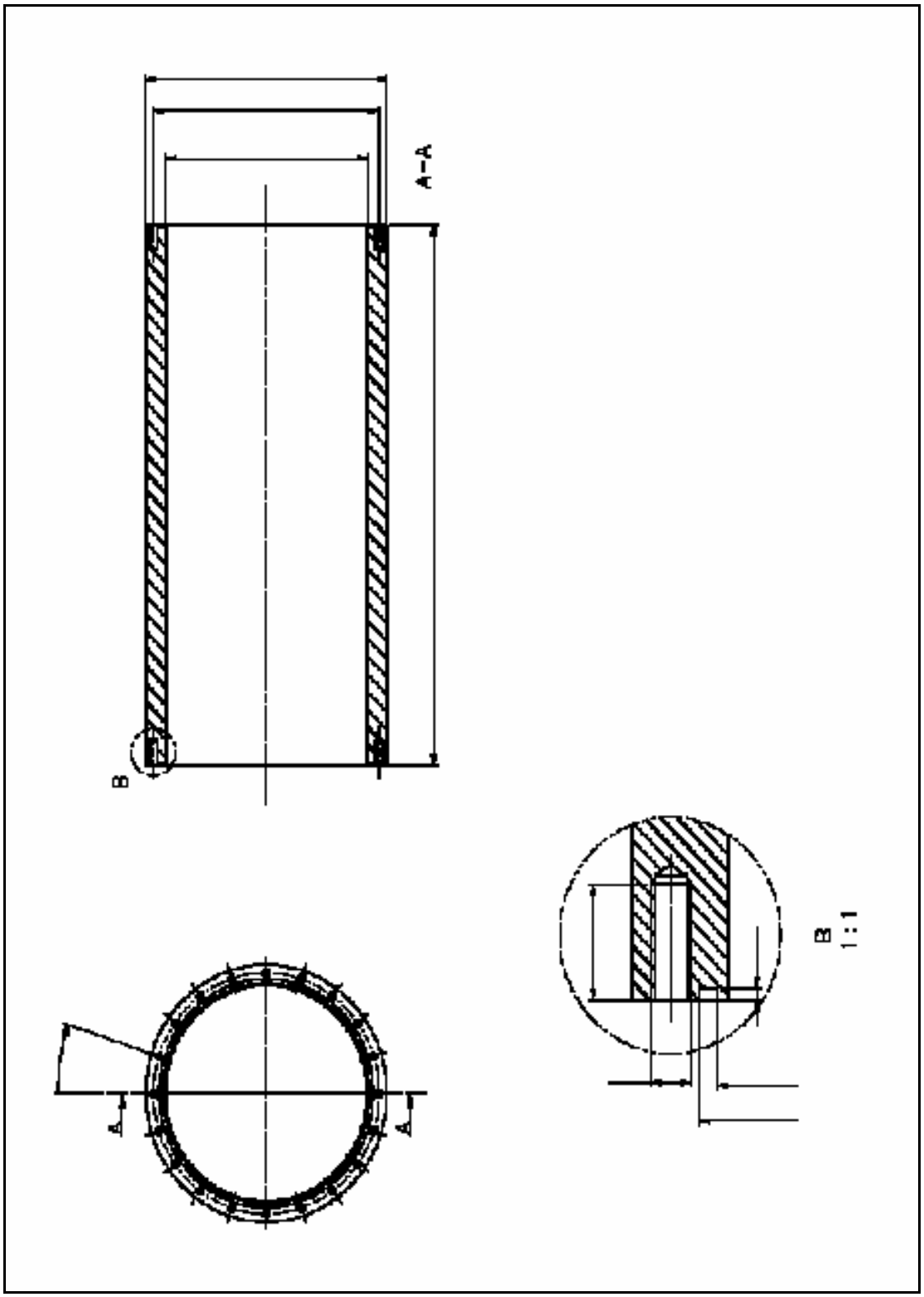

Figure 88. Technical drawing of Tank Body

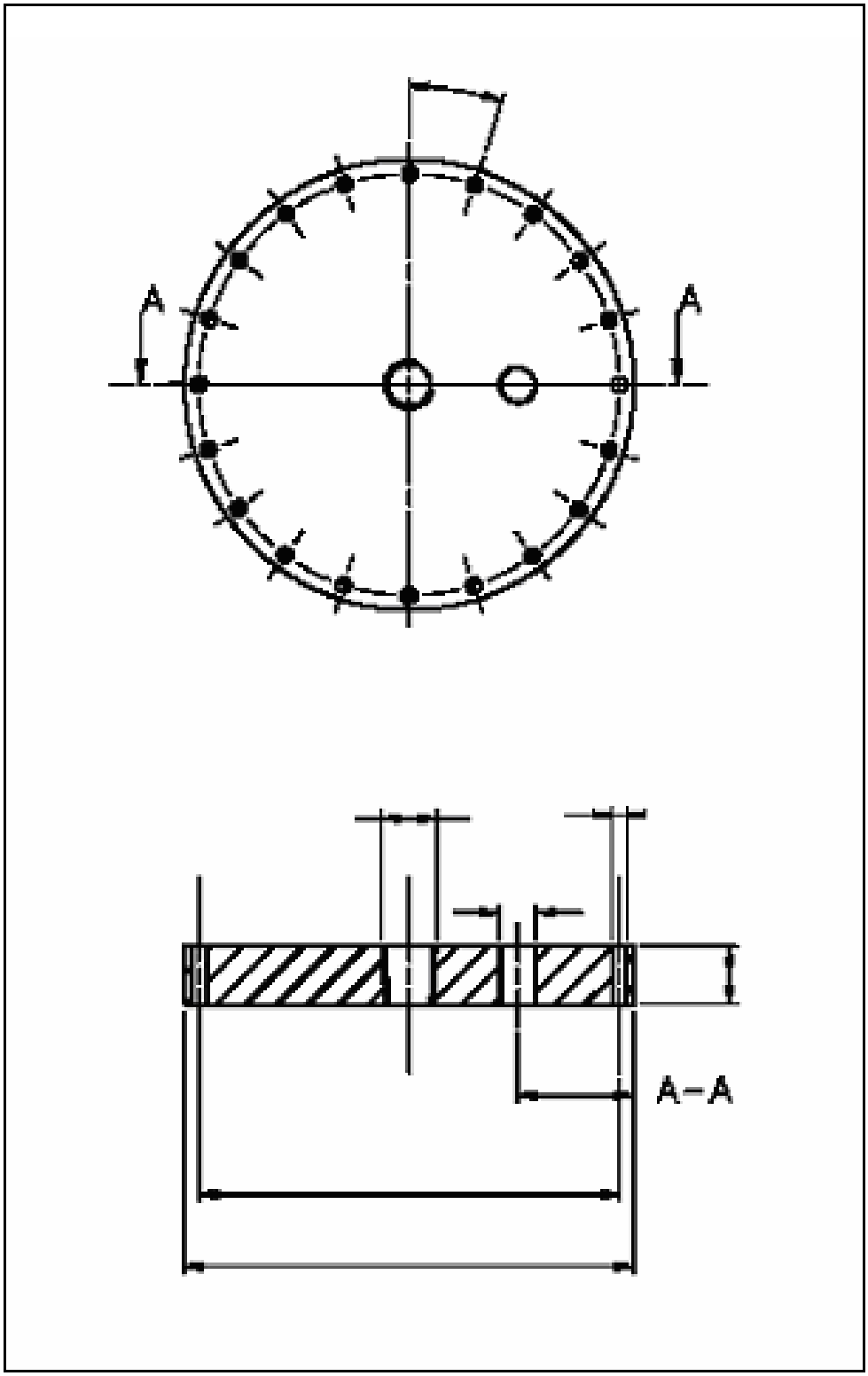

Figure 89. Technical drawing of Top Plate

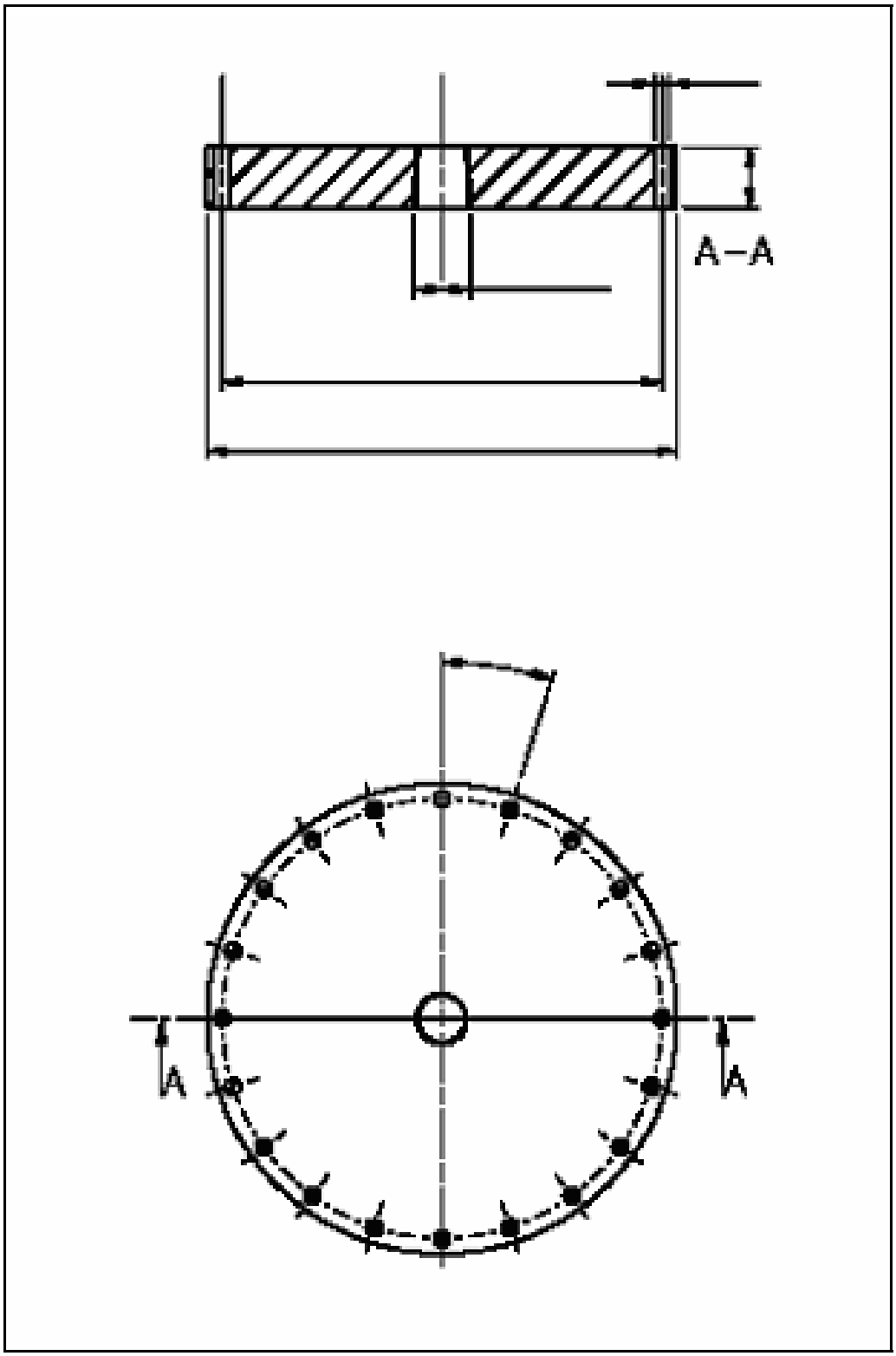

Figure 90. Technical drawing of Bottom Plate

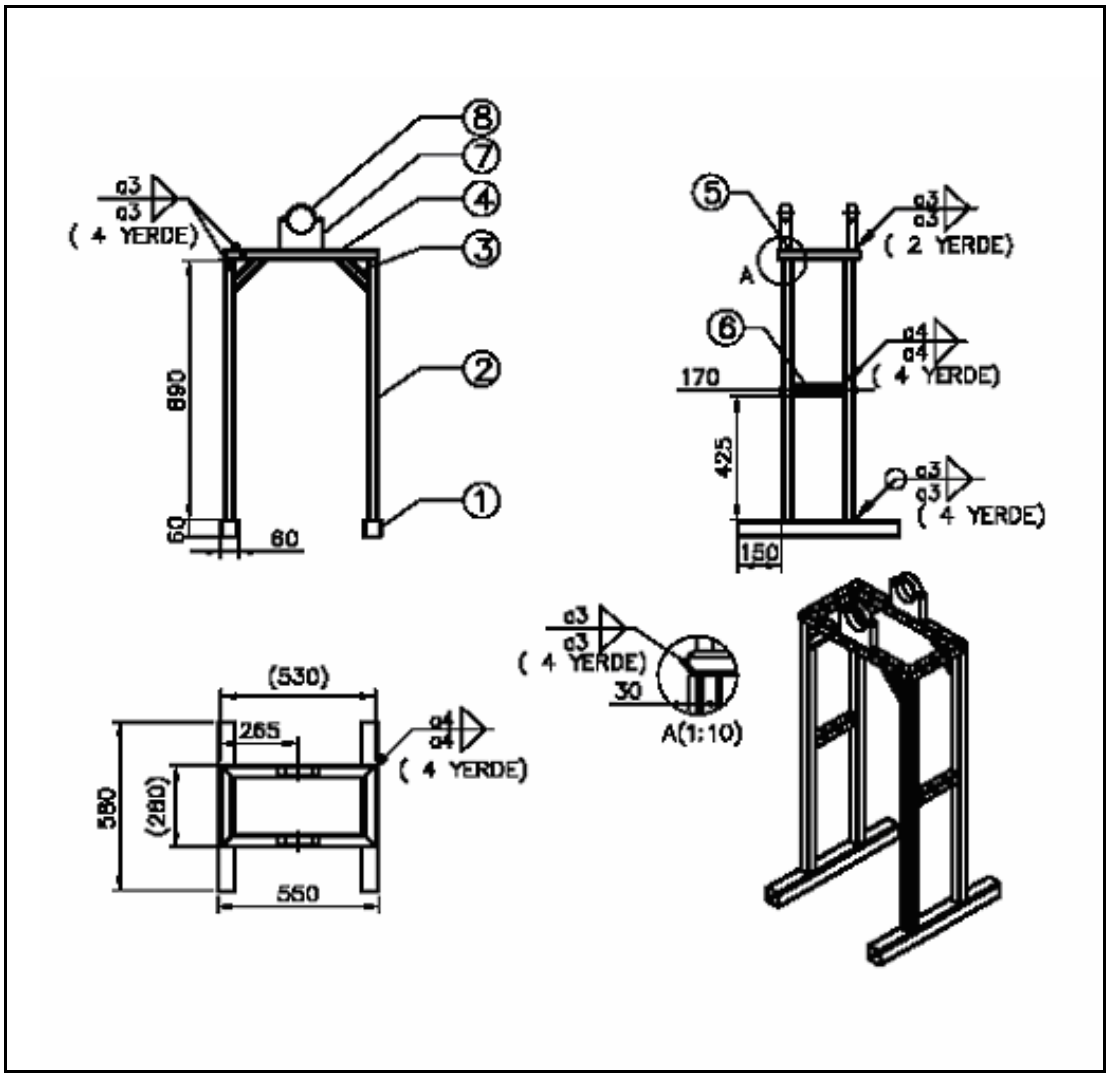

Figure 91. Technical drawing of Base

B. SPECIFICATIONS

Rupture Disc Specifications

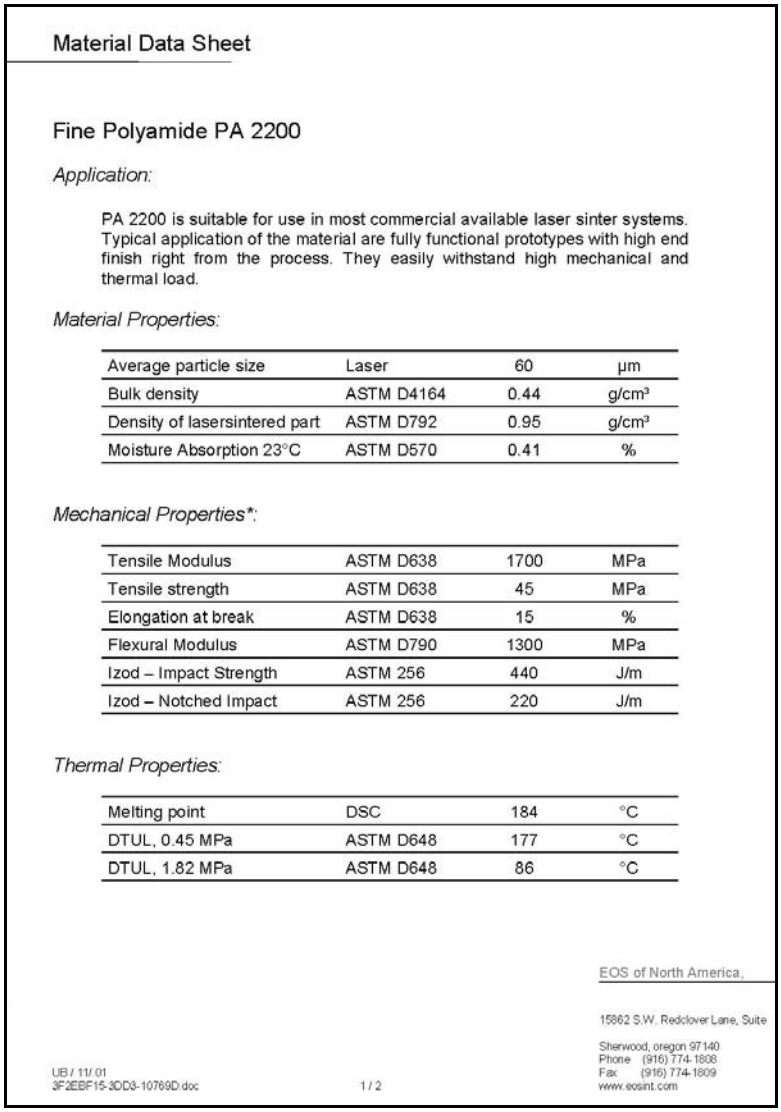

Material Data Sheet

Fine Polyamide PA 2200

Application:

PA 2200 is suitable for use in most commercial available laser sinter systems. Typical application of the material are fully functional prototypes with high end finish right from the process. They easily withstand high mechanical and thermal load.

Material Properties:

Average particle size	Laser	60	µm
Bulk density	ASTM D4164	0.44	g/cm³
Density of lasersintered part	ASTM D792	0.95	g/cm³
Moisture Absorption 23°C	ASTM D570	0.41	%

Mechanical Properties:*

Tensile Modulus	ASTM D638	1700	MPa
Tensile strength	ASTM D638	45	MPa
Elongation at break	ASTM D638	15	%
Flexural Modulus	ASTM D790	1300	MPa
Izod – Impact Strength	ASTM 256	440	J/m
Izod – Notched Impact	ASTM 256	220	J/m

Thermal Properties:

Melting point	DSC	184	°C
DTUL, 0.45 MPa	ASTM D648	177	°C
DTUL, 1.82 MPa	ASTM D648	86	°C

EOS of North America,

15862 S.W. Redclover Lane, Suite

Sherwood, oregon 97140
Phone (916) 774-1808
Fax (916) 774-1809
www.eosint.com

UB / 11/ 01
3F2EBF15-3DD3-10769D.doc

1 / 2

Figure 92. Mechanical data sheet of the rupture disc material

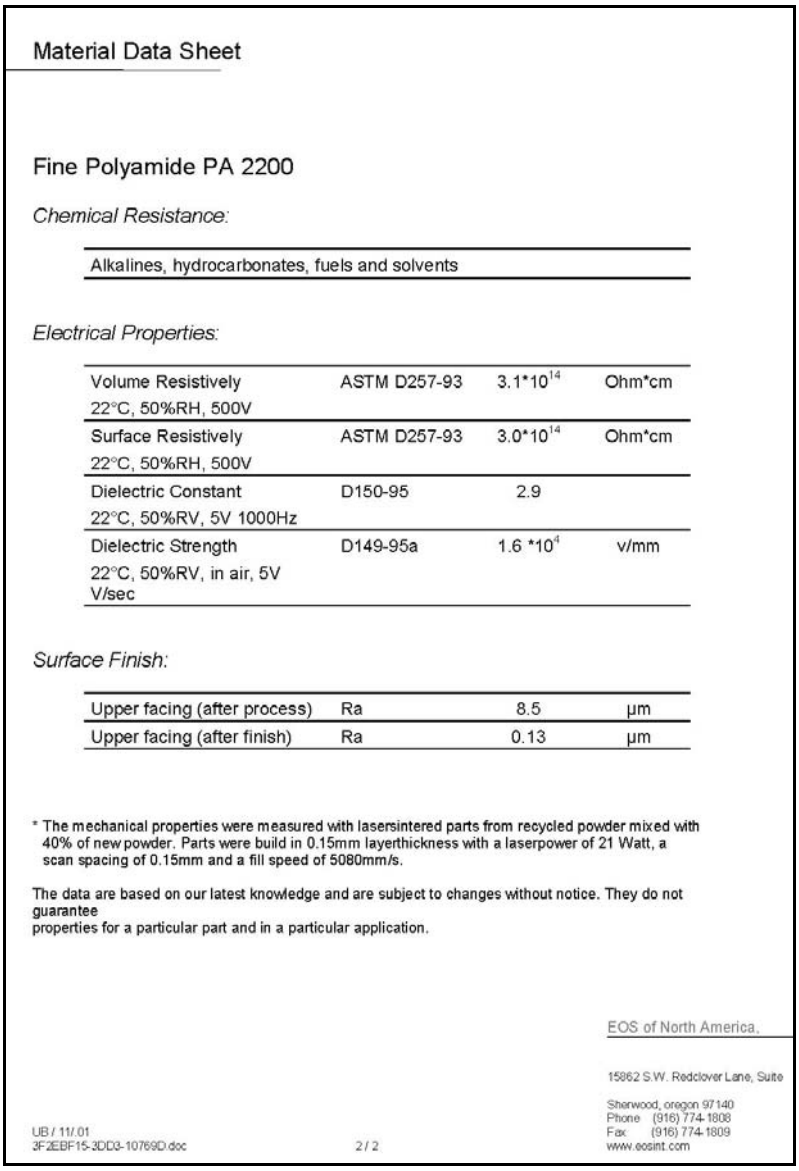

Material Data Sheet

Fine Polyamide PA 2200

Chemical Resistance:

Alkalines, hydrocarbonates, fuels and solvents

Electrical Properties:

Volume Resistively 22°C, 50%RH, 500V	ASTM D257-93	$3.1*10^{14}$	Ohm*cm
Surface Resistively 22°C, 50%RH, 500V	ASTM D257-93	$3.0*10^{14}$	Ohm*cm
Dielectric Constant 22°C, 50%RV, 5V 1000Hz	D150-95	2.9	
Dielectric Strength 22°C, 50%RV, in air, 5V V/sec	D149-95a	$1.6*10^{4}$	v/mm

Surface Finish:

Upper facing (after process)	Ra	8.5	µm
Upper facing (after finish)	Ra	0.13	µm

* The mechanical properties were measured with lasersintered parts from recycled powder mixed with 40% of new powder. Parts were build in 0.15mm layerthickness with a laserpower of 21 Watt, a scan spacing of 0.15mm and a fill speed of 5080mm/s.

The data are based on our latest knowledge and are subject to changes without notice. They do not guarantee
properties for a particular part and in a particular application.

EOS of North America,

15862 S.W. Redclover Lane, Suite

Sherwood, oregon 97140
Phone (916) 774-1808
Fax (916) 774-1809
www.eosint.com

Figure 93. Mechanical data sheet of the rupture disc material – Cont.

Pressure Transducer Specifications

Pressure – PAG

KISTLER

1 ... 2

Quarz-Hochdrucksensor
Capteur de haute pression a quartz
Quartz High Pressure Sensor

701A

Quarz Drucksensor zum Messen dynamischer und quasistatischer Drücke bis 250 bar bei Temperaturen bis 200 °C.

Capteur de pression à quartz pour mesurer des pressions dynamiques et quasistatiques jusqu'à 250 bar à des températures jusqu'à 200 °C.

Quartz pressure sensor for measuring dynamic and quasistatic pressures up to 250 bar at temperatures up to 200 °C.

- hohe Empfindlichkeit
  haute sensibilité
  hight sensitivity
- Temperaturen bis zu 200 °C
  Températures jusqu'à 200 °C
  Temperatures up to 200 °C

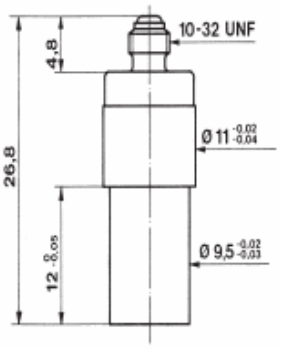

2:1

Technische Daten	Données techniques	Technical Data		
Bereich Kalibrierte Teilbereiche	Gamme Gammes partielles étalonnées	Range Calibrated partial ranges	bar bar bar	0 ... 250 0 ... 25 0 ... 2,5
Überlast	Surcharge	Overload	bar	400
Empfindlichkeit	Sensibilité	Sensitivity	pC/bar	≈ -80
Eigenfrequenz	Fréquence propre	Natural frequency	kHz	≈70
Linearität	Linéarité	Linearity	%FSO	≤ ±0,5
Beschleunigungsempfindlichkeit	Sensibilité aux accélérations	Acceleration sensitivity	bar/g	<0,001
Betriebstemperaturbereich	Gamme de température d'utilisation	Operating temperature range	°C	-150 ...200
Temperaturkoeffizient der Empfindlichkeit	Coefficient de température de la sensibilité	Temperature coefficient of sensitivity	°C-1	$<10^{-4}$
Isolationswiderstand	Résistance d'isolement	Insulation resistance	Ω	$\geq 10^{13}$
Stossfestigkeit	Résistance au choc	Shock resistance	g	5000
Kapazität	Capacité	Capacitance	pF	9
Gewicht	Poids	Weight	g	8,5
Stecker, Teflon-Isolator	Connecteur, isolateur en téflon	Connector, teflon insulator		10-32 UNF

1 N (Newton) = 1 kg·m·s^{-2} = 0,1019... kp = 0,2248... lbf; 1 kp = 1 kgf = 9,80665 N; 1 inch = 25,4 mm; 1 kg = 2,2046... lb; 1 Nm = 0,73756... lbft

000-050m-06.95 (DB03.701Am-06.95)

Beschreibung

Der zu messende Druck wirkt über die Membrane auf das Quarzkristall Messelement, das den Druck p (bar) in eine elektrische Ladung Q (pC = pico-Coulomb) umwandelt. Die Membrane aus rostfreiem Stahl ist mit dem Sensorgehäuse aus rostfreiem Stahl hermetisch und bündig verschweisst. Die Quarze sind in hochempfindlicher Anordnung (Transversaleffekt) in der Quarzkammer eingebaut, die mit dem Gehäuse hermetisch verschweisst ist.

Der Stecker-Anschluss ist mit dem Gehäuse verschweisst, jedoch ist sein Teflon-Isolator nicht dicht.

Description

Par l'intermédiaire du diaphragme, la pression agit sur l'élément de mesure à quartz qui transforme la pression p (bar) en charge électrique Q (pC = pico-Coulomb). Le diaphragme en acier inoxydable est soudé hermétiquement, au ras du front, au boîtier en acier inoxydable. Les éléments à quartz sont montés en un ensemble de haute sensibilité (effet transversal) dans la chambre à quartz, elle-même soudé hermétiquement au boîtier.

La prise électrique est soudée au boîtier, cependant son isolateur en téflon n'est pas rigoureusement étanche.

Description

The measured pressure acts through the diaphragm on the quartz crystal measuring element, which transforms the pressure p (bar) into an electrostatic charge Q (pC = pico-Coulomb). The stainless steel diaphragm is welded flush and hermetically to the stainless steel sensor body. The quartz elements are mounted in a highly sensitive arrangement (transversal effect) in the quartz chamber, which is welded hermetically to the body.

The connector is welded to the body, but its teflon insulator is not absolutely tight.

Kistler Instrumente AG Winterthur, CH-8408 Winterthur, Switzerland, Tel. (052) 224 11 11 Kistler Instrument Corp., Amherst, NY 14228-2171, USA, Phone (716) 691-5100

Figure 94. Data sheet of the pressure transducers

Anwendung

Der Drucksensor 701A eignet sich besonders für die Messung schneller Druckverläufe. Bei besonders beschränkten Einbauverhältnissen oder sehr hohen Messfrequenzen ist der Drucksensor 601 zu verwenden.

Typische Anwendungen:
Druckmessungen an Verbrennungsmotoren, Kompressoren, pneumatischen und hydraulischen Anlagen (ausgenommen Einspritzpumpen).

Application

Le capteur 701A est adapté à la mesure de variations rapides de pression. On choisit le capteur miniature 601 pour des dispositifs à dimensions réduites ou pour les fréquences très élevées.

Exemples d'application:
Mesure de pressions de moteurs à combustion interne, compresseurs, installations pneumatiques et hydrauliques (à l'exception des pompes à injection).

Application

The quartz pressure sensor 701A is suited for dynamic pressure measurements. For very high frequencies or reduced mounting space the sensor 601 is used.

Typical applications:
Pressure measurements on combustion engines, compressors, pneumatic and hydraulic installations (except injection pumps).

Montage

Der Sensor kann mittels eines Montagenippels (Fig. 1) oder eines Steckernippels (Fig. 2) im Messobjekt oder dem Adapter montiert werden. Bei der Montage nach Fig. 2 werden Sensor und Steckernippel zu einer Montageeinheit zusammengeschraubt. Die Trennfläche kann mit "Loctite" gedichtet werden.

Siehe auch Datenblätter für:

Werkzeuge	4.012
Adapter	4.015
Steckernippel	4.014
Kabel	15.035

Montage

Le capteur peut être monté directement dans le dispositif de mesure ou dans l'adaptateur à l'aide d'un écrou de montage (fig. 1) ou d'un écrou connecteur (fig. 2). Pour le montage selon fig. 2, le capteur et l'écrou connecteur forment une unité. La jonction capteur - écrou connecteur peut être rendue étanche avec du "Loctite".

Voir aussi les notices techniques suivantes:

Outillage	4.012
Adaptateurs	4.015
Ecrous connecteurs	4.014
Câbles	15.035

Mounting

The sensor can be mounted directly into the measuring object or the adapter by means of a mounting nut (fig. 1) or a connecting nipple (fig. 2). When mounted with a connecting nipple, the latter is preassembled with the sensor to a mounting unit. The junction between nipple and sensor can be sealed with "Loctite".

See also datasheets for:

Tools	4.012
Adapters	4.015
Connecting nipples	4.014
Cables	15.035

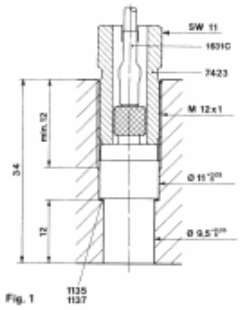

Fig. 1

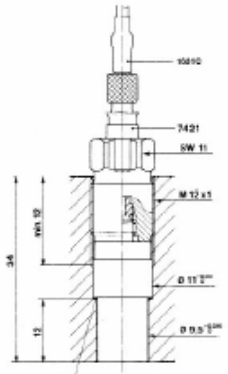

Fig. 2

Zubehör	Typ
Cu-Dichtung	1135
Ni-Dichtung	1135A
Teflon-Dichtung	1137
Schlüssel für Steckernippel 7421	1303
Stufenbohrer	1333
Ausziehwerkzeug für 10-32 UNF	1311
Montagenippel SW8	7423
Steckernippel 10-32UNF/10-32UNF	7421
Steckernippel 10-32UNF/BNC	7401
Steckernippel 10-32UNF/TNC	7411
Steckernippel luftgekühlt 10-32UNF/10-32UNF	7461
Schrumpfschlauch für Stecker	1021
Montageadapter M14 x 1,25	7501
Montageadapter M5	7503
Kühladapter M18 x 1,5	7505
Kühladapter M14 x 1,25	7507

Accessoires	Type
Joint en cuivre	1135
Joint en nickel	1135A
Joint en téflon	1137
Clé pour écrou connecteur 7421	1303
Aléseuse progressive	1333
Outil extracteur pour 10-32 UNF	1311
Ecrou de montage OCW8	7423
Ecrou connecteur 10-32UNF/10-32UNF	7421
Ecrou connecteur 10-32UNF/BNC	7401
Ecrou connecteur 10-32UNF/TNC	7411
Ecrou connecteur refroidi par air 10-32UNF/10-32UNF	7461
Gaine thermorétractable pour connecteur	1021
Adaptateur de montage M14 x 1,25	7501
Adaptateur de montage M5	7503
Adaptateur refroidi M18 x 1,5	7505
Adaptateur refroidi M14 x 1,25	7507

Accessories	Type
Copper seal	1135
Nickel seal	1135A
Teflon seal	1137
Key for connecting nipple 7421	1303
Step drill	1333
Extraction tool 10-32 UNF	1311
Mounting nut WS8	7423
Connecting nipple 10-32UNF/10-32UNF	7421
Connecting nipple 10-32UNF/BNC	7401
Connecting nipple 10-32UNF/TNC	7411
Connecting nipple air cooled 10-32UNF/10-32UNF	7461
Heat-shrink tubing for connector	1021
Mounting adapter M14 x 1,25	7501
Mounting adapter M5	7503
Cooling adapter M18 x 1,5	7505
Cooling adapter M14 x 1,25	7507

000-050m-06.95 (D803.701Am-06.95)

Figure 95. Data sheet of the pressure transducers – Cont.

Thermocouple Specifications

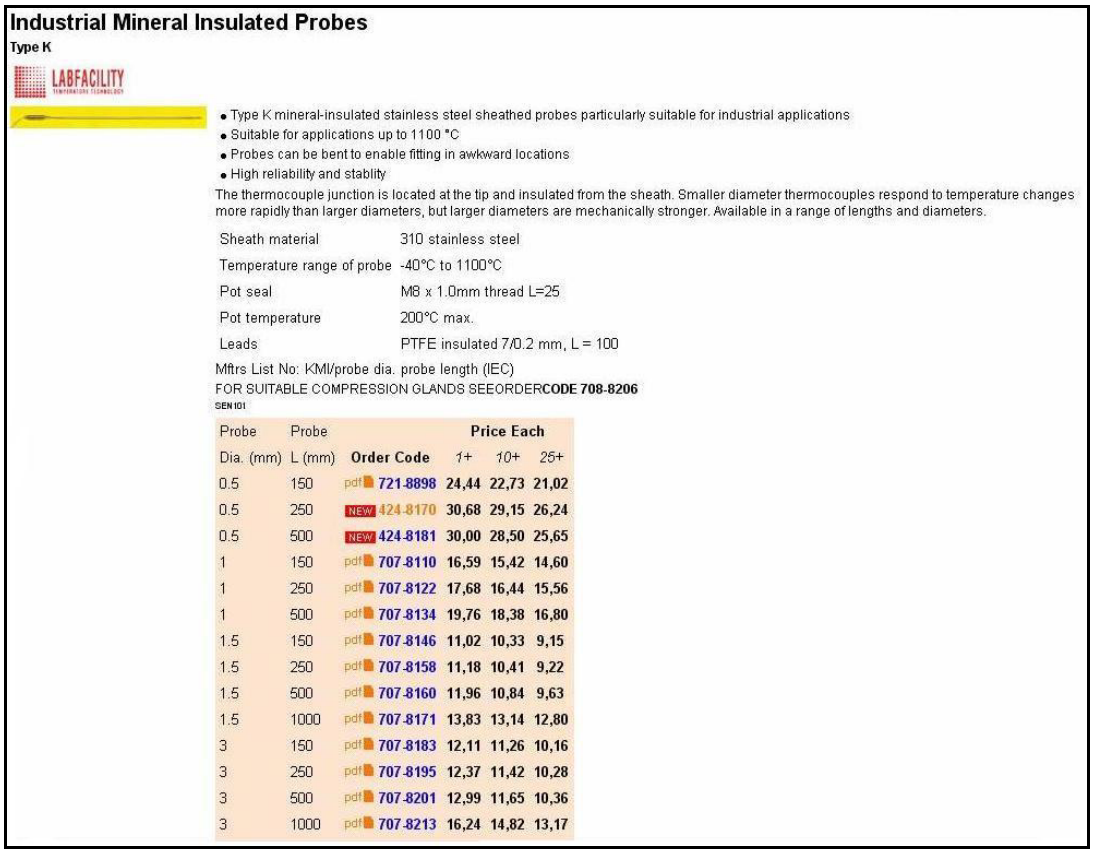

Industrial Mineral Insulated Probes

Type K

LABFACILITY

- Type K mineral-insulated stainless steel sheathed probes particularly suitable for industrial applications
- Suitable for applications up to 1100 °C
- Probes can be bent to enable fitting in awkward locations
- High reliability and stablity

The thermocouple junction is located at the tip and insulated from the sheath. Smaller diameter thermocouples respond to temperature changes more rapidly than larger diameters, but larger diameters are mechanically stronger. Available in a range of lengths and diameters.

Sheath material	310 stainless steel
Temperature range of probe	-40°C to 1100°C
Pot seal	M8 x 1.0mm thread L=25
Pot temperature	200°C max.
Leads	PTFE insulated 7/0.2 mm, L = 100

Mftrs List No: KMI/probe dia. probe length (IEC)

FOR SUITABLE COMPRESSION GLANDS SEEORDER**CODE 708-8206**

SEN101

Probe Dia. (mm)	Probe L (mm)	Order Code	Price Each 1+	10+	25+
0.5	150	pdf 721-8898	24,44	22,73	21,02
0.5	250	NEW 424-8170	30,68	29,15	26,24
0.5	500	NEW 424-8181	30,00	28,50	25,65
1	150	pdf 707-8110	16,59	15,42	14,60
1	250	pdf 707-8122	17,68	16,44	15,56
1	500	pdf 707-8134	19,76	18,38	16,80
1.5	150	pdf 707-8146	11,02	10,33	9,15
1.5	250	pdf 707-8158	11,18	10,41	9,22
1.5	500	pdf 707-8160	11,96	10,84	9,63
1.5	1000	pdf 707-8171	13,83	13,14	12,80
3	150	pdf 707-8183	12,11	11,26	10,16
3	250	pdf 707-8195	12,37	11,42	10,28
3	500	pdf 707-8201	12,99	11,65	10,36
3	1000	pdf 707-8213	16,24	14,82	13,17

Figure 96. Data sheet of the thermocouple

Data Acquisition System Specifications

Measure & Analyze – MCA

KISTLER
measure. analyze. innovate.

Charge Meter

Type 5015A...

Universally Applicable for Piezoelectric Measuring Technology

This instrument can be used wherever mechanical quantities are measured with piezoelectric sensors. Piezoelectric sensors produce an electric charge which varies in direct proportion to the load acting on the sensor.

- Single-channel charge amplifier
- Piezotron® input (option)
- Measure-jump compensated
- Liquid crystal display (128x128 pixels)
- Menu-driven operation
- Direct signal evaluation
- Flexible adjustment of high-pass and low-pass filters
- Compatible with Charge Amplifier Type 5011B
- PC-Software and Virtual Instrument Driver for LabVIEW™

Description

The Type 5015A... is not only a charge amplifier but an universal Charge Meter with a graphical liquid crystal display. However, the 19"-rack module is also suitable for measurements in an industrial environment. It can display instantaneous, peak and average values as well as reference deviations. State-of-the art technology allows the naturally occurring interference to be almost entirely eliminated. The instrument is distinguished firstly by its excellent technical data and secondly by its extremely simple operation.

Application

The instrument has been designed as the successor to the successful charge amplifier Type 5011B for use in research, development and the laboratory.

Technical Data

Charge Input		
Connector Type	BNC neg.	
Measuring range FS	pC	±2 ... 2'200'000
Measuring error		
Range FS <10 pC	%	<±3
Range FS <100 pC	%	<±1
Range FS ≥100 pC	%	<±0,5
Drift, measuring mode DC (Long)		
at 25 °C	pC/s	<±0,03
at 50 °C	pC/s	<±0,3
Max. common mode voltage between input and output ground	V	<±30
Overload	%FS	≈±105

000-297e-11.03 (DB11.5015Ae)

Figure 97. Data sheet of the data acquisition system

KISTLER
measure. analyze. innovate.

Voltage Input (Piezotron®)		
Connector Type	BNC neg.	
Measuring range FS	mV	±2 ... 20'000
Measuring error		
Range FS <10 mV	%	<±3
Range FS <100 mV	%	<±1
Range FS ≥100 mV	%	≤±0,5
Drift, measuring mode voltage		
at 25 °C	mV/s	<±0,03
at 50 °C	mV/s	<±0,3
Max. common mode voltage between input and output ground	V	<±30
Overload	%FS	≈±105
Piezotron mode		
Supply current	mA	4 ±10 %
Input voltage swing	V	0 ... 20

Voltage Output		
Connector Type	BNC neg.	
Output range FS	V	±10/±5/±2,5/±2
Output current	mA	<±2
Output impedance	Ω	≈10
Measure-jump	Compensated	
Measure-jump	mV	<±3
Correction time, inclusive reed-relay delay time	ms	<15 1)
Zero errors	mV	<±2
Output interference (0,1 Hz ... 1 MHz), Type 5015Axxx0		
Range FS, LP filter off		
2,000 ... 9,999 pC	mVpp	<140 ... <40
10,00 ... 99,99 pC	mVpp	<30 ... <10 1)
100,0 ... 999,9 pC	mVpp	<15 ... <7 1)
...	mVpp	<15 ... <7 1)
0,220 ... 2,200 nC	mVpp	<15 ... <7 1)
Range FS, LP filter ≤30 kHz		
2,000 ... 9,999 pC	mVpp	<60 ... <20
10,00 ... 99,99 pC	mVpp	<20 ... <7 1)
...	mVpp	<10 ... <5 1)
0,220 ... 2,200 nC	mVpp	<10 ... <5 1)
Output interference (0,1 Hz ... 1 MHz), Type 5015Axxx1		
Range FS, LP filter off		
2,000 ... 9,999 pC, mV	mVpp	<220 ... <50
10,00 ... 99,99 pC, mV	mVpp	<50 ... <12 1)
100,0 ... 999,9 pC, mV	mVpp	<20 ... <7 1)
...	mVpp	<20 ... <7 1)
0,220 ... 2,200 nC	mVpp	<20 ... <7 1)
Range FS, LP filter ≤30 kHz		
2,000 ... 9,999 pC, mV	mVpp	<180 ... <50 1)
10,00 ... 99,99 pC, mV	mVpp	<30 ... <10 1)
100,0 ... 999,9 pC, mV	mVpp	<10 ... <5 1)
...	mVpp	<10 ... <5 1)
0,220 ... 2,200 nC	mVpp	<10 ... <5 1)

1) Values valid from MCC version V2.xx

Frequency Response		
DC (Long), LP-filter off		
Bandwidth (-3 dB)	kHz	≈0 ... 200
Group delay	µs	≈10

High-pass Filter (1st order)		
Analog high-pass filter		
DC (Long)		
Range FS Charge, (Voltage)		
≥2 pC, (mV)	s	10'000
≥1'000 pC, (mV)	s	100'000
Time constants		
Medium	s	10/100/1'000/2'200
Short	s	0,1/1/10/220
Tolerance	%	<±20

Digital high-pass filter computed by DSP

Time constants		
Range FS Charge, (Voltage)		
≥2 pC, (mV)	s	0,01/0,1/1
≥100 pC, (mV)	s	0,01/0,1/1/10
≥1'000 pC, (mV)	s	0,01/0,1/1/10/100
≥10'000 pC, (mV)	s	0,01/0,1/1/10/100
Tolerance	%	<±20
Cutoff frequencies		
–3 dB	Hz	16/1,6/0,16/0,016/ 0,0016
–10 %	Hz	30/3/0,3/0,03/0,003
–5 %	Hz	50/5/0,5/0,05/0,005
–1 %	Hz	100/10/1/0,1/0,01
Tolerance	%	<±20

000-297e-11.03 (DB11.5015Ae)

Figure 98. Data sheet of the data acquisition system – Cont.

KISTLER
measure. analyze. innovate.

Low-pass Filter

Digital low-pass filter computed by DSP

Filter Type	IIR, linear Phase	
Order		2. or 5.
Cutoff frequency (–3 dB)	Hz	5 ... 30'000
Steps		1/2/3/5
Tolerance	%	<±10

Signal Evaluation

Sample rates		
LP-filter on	ksps	400
LP-filter off	ksps	1'000
Minimum pulse width for peak-peak value detection		
LP-filter 5 Hz ... 30 Hz	µs	>2'500
LP-filter 50 Hz ... 300 Hz	µs	>250
LP-filter 500 Hz ... 3 kHz	µs	>25
LP-filter 5 kHz ... 30 kHz	µs	>2,5
LP-filter off	µs	>1
Max. integration time for mean value	min	<75
Integration time for the updating rate of the liquid crystal display		
Instant value	ms	300
Characteristic values	ms	300
Bar graph	ms	17,5

Remote Control

Connector Type		MiniDin round socked
Pin allocation		
Inputs with internal pull-up resistor		
Pin 4 (input)		Window (remote)
Pin 5 (input)		Measure (remote)
Pin 6		DGND
Input voltage		
logic inactive or input open	V	3,5 ... 30
logic active	V(mA)	0 ... 1 (0 ... 4)
Delay time		
Window (remote)	ms	<0,5
Measure (remote)	ms	<15

Digital Measuring Data Transfer

The instrument provides a continuos measuring data transfer via the serial interface to a PC. For this the PC software (Windows©) of the VI driver (LabVIEW™) is required. This feature is not available on the IEEE-488 interface.

Sampling rates	ksps	0,1/0,25/0,5/1

RS-232C Interface (Electrically Separated)

EIA-standard		RS-232C
Connector Type		DB-9S (D-Sub)
Pin allocation		
Pin 2		RxD
Pin 3		TxD
Pin 5		SG
Max. cable length at		
9'600 bps	m	<15
19'200 bps	m	<15
38'400 bps	m	<12
57'600 bps	m	<10
115'200 bps	m	<5
Max. input voltage, continues	V	<±20
Max. voltage between Signal ground and protective ground	V_{RMS}	<20
Baud rates	bps	1'200/9'600/ 19'200/38'400/ 57'600/115'200
Data-bit		8
Stop-bit		1
Parity		none
SW handshake		none

IEEE-488 Interface (Option)

Standard		IEEE-488.1-1987
Connector Type		Microribbon series 57 (24-pole)
Max. distance between devices	m	2
Max. bus length	m	20
Max. number of devices		15
Adress range		0 ... 30
Functions		Listener and Talker
Interface-functions		SH1, AH1, L4, LE0, T6, TE0, SR1, RL2, PP0,DC1, DT1, C0, E1
Multiline commands		DCL, SDC, GET, UNL, UNT, SPE, SPD
Uniline commands		IFC, REN, EOI, SRQ, ATN

000-297e-11.03 (DB11.5015Ae)

Figure 99. Data sheet of the data acquisition system – Cont.

KISTLER
measure. analyze. innovate.

Power Supply Connection		
Power plug (2P+E, protection class I)		IEC 320C14
Supply voltage setable	V~	115/230
Supply voltage tolerance	%	–22, +15
Supply frequency	Hz	48 ... 62
Consumption	VA	≈20
Voltage between Signal ground and protective ground	V_{RMS}	<50
Fuses		
F1 (slow)	mA	100
F2 (slow)	mA	100

Remaining Data		
IP-Degree of protection		IP40, IEC 60529
Operating temperature	°C	0 ... 50
Storage temperature	°C	–10 ... 70
Rel. humidity, not condensing	%	10 ... 80
Vibration steadiness (20 Hz ... 2 kHz, duration 16 min, cycle 2 min.)	g	<10
Shock steadiness (1ms)	g	<200
Housing dimensions		
with frame (wxhxd)	mm	105,3x142x253,15
without frame (wxhxd)	mm	71,12x128,7x230
Front panel (according DIN 41494, part 5)	HT/TE	3/14
Weight	kg	≈2,3

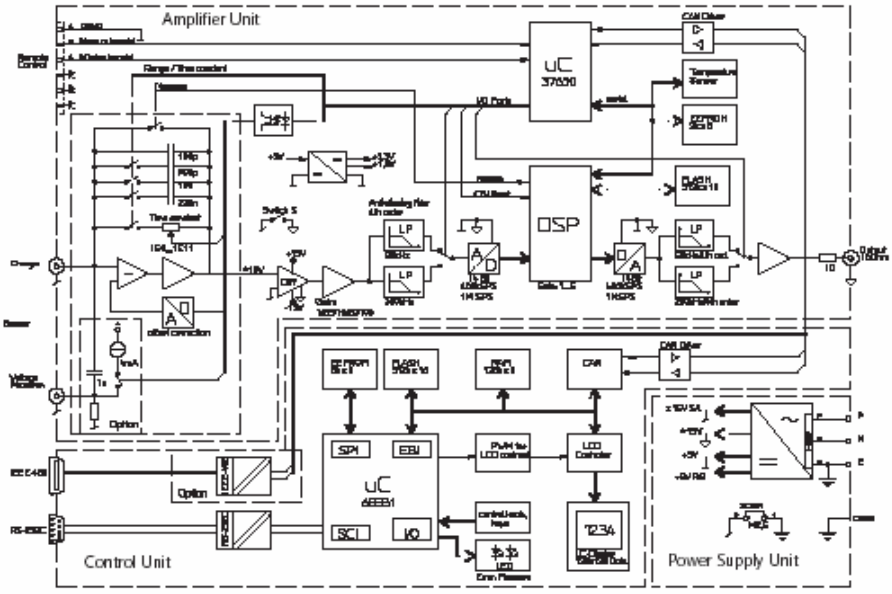

Fig. 1: Block Diagram of charge meter Type 5015A...

000-297e-11.03 (DB11.5015Ae)

Figure 100. Data sheet of the data acquisition system – Cont.

C. SUB SYSTEM EXPERIMENTAL RESULTS

Rupture Disc Validation Test Results

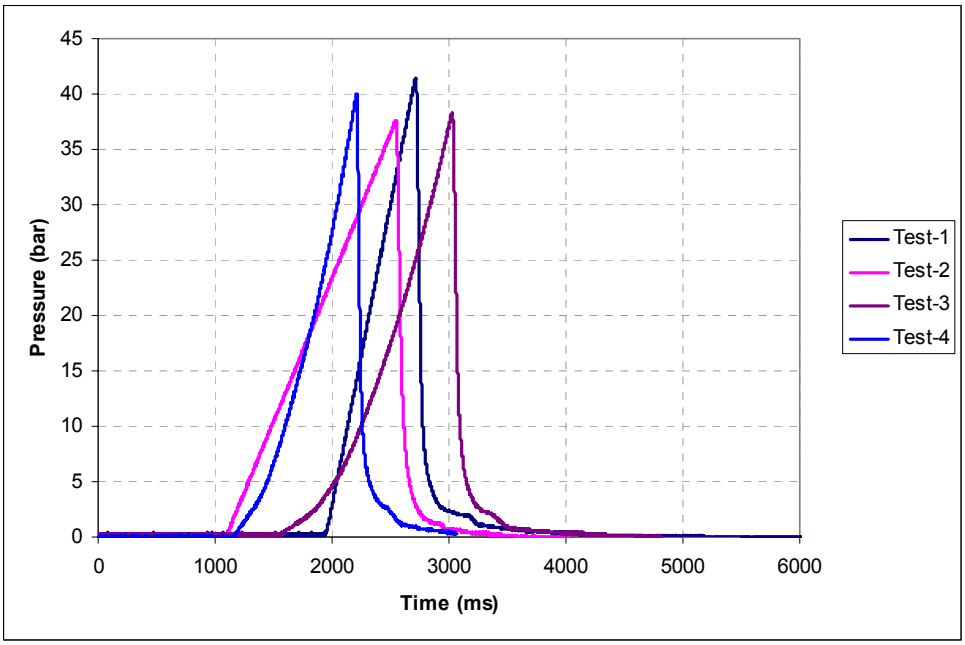

Figure 101. Rupture Disc Burst Pressure Determination Tests – (t = 3 mm)

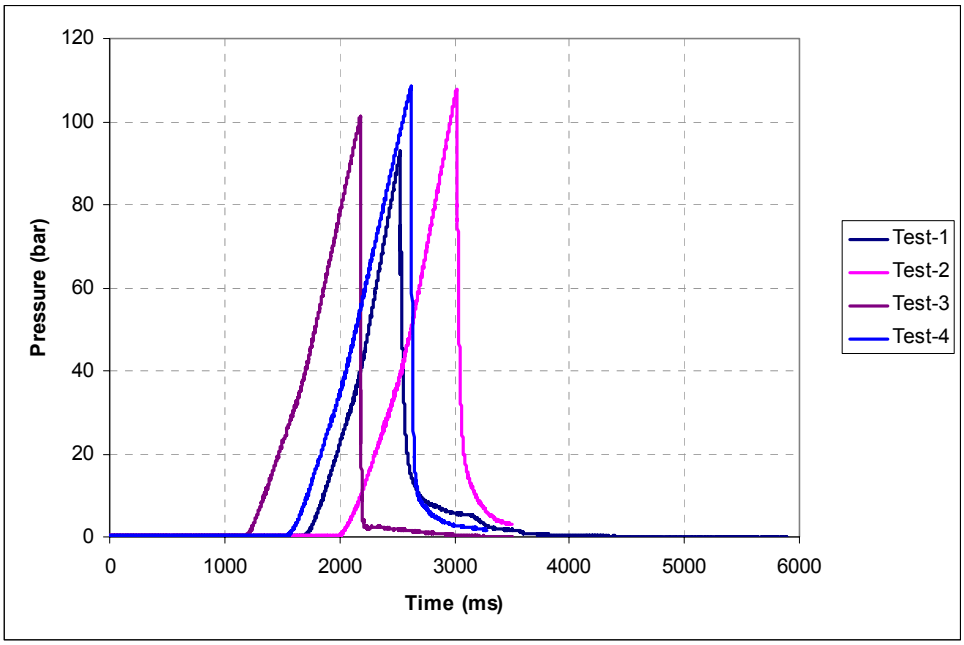

Figure 102. Rupture Disc Burst Pressure Determination Tests – (t = 4 mm)

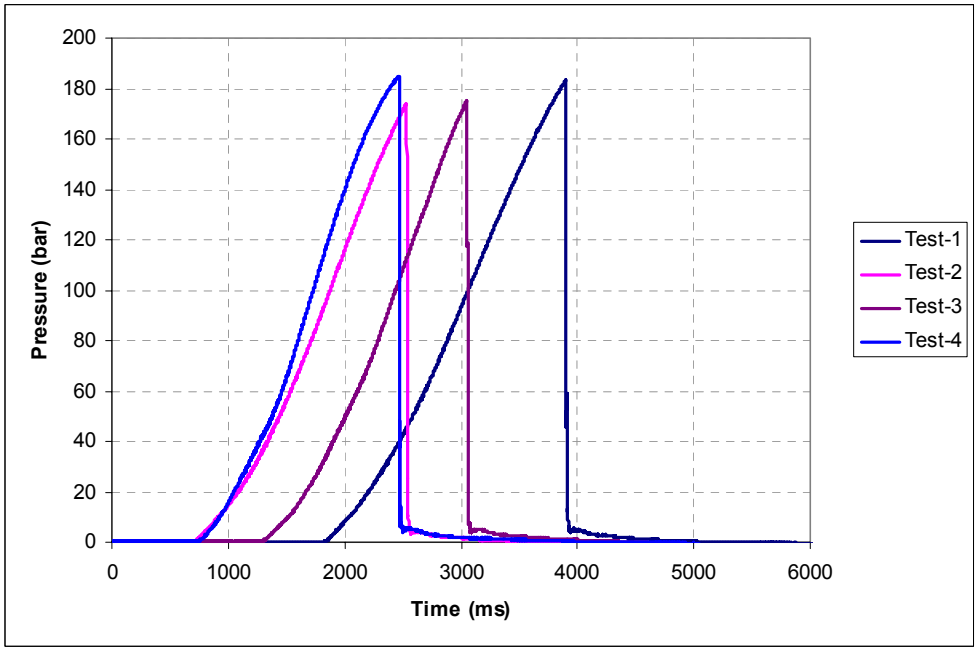

Figure 103. Rupture Disc Burst Pressure Determination Tests – (t = 5 mm)

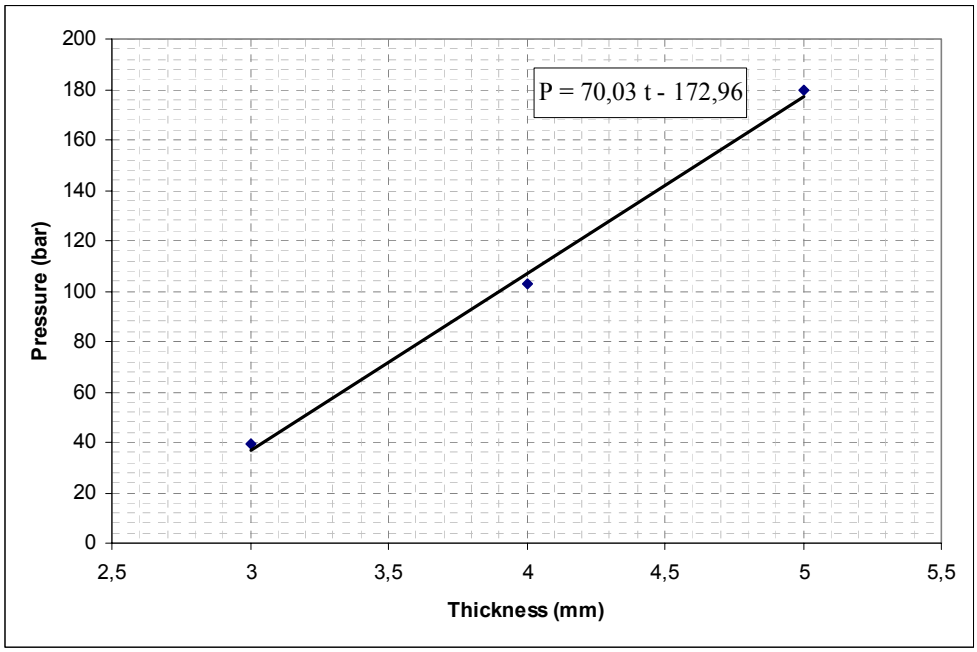

Figure 104. Rupture Disc Pressure vs. Thickness Variation

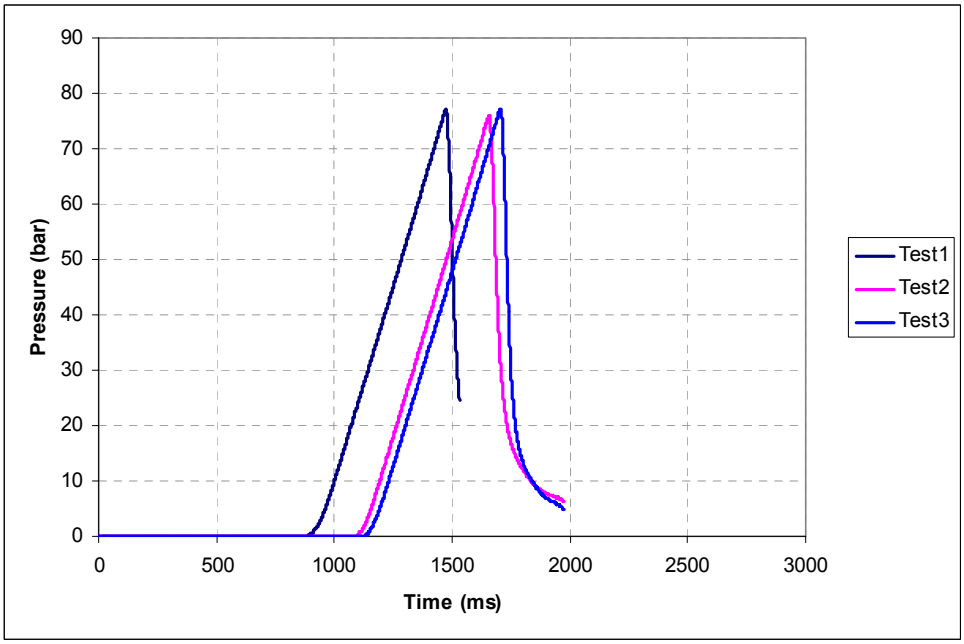

Figure 105. Rupture Disc Burst Pressure Determination Tests – (t = 3.4 mm)

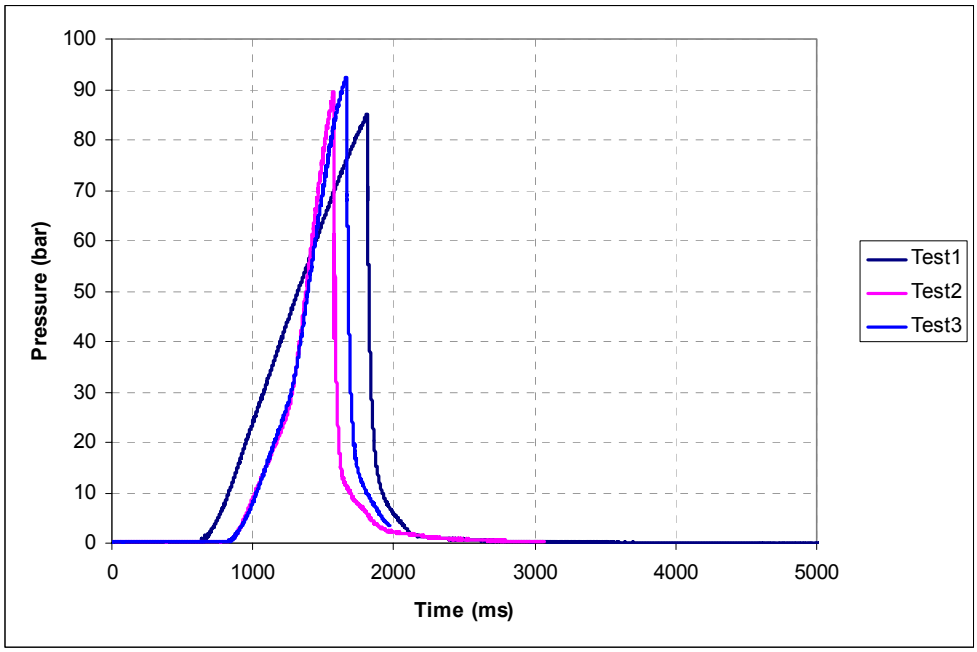

Figure 106. Rupture Disc Burst Pressure Determination Tests – (t = 3.5 mm)